

8-2017

Superfine Powdered Activated Carbon (S-PAC) Coupled with Microfiltration for the Removal of Trace Organics in Drinking Water Treatment

Erin Partlan

Clemson University, erpartlan@gmail.com

Follow this and additional works at: https://tigerprints.clemson.edu/all_dissertations

Recommended Citation

Partlan, Erin, "Superfine Powdered Activated Carbon (S-PAC) Coupled with Microfiltration for the Removal of Trace Organics in Drinking Water Treatment" (2017). *All Dissertations*. 2011.

https://tigerprints.clemson.edu/all_dissertations/2011

This Dissertation is brought to you for free and open access by the Dissertations at TigerPrints. It has been accepted for inclusion in All Dissertations by an authorized administrator of TigerPrints. For more information, please contact kokeefe@clemson.edu.

**SUPERFINE POWDERED ACTIVATED CARBON (S-PAC) COUPLED WITH
MICROFILTRATION FOR THE REMOVAL OF TRACE
ORGANICS IN DRINKING WATER TREATMENT**

A Dissertation
Presented to
the Graduate School of
Clemson University

In Partial Fulfillment
of the Requirements for the Degree
Doctor of Philosophy
Environmental Engineering

by
Erin Partlan
August 2017

Accepted by:
David Ladner, Committee Chair
Tanju Karanfil
Cindy Lee
O. Thompson Mefford

ABSTRACT

Anthropogenic contaminants—such as pharmaceuticals and personal care products—are an area of emerging concern in the treatment of drinking water. An integrated activated carbon membrane coating consisting of superfine powdered activated carbon (S-PAC) with particle size near or below one micrometer was explored to enhance removal of trace synthetic organic contaminants (SOCs) from water. S-PAC was chosen for its fast adsorption rates relative to conventionally sized PAC and atrazine was chosen as a model SOC. S-PAC and microfiltration membranes have a symbiotic relationship; membrane filtration separates S-PAC from water, while S-PAC adds capacity for a membrane process to remove soluble components. Three aspects of S-PAC in conjunction with membranes were examined, fouling by S-PAC on the membrane, effects of S-PAC production on material parameters, and modeling of S-PAC adsorption with and without a membrane.

Fouling caused by carbon particles can result in marked reduction of filtration rate and an increased cost of operation. Since larger carbon particles foul less than smaller particles, while smaller carbons have faster adsorption performance, states of carbon aggregation were tested for filtration. Particles aggregated using the coagulant ferric chloride resulted in improved flux, while aluminum sulfate and polyaluminum chloride resulted in the same or worse filtration rates. A calcium chloride control showed that increased effective particle size via divalent bridging was very successful in reducing fouling. While particle size increased with conventional coagulants, the unflocculated metal precipitates likely contributed to membrane fouling.

The methods of producing S-PAC determine material properties that affect both adsorption and filtration performance. In-house S-PACs—including multiple sizes of several carbon types—were prepared by wet bead milling and measured for both physical and chemical material parameters. Physical parameters, aside from particle size, did not change deterministically with milling duration, although stochastic changes were observed. Chemical measurements revealed a heavily oxidized external particle surface resulting from a high energy milling environment. Surfaces of interior pores appeared to be unaffected.

Adsorption via batch kinetics and adsorption via S-PAC coating were modeled with analytical and computational models, respectively, using experimental data produced from the in-house S-PACs. The experimental data showed that removal of atrazine by S-PAC membrane coating correlated most strongly to a combination of oxygen content and the specific external surface area, while membrane fouling correlated to particle size and the specific external surface area. Batch kinetics data were modeled with the homogeneous surface diffusion model (HSDM) while membrane coating data were modeled with computational fluid dynamics (CFD). The fitted models required isotherm parameters indicative of an adsorbent with more capacity than was measured for S-PAC experimentally. Lastly, surface diffusion coefficients were neither constant nor varied with any measured material parameter. However, both model parameters correlated with overall atrazine removal, which indicates that model fits are related to performance, but it is not yet clear how they are connected.

DEDICATION

To my parents, Eva and Martin

ACKNOWLEDGMENTS

I would like to express my sincere appreciation to my advisor Dr. David Ladner and committee members, Drs. Cindy Lee, Tanju Karanfil, and O. Thompson Mefford for providing me with their valuable guidance, continuous support and inspiration. I am also thankful to my EEES family including all faculty, staff and students for their endless support.

Special thanks go to the researchers working on carbon research that have worked with me in data collection and data analysis: Kathleen Davis, Pauline Amaral, Mengfei Li, Semra Bakkaloglu, Onur Guven Apul, and Yiran Ren. Financial support was provided by National Science Foundation (CBET 1236070) research grant with additional support through the NSF East Asia and Pacific Summer Institute (EAPSI) Fellowship and the Fellowship for Membrane Technology sponsored by the National Water Research Institute (NWRI) and the American Membrane Technology Association (AMTA).

TABLE OF CONTENTS

	Page
TITLE PAGE	i
ABSTRACT.....	ii
DEDICATION	iv
ACKNOWLEDGMENTS	v
TABLE OF CONTENTS.....	vi
LIST OF TABLES	viii
LIST OF FIGURES	x
1. PROSPECTUS	1
Introduction	1
Research Objectives	4
2. BACKGROUND.....	7
Persistent Organic Pollutants	7
Activated Carbon.....	13
Superfine Carbon.....	22
Membrane Separations	27
Colloidal Stability	35
Adsorption Modeling	38
3. MICROFILTRATION OF AGGREGATED S-PAC UNDER NATURAL AND CHEMICALLY ENHANCED COAGULATION	47
Motivation	47
Materials and Methods	47
Preliminary Work	53
Results	56
Discussion	70
Conclusions	72

Table of Contents (Continued)

	Page
4. EFFECT OF BEAD MILLING ON CHEMICAL AND PHYSICAL CHARACTERISTICS OF S-PAC	74
Motivation	74
Materials and Methods	74
Results and Discussion	77
Conclusions	97
5. S-PAC MEMBRANE COATING ANALYSIS VIA MODELING.....	98
Motivation	98
Experimental Data Set.....	98
Homogeneous Surface Diffusion Model.....	105
CFD Packed Bed Reactor Model	115
Discussion	128
Conclusions	132
6. CONCLUSIONS AND RECOMMENDATIONS.....	133
Summary and Conclusions.....	133
Recommendations for Future Work	134
APPENDICES	139
A: HSDM Model	140
REFERENCES	151

LIST OF TABLES

Table		Page
2.1.	Properties of selected synthetic organic chemicals of environmental concern.....	10
2.2.	Summary of published literature regarding S-PAC. Size is reported in all studies but other properties are reported less frequently.....	25
3.1.	Particle size distribution of milled S-PAC.....	48
3.2.	Test matrix of feedwater composition. All trials used a carbon concentration of 5 mg/L. Ionic strength was held constant at 10 mM in trials containing ionic compounds.	51
3.3.	Trials with varied ferric chloride dose resulted in trends in slope increase and atrazine removal. The pH correlated directly with the ferric chloride dose and did not affect performance. Neither was turbidity an indicator of performance.	67
4.1.	Measured characteristics of parent PAC materials: specific surface area, total pore volume, and point of zero charge (pH_{PZC}). Seven PACs were milled including coal, wood, and coconut shell based materials.	75
4.2.	Elemental analysis of PAC and S-PAC for four carbons in terms of carbon content, hydrogen content, and nitrogen content by weight percent.....	83
4.3.	Surface charge properties measured by point of zero charge, isoelectric point, and percent oxygen content. The difference between pH_{PZC} and pH_{IEP} is shown as ΔpH . Carbons are distinguished by material and milling time. Dashed lines indicate that measurements were not taken.....	85
4.4.	Surface area and pore volume measurements for seven activated carbons.	91
4.5.	Characteristics for S-PAC reported in literature.....	95
5.1.	Batch kinetics data for 15 ppb of atrazine in DDI onto 2.5 mg/L of each milled carbon.....	99

List of Tables (Continued)

Table	Page
5.2. Atrazine permeated through carbon cakes formed from 1 mg of carbon on a microfiltration membrane. S-PACs are labeled according to their extent of milling. Non-milled PAC and a no carbon condition were used for comparison.....	101
5.3. The normalized flux and total atrazine removal resulting from each carbon cake. Both correlate slightly with the particle size.....	102
5.4. Input parameters for HSDM model.....	106
5.5. Diffusion coefficients determined using minimization of error (sum of squared normalized residuals) to best describe each data set.....	109
5.6. Parameter inputs to the COMSOL model.....	119
5.7. Use of experimental data and the Carman-Kozeny equation to determine carbon permeability within the COMSOL model using a Kozeny constant of 7.....	121
5.8. Summary of model parameter results for the best fit to each data set through HSDM modeling and CFD modeling. For comparison, the Freundlich equilibrium, q_e , is calculated for each set of Freundlich parameters for a concentration of 15 ppb atrazine.....	130

LIST OF FIGURES

Figure	Page
2.1.	Two planes of uniform spheres in a hexagonal close packed arrangement. Left: The base layer demonstrates the hexagonal arrangement. Right: An isometric view shows that the next plane is offset from the first, but is also in hexagonal arrangement. 33
3.1.	Benchscale filtration apparatus using Amicon dead-end filtration cell and operated by constant pressure from a gas cylinder. Data of permeate mass over time is collected by computer. 50
3.2.	Membrane coating using activated carbon of three effective sizes. The largest size is the parent PAC, the smallest size is the fully dispersed probe sonicated S-PAC, and the bath sonicated S-PAC has an effective size between the two. 54
3.3.	Left: Flux decline due to filtration of fully dispersed carbon at varied pH. Right: Translating flux decline into cake resistance reveals a linearly increasing resistance with increasing mass on the membrane. 55
3.4.	Increases in particle size over time as a result of natural aggregation processes is observable at a very high particle concentration of 1000 mg/L. Particle size increase at 20 mg/L and 100 mg/L are not observed over the measurement time frame. Linear fit lines of particle size increase after an initial 30% increase are used as an indicator of aggregation rate. 56
3.5.	Particle size increase as a result of ionic strength. CaCl_2 ions resulted in much faster aggregation than NaCl or KCl at the same concentrations. 57
3.6.	Normalized attachment efficiencies as a result of monovalent Na^+ , Cl^- , and K^+ ions, and divalent Ca^{2+} ions. a) Particles in NaCl up to 100 mM, b) Particles in KCl up to 100 mM, c) Particles in CaCl_2 up to 10 mM. DLVO models for each salt are shown as red dashed lines. 58

List of Figures (Continued)

Figure	Page
3.7. Visual observation of samples from jar tests after slow mixing. Image width is 10 mm. Clockwise from top left: carbon only in DDI at pH 7, carbon in 10 mM NaCl at pH 7, carbon in ferric chloride and DDI at pH 7, carbon in ferric chloride, 10 mM NaCl and DDI at pH 7.	59
3.8. Growth in cake resistance associated with carbon fed to the membrane at pH 7 under no ionic strength, 10 mM NaCl, and 0.5 mM CaCl ₂ + 8 mM NaCl.	61
3.9. Growth in cake resistance associated with carbon fed to the membrane using ferric chloride at pH 6 and pH 7, alum at pH 7, and PACl at pH 7.	61
3.10. Growth in cake resistance associated with carbon fed to the membrane with NaCl using ferric chloride at pH 7 and PACl at pH 6 and pH 7.	62
3.11. Growth in cake resistance associated with carbon fed to the membrane with NaCl and Ca ²⁺ using ferric chloride at pH 7.	62
3.12. Growth in cake resistance from supernatant of ferric chloride and alum coagulation at pH 7 after settling for 20 minutes. Equivalent carbon dosed refers to the carbon used to treat the volume filtered, but not necessarily the carbon mass filtered.	64
3.13. Turbidity was not a good predictor of filtration performance. Tests with settling had low turbidity, as expected, but tests without settling performed even better.	64
3.14. Replicates of filtration performance for four filtration scenarios: carbon in 10 mM NaCl, carbon in 0.5 mM CaCl ₂ and 8 mM NaCl, carbon with 37 μM ferric chloride in 10 mM NaCl, and carbon in 37 μM aluminum via PACl.	65
3.15. Atrazine concentrations in the permeate from 15 ppb atrazine in DDI filtered through carbon cakes formed from aggregated carbon. All trials with ferric chloride resulted in	

List of Figures (Continued)

Figure	Page
breakthrough, whereas trials without ferric chloride did not see breakthrough.....	66
3.16. Growth in cake resistance associated with carbon aggregated with varied doses of ferric chloride. All trials include 60 mg/L of alkalinity as CaCO ₃ and 10 mM ionic strength as NaCl.....	68
3.17. Atrazine removal is not heavily impacted by ferric dose, noted by data label, until very high doses. Moderate doses removed over 90% of atrazine, while no dose resulted in 100% atrazine removal.	68
3.18. Addition of ferric chloride to direct filtration schemes containing NOM do not result in improved filtration performance.	69
3.19. Atrazine is removed well by carbon alone and even carbon with NOM, however, the addition of ferric chloride negatively impacts atrazine removal.	70
4.1. Particle size of milled carbons with milling times varied from one pass through the mill to 6.3 hours. Data is split into two panes to avoid excessive overlap.....	79
4.2. Scanning electron microscopy images (10K magnification) of all forms of BC1, including PAC (A) and all S-PACs. Particles visibly decrease in size as milling increases from 1 pass (B) to 15 min (C), 30 min (D), 1 hr (E), 2 hrs (F), and 6 hrs (G).	80
4.3. Scanning electron microscopy images (20K magnification) of BC1 after milling for 1 hr (A), 2 hrs (B), and 6 hrs (C). Particle size differences are apparent.	81
4.4. Concentration of particles increases as particle size decreases. Concentrations were calculated from measured average particle sizes and conservation of mass.....	82

List of Figures (Continued)

Figure	Page
4.5. Ash content of PAC and S-PAC with the longest milling time for each carbon. Milling times are denoted by color. No trends are seen in changes between PAC and S-PAC.	84
4.6. Decreases in pH_{pzc} correlated strongly with increases in weight percent of oxygen while pH_{IEP} measurements did not correlate with oxygen. Linear regression of pH_{PZC} data found R^2 values of 0.83, 0.93, 0.98, 0.95, and 0.90 for BC1, BC2, BC3, WD, and CS, respectively. Linear regression of pH_{IEP} data found R^2 values of 0.00, 0.49, 0.07, and 0.50 for BC1, BC2, WD, and CS, respectively.	86
4.7. The difference between pH measured using the pH_{PZC} method and the electrokinetic measurement of the isoelectric point is correlated with the S-PAC	88
4.8. Oxygen increased with newly revealed surface area as a result of milling. External surface area was calculated from Z-avg particle size measurements.	88
4.9. Illustration of PAC pulverization into S-PAC with proposed rapid surface oxidation.	89
4.10. Oxygen increases correlated with the content of select metals in the carbons, averaged between PAC and the longest milled S-PAC. Linear regression was performed without the outlier LC2 for divalent elements, and without the outliers LC1 and LC2 for total ash.	90
5.1. Normalized concentration in the liquid phase from batch adsorption kinetics experiments. 2.5 mg/L of carbon and 15 ppb of atrazine was used in each experiment.	99
5.2. Permeate concentration as a function of the volume filtered. Minimum adsorption occurred through the membrane, as seen by the No Carbon data. Breakthrough occurred immediately and consistently through the PAC layer, while S-PACs provided higher removals. Breakthrough is seen partway through in 1-pass carbon and at the end for 2-hours carbon.	101

List of Figures (Continued)

Figure	Page
5.3. Permeate concentration as a function of time. A log y-axis is used to show S-PAC data more clearly. The flux through the 6-hours carbon cake was significantly lower than the other cakes and the filtration took more than twice as long.	102
5.4. Flux values measured experimentally compared with predicted flux values. PAC and 1-pass S-PAC are predicted independent of other parameters, while all other carbon fluxes are predicted from their specific external surface area.....	103
5.5. Percent of atrazine removed as measured experimentally and predicted from the specific external surface area and oxygen content of each carbon.	104
5.6. Literature data fit with the developed HSDM model (Badruzzaman et al., 2004). Error minimized surface diffusion coefficients are similar to reported fitted values.	107
5.7. PAC modeled with HSDM using the measured Freundlich parameters and parameters chosen to best fit the experimental data.....	110
5.8. 1 pass S-PAC modeled with HSDM using the measured Freundlich parameters and parameters chosen to best fit the experimental data.....	110
5.9. 15 min S-PAC modeled with HSDM using the measured Freundlich parameters and parameters chosen to best fit the experimental data.....	111
5.10. 30 min S-PAC modeled with HSDM using the measured Freundlich parameters and parameters chosen to best fit the experimental data.....	111
5.11. 1 hr S-PAC modeled with HSDM using the measured Freundlich parameters and parameters chosen to best fit the experimental data.....	112

List of Figures (Continued)

Figure	Page
5.12. 2 hrs S-PAC modeled with HSDM using the measured Freundlich parameters and parameters chosen to best fit the experimental data.....	112
5.13. 6 hrs S-PAC modeled with HSDM using the measured Freundlich parameters and parameters chosen to best fit the experimental data.....	113
5.14. Scanning electron microscopy (SEM) image of 4 mg of WC800 6 hour milled carbon on a 21 mm diameter microfiltration membrane.	116
5.15. Representation of a slice of a column section of a packed bed reactor created in COMSOL Multiphysics 5.2. The column is 3 μm in height with a radius of 3 μm . The membrane layer is modeled with a 0.1 μm thickness.....	117
5.16. Pressure drop over 10 μm carbon columns on a membrane support. Columns with larger particle sizes see less pressure drop over the cake than those with smaller particle sizes.....	124
5.17. Permeate concentration of models with all S-PAC sizes using parameters for best fit of 1-pass S-PAC data. $D_s = 5 \times 10^{-10}$ cm^2/min , $K_{fl} = 0.1$ cm/s , $K_F = 8$ mol/kg , $1/n = 0.1$, and $k_{ads} = 50$. Parameters that result in good fits to 1-pass data (628 nm) do not result in good fits for other S-PAC data.....	125
5.18. Concentration over the height of the simulated 628 nm carbon cake at various time points in the simulation.....	126
5.19. Permeate concentration of best fit models for S-PAC sizes except 1 pass. All models used the same isotherm parameters. 15 min (432 nm) data and 30 min (398 nm) data were modeled with $D_s = 1.5 \times 10^{-6}$ cm^2/min , while 1 hr, 2 hrs (330 nm) and 6 hrs (230 nm) data were modeled with $D_s = 5 \times 10^{-7}$ cm^2/min	127

List of Figures (Continued)

Figure	Page
5.20. Concentrations within a pellet situated at $z = 2 \mu\text{m}$. Left: Concentration of liquid-phase species. Right: Concentration of solid-phase species.....	128
5.21. HSDM and CFD model parameters correlated to the overall atrazine removal through carbon coatings. The dashed line is provided for a 1:1 reference.	131
A.1. Excel input file, HSDMin.xlsx, modified from To.....	140

CHAPTER ONE

PROSPECTUS

Introduction

New problems facing drinking water treatment plants include the deterioration of source water quality due to increased presence of synthetic organic compounds (SOCs) (Barnes et al., 2008). SOCs such as pharmaceutical and personal care products (PPCPs) and pesticides are introduced to drinking water sources via domestic wastewater effluent and stormwater runoff. SOCs pose difficulties since they are not removed by conventional wastewater treatment unit processes and concentrations may be compounded by de facto water reuse (Stackelberg et al., 2004). De facto wastewater reuse—the intake of treated wastewater at drinking water treatment plants—has increased in recent years; estimates of peak reuse during seasonal low flow periods are as high as 100% in some plants (Rice et al., 2013). The importance of removing trace contaminants will only continue to grow as planned direct and indirect potable reuse projects gain popularity (Leverenz et al., 2011).

Activated carbon is an established material for the adsorption and removal of unwanted compounds and is added to treatment trains to target soluble constituents (Osantowski and Wullschleger, 1986; Clark and Lykins, 1990; Crittenden et al., 2005). The graphitic surface properties of activated carbon combined with high surface area after activation make it an ideal adsorbent for water treatment (Boehm, 2002). Activated carbon removes many types of soluble components, including dissolved natural organic matter (NOM) and compounds contributing taste and odor such as geosmin and 2-methylisoborneol (2-MIB).

Originally, granular activated carbon (GAC) was used as column filtration media. Further development of activated carbon technology resulted in the production of powdered activated carbon (PAC) from GAC, which allowed activated carbon to be added directly to the flow stream (Snoeyink and Chen, 1985). A recent development in activated carbon technology is to further reduce the size of PAC to very small sizes, termed superfine powdered activated carbon (S-PAC) (Matsui et al., 2004). To date, S-PAC production and testing has been limited to academic researchers and academically affiliated municipal pilot studies. S-PAC has shown improved kinetics over PAC for the adsorption of small-molecule contaminants, and similar kinetics but higher adsorption capacities on a mass basis for larger molecules such as natural organic matter (NOM) (Matsui et al., 2006, 2012; Ellerie et al., 2013). The mechanism for faster adsorption lies in shortened diffusion-limited adsorption pathways, which allow faster access to adsorption sites for small molecules (Matsui et al., 2009a).

Improved kinetics for circumvention of competitive adsorption is the primary motivation for pursuing S-PAC. Competition with NOM results in limited available adsorption capacity for SOCs and low contaminant concentrations mean there is a limited driving force for adsorption. As a result, when PAC is applied for the removal of trace contaminants, higher doses are required than for the adsorption of large and prevalent molecules such as NOM. S-PAC technology is a potential solution for anticipated regulations regarding emerging contaminants and may have applications in direct potable water reuse (DPR) in addition to conventional drinking water treatment. In DPR, wastewater undergoes advanced treatment to create potable drinking water. Any

anthropogenic compounds that are not removed in treatment will be consumed and disposed in wastewater, which is again treated by DPR to create drinking water, thus creating a closed loop resulting in magnification of contaminant concentrations.

However, the question remains as to how to strategically apply S-PAC. Due to the nearly colloidal nature of S-PAC particles, it is not possible to use sedimentation or media filtration for removal, as would be employed in PAC applications. One solution is to use membranes for separations. Membranes with nominal pore size smaller than S-PAC particles will reject S-PAC via size exclusion, though at the cost of reduced membrane flux. While the membrane can simply be used to catch S-PAC that is dosed ahead of the membrane, previous studies have shown the potential for S-PAC deposited as a coating onto the membrane surface to be highly effective for contaminant removal (Heijman et al., 2009a; Ellerie et al., 2013).

The following set of studies included both membrane application scenarios, beginning with membrane removal of dosed S-PAC under drinking water treatment scenarios. Next, in-house production of S-PAC was conducted to determine the effects of particle size with regards to membrane application and to determine the physical and chemical properties of S-PAC, which was motivated by limited literature reporting multiple material properties. Lastly, a modeling effort sought to understand the mechanisms by which S-PAC coatings on microfiltration membranes are able to remove contaminants despite an extremely limited contact time.

Research Objectives

The focus of this research is on the performance of S-PAC in combination with membranes with regards to variation in S-PAC material parameters and application conditions. This work does not set out to show the difference in adsorption performance between S-PAC and PAC, which has been established in the literature. There were three primary objectives that encompass an understanding of fundamental mechanisms as well as decision outcomes for potential application. The first objective examined how aggregated S-PAC interacts with membrane filtration. The second objective pursued understanding of S-PAC behavior through material analysis of S-PAC produced under known and controlled conditions. The third objective considered S-PAC behavior through the lens of analytical and computational models.

Objective 1: Aggregation of S-PAC

Objective 1 addressed S-PAC applied under coagulation and flocculation conditions and removed via dead-end microfiltration. Preliminary experiments regarding dead-end filtration of PAC and S-PAC found a correlation between flux decline and particle size. The hypothesis of this objective was if S-PAC aggregated with chemical coagulants results in higher membrane fluxes than non-aggregated S-PAC, then increased effective particle size via conventional water treatment processes improves filtration performance. S-PAC aggregation was tested with conventional chemical coagulants for

water treatment. The resulting flocs were observed visually, measured for turbidity, filtered by dead-end microfiltration, and tested for atrazine removal through the carbon cake.

Objective 2: Characterization of S-PAC

The second objective examined variables introduced through the production of S-PAC with broad material characterization covering both physical and chemical properties. Previous studies have reported limited data regarding S-PAC and its parent PAC, as well as limited reporting of milling conditions. The hypothesis was that if PAC milled for various durations produces S-PACs with characteristics that vary as a function of milling time, then milling causes deterministic material changes. Several commercial carbons of varied original materials were milled in-house to produce multiple S-PACs each, which were measured for particle size, specific surface area, point of zero charge, isoelectric point, chemical composition including oxygen, and ash content.

Objective 3: Transport Modeling

Objective 3 was motivated by experimental and modeling work performed by Jaclyn Ellerie (Ellerie, 2012; Ellerie et al., 2013). Ellerie used the homogeneous surface diffusion model (HSDM), which is used to model both GAC and PAC column reactors, to fit adsorption data from membrane coatings and found the model to be insufficient to predict adsorption results. In this work, a larger data set of membrane coatings and batch adsorption kinetics was available using the S-PACs produced in the second objective (Amaral et al., 2016). HSDM was used to model batch kinetics data while computational fluid dynamics (CFD) using multiphysics solutions was used to model adsorption through

a carbon coating. The hypothesis was that if both data sets are modeled well with the same set of fitting parameters, then the parameters will indicate the mechanism of S-PAC adsorption as it differs from PAC adsorption.

CHAPTER TWO

BACKGROUND

Persistent Organic Pollutants

Certain organic compounds resist degradation under natural environmental conditions, therefore considered persistent organic pollutants (POPs), and may pose risks to human and environmental health. Contaminants that have been identified as potential hazards but their effects have not been well established may be considered contaminants of emerging concern (CECs). Naturally occurring compounds can usually be broken down within the environment; therefore, most POPs have anthropogenic origin. Categories of CECs include antibiotics, hormones, and other pharmaceuticals as well as industrial and household chemicals such as plasticizers, surfactants, fire retardants, and pesticides (Bhandari et al., 2009).

Health concerns have come to light for these compounds for two reasons; first, improvements in chemical detection have allowed for environmental surveys to reveal the presence of many anthropogenic compounds in natural waters, and second, increased water scarcity leads to more human exposure to these compounds (Bhandari et al., 2009). Since detection of and subsequent concern over these compounds are relatively recent, long term health effects have not yet been determined. Additionally, while detection is now possible at the parts per trillion level, the procedures required for detection—namely spectrometry methods in conjunction with solid phase extraction—are both lengthy and cumbersome.

Organic Pollutant Removal

Many contaminants of consumer origin first pass through municipal wastewater treatment before discharge to the environment. Other contaminants, such as agriculturally applied pesticides, typically do not pass through municipal treatment and enter environmental water bodies through surface runoff (Luo et al., 2014). In municipal treatment, contaminants may be removed via sorption or partitioning into primary sludge solids, especially lipophilic portions. Biodegradation of contaminants via wastewater secondary activated sludge is a function of sludge age and varies for each contaminant; conventional secondary sludge treatment fully degraded the compounds ibuprofen, caffeine, naproxen, and triclosan, while much longer sludge ages were required to degrade compounds such as the insecticide lindane (Nyholm et al., 1992; Thomas and Foster, 2005). Lastly, oxidation processes used for wastewater disinfection, including free chlorine, chloramine, and ozone, can degrade some SOCs, with ozone being the most effective at doses currently used for wastewater disinfection (Huber et al., 2005a, 2005b). While municipal wastewater treatment is somewhat effective at contaminant removal, the remaining concentrations of those compounds resistant to removal may still pose human health threats when present in drinking water sources.

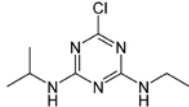
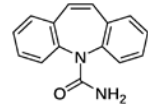
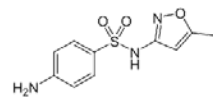
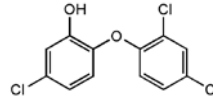
In municipal drinking water treatment, the treatment unit processes with the ability to remove contaminants are activated carbon adsorption and advanced oxidation (Bhandari et al., 2009). Reverse osmosis is also useful for removing soluble compounds but is only present in a limited number of drinking water treatment plants. It is theoretically possible to have contaminant sorption to precipitates during chemical coagulation; however,

removals were found to be limited (Adams et al., 2002; Westerhoff et al., 2005). Additionally, while activated carbon adsorption was found to be effective, ion exchange adsorption was not effective at removing organic contaminants (Adams et al., 2002). The caveat to activated carbon usage is the potentially high carbon dose required to significantly reduce contaminant concentrations (Adams, 2009). One study used carbon doses of 5–50 mg/L and a contact time of 4 hours to test removals of several antibiotics (Adams et al., 2002). They found a mean removal of 50% using 5 mg/L of carbon, 80% removal using 10 mg/L of carbon, 90% removal using 20 mg/L of carbon, and 100% removal using 50 mg/L of carbon. Another study used a carbon dose of 5 mg/L and a contact time of 4 hours to find 98% removal of triclosan, 80% removal of carbamazepine, and 16% removal of sulfamethoxazole, among other compounds (Westerhoff et al., 2005).

Properties of Organic Pollutants

The response of contaminants to various removal techniques is a function of the contaminant properties. Several small-size organic molecules are shown with their attributes (Table 2.1); the acid dissociation coefficient pK_a , which affects ionization, the octanol-water coefficient $\log K_{ow}$, which describes water solubility, and molecule planarity are factors that may affect adsorption. Structure activity relationships (SAR) can be used to predict the activity characteristics from molecular composition alone through analysis of structurally similar and more thoroughly investigated compounds (Allen and Shonnard, 2001). In natural environments, compounds leave the water phase through several methods, including volatilization, sorption, and biodegradation/biotransformation, that can be predicted by SAR for compounds without experimental data (Gurr and Reinhard, 2006).

Table 2.1. Properties of selected synthetic organic chemicals of environmental concern.

Name (classification)	MW [g/mol]	pKa	Log K_{ow}	Structure
Atrazine (pesticide)	215.6	1.6	2.61	
Carbamazepine (pharmaceutical)	236.7	< 2	2.45	
Sulfamethoxazole (pharmaceutical)	285.5	5.7	0.89	
Triclosan (personal care product)	289.6	7.9	4.76	

Volatilization is the partitioning of a compound into the gaseous phase, which is described by the Henry's Law coefficient, K_H . A relationship between structure and activity has been derived to determine K_H from molecular bonds, where n_i is the number of bond contributions of type h_i , and n_j is the number of groups with corrections of type c_j given in a reference table (Equation 2.1) (Allen and Shonnard, 2001).

$$-\log K_H = \sum n_i h_i + \sum n_j c_j \quad \text{Eq. 2.1}$$

Sorption in the water column is primarily to soils and other organic content, and the rate of partitioning into that phase is described by the organic carbon-water partition coefficient, K_{oc} . Since this is a highly important parameter for understanding contaminant fate and transport, data exist for K_{oc} values for many organic contaminants, but it is still valuable to predict K_{oc} for new compounds. K_{oc} can be predicted by a term called molecular connectivity, 1x , which is a function of molecular structure, as well as functional groups, where n_j is the number of groups with corrections of value P_j (Equations 2.2 and 2.3) (Allen and Shonnard, 2001).

$$\log K_{oc} = 0.53 * {}^1x + 0.62 + \sum n_j P_j \quad \text{Eq. 2.2}$$

$${}^1x = \sum (\delta_i \cdot \delta_j)^{-\frac{1}{2}} \quad \text{Eq. 2.3}$$

Biodegradability, I , is not a specific molecular property, but SAR can predict whether a compound will persist for environmental lifetimes on the order of days, months, or years. Using a similar group contribution method to the above relationships, I is predicted by f_i number of groups with a_i value and the molecular weight modified by a_m (Equation 2.4) (Allen and Shonnard, 2001). The weighting values have been determined by linear correlation with estimates of biodegradation compiled from multiple datasets of biodegradability related factors such as the change over time in biological oxygen demand (BOD) (Raymond et al., 2001).

$$I = 3.199 + \sum a_i f_i + a_m(MW) \quad \text{Eq. 2.4}$$

Activated carbon adsorption itself is not predicted through such relationships, but there are a number of molecular properties that are contributing components. Some characteristic components can be predicted; molecular size is an understated outcome of SAR but is a key element in diffusion and adsorption within porous structures that can be as small as 2 nm in diameter. Molecule planarity is also a factor in addition to molecular weight since it describes the volume that molecules occupy and volume is limited within carbon pores (Zhang et al., 2010; Bakkaloglu, 2014). Solubility, S , and the octanol-water partition coefficient, K_{ow} , are both related to molecule hydrophobicity and are properties that can be predicted by SAR (Equations 2.5 and 2.6). Hydrophobicity affects partitioning into lipophilic phases and adsorption to hydrophobic surfaces such as the graphitic material of activated carbon (Wu and Pendleton, 2001; Zhang et al., 2011). Atrazine is a polar, planer molecule of relatively small molecular size and moderate solubility, while carbamazepine is a similarly sized molecule with similar solubility but is nonplanar; in a comparative study, activated carbon adsorption of atrazine was faster and had a higher equilibrium concentration than carbamazepine (Bakkaloglu, 2014). Organic contaminants, which include PPCPs, are typically polar compounds due to desired interactions with human systems. Smaller adsorption capacity has been attributed to compound solubility (Li et al., 2002).

$$\log S = 0.796 - 0.854(\log K_{ow}) - .00278(MW) + \sum h_j \quad \text{Eq. 2.5}$$

$$\log K_{ow} = 0.229 + \sum n_i f_i + \sum n_j f_j \quad \text{Eq. 2.6}$$

The acid dissociation constant, pK_a , is also an important component. Compounds with dissociation constants less than 7, often described as acidic compounds, do not exist in their ionized form in natural waters that tend to have a pH of 7–8, thus they are primarily sorbed via physical processes such as hydrogen bonding and van der Waals attraction instead of strong chemical sorption or charge-based electrostatic sorption (Weber JR et al., 1991; Delle Site, 2001). While there is no SAR for determining pK_a , fortunately, the measurement is fairly simple.

In addition to contaminant properties, activated carbon also plays a role as a confounding factor in sorbate-sorbent interactions since its surface functional groups contribute to charge and hydrophobicity, and surface interactions can change as a function of the pH and ionic strength of the bulk fluid. As an example of sorbent-sorbate interactions affected by sorbent properties, pi-bond interactions can be disrupted by chemisorbed oxygen on the sorbate surface and thus weaken adsorption of molecules such as phenolic compounds that sorb via those interactions (Dabrowski et al., 2005).

Activated Carbon

Activated carbon is a commonly used technology for the adsorption of unwanted compounds in drinking water treatment (Osantowski and Wullschleger, 1986). Of surface water treatment plants in the U.S. employing activated carbon, the majority use it for

seasonal treatment of taste and odor compounds, though some use it for control of natural organic matter (NOM) or synthetic organic contaminants (SOCs) (Crittenden et al., 2005). The choices available for activated carbon include variations in size, whether the carbon is granular (GAC), powdered (PAC), or extruded, and variations in the carbon source material, which can result in different physical and chemical material properties (Clark and Lykins, 1990).

Material Production

Activated carbon is produced from the carbonization and activation of high carbon content precursor materials containing low inorganic matter including coal, wood, coconut shells, walnut shells, and peat (Clark and Lykins, 1990; Dabrowski et al., 2005). During carbonization, water and organic compounds are volatilized thermally using temperatures of 300–500°C. Activated carbons share similar structure despite differences in precursors because the activation process shifts the structure of carbon molecules into that of graphitic plates (Shimodaira and Masui, 2002).

Activation refers to the removal of any remaining organic matter, including organic carbon, to reveal a porous internal structure with high capacity for adsorption, and can be performed either thermally or chemically. Carbons with 400 to 2000 meters squared of surface area per gram of carbon (m^2/g) are considered useful as an adsorbent (Neely and Isacoff, 1982). Thermal activation requires heating materials to temperatures of 700–900°C in the presence of water, oxygen, and carbon-dioxide (Neely and Isacoff, 1982). Chemical preparation of activated carbon does not require a carbonization step prior to activation; activation is initiated by impregnating uncarbonized material with chemical compounds,

such as phosphoric acid, before heating to carbonization temperatures (McDougall, 1991). Activated carbon particle size depends on the precursors—small precursors, such as sawdust, lead to powdered forms—though PAC can also be formed by crushing GAC. Some activated carbon is produced through extrusion to produce an activated carbon of highly uniform size (McDougall, 1991).

Resistance to abrasion is often a factor considered during selection of GAC due to the need to reduce carbon losses during backwashing and regeneration (Abram, 1973). Abrasion resistance is evaluated by measuring particle degradation. While material hardness and degradation due to impact are directly correlated for solid materials, for porous and brittle materials such as activated carbon, impacts can remove fractions of particles more easily than would be predicted by hardness. The ball pan method is the American Society for Testing and Materials (ASTM) standard for testing hardness in GAC and consists of abrading carbon against steel balls (ASTM Standard D3802-10, 2010). Studies of PAC hardness have used variations of this method, including an abbreviated ball pan method and stirring/self-abrasion methods (Toles et al., 2000; Yalcin and Arol, 2002).

Carbon losses are not a concern for PAC, since they are not regenerated, but PAC hardness can be a concern if applied in conjunction with polymeric membranes that can be abraded by PACs (Glucina et al., 1997; Stoquart et al., 2012). In contrast, ceramic membrane materials are harder than activated carbon and would not encounter such difficulty. A direct measurement of material hardness can be performed with the Mohs hardness test, which involves scratching the test material against standard materials and assigning a hardness rating of 1–10 based on visual assessment of indentation on the

standard material. Activated carbon is relatively soft with a Mohs hardness between 2 and 3, even for carbons of differing source material (Patni et al., 2008). Thus, variation in carbon hardness is not significant enough to register on the Mohs hardness scale. In most cases, the hardness of the carbon precursor translates into a harder carbon, such that hardness decreases from coconut shell to anthracite coal, bituminous coal, lignite coal, and wood (Greenbank and Spotts, 1993). However, some wood carbons have been produced with abrasion resistance comparable to coconut shell-based carbons (Hernández et al., 2014).

Physical Adsorption Parameters

The primary benefit of activated carbon as an adsorbent is its high internal surface area; however, two carbons with the same specific surface area may still perform differently because of other properties, such as pore size distribution and surface functional groups (Karanfil and Kilduff, 1999; Karanfil et al., 1999; Li et al., 2002; Quinlivan et al., 2005). Physically, adsorption to activated carbon can be determined by the size of pore channels, which are typically categorized into macropores as those larger than 50 nm, mesopores as between 2 and 50 nm, and micropores as smaller than 2 nm (Smíšek and Černý, 1970). Additionally, consideration of primary micropores—those smaller than 1 nm—can be useful since molecules have high adsorption strength in this range and even the smallest NOM molecules are too large for these pore widths (Pelekani and Snoeyink, 2000). Pores from 1–2 nm are termed submicropores. Small pore widths are able to be measured experimentally via nitrogen adsorption under controlled pressure since diatomic nitrogen has a diameter of approximately 0.3 nm and is able to penetrate the smallest pores.

Pore sizes are stronger determining factors for carbon performance than total surface area, which can lead to more capacity only if the pore sizes are appropriate for the target molecules. For example, large molecules cannot access smaller pores, thus capacity in the form of micropores goes unused. Also, pore widths similar in size to molecular diameters increases the adsorption strength since the molecule will be bound by adsorption site potentials from both sides of a pore (Martin, 1980; Li et al., 2002). Depending on the target molecule to be removed, variations in these characteristics can be advantageous to optimization of adsorption capacity or kinetics.

Lastly, the diameter of the carbon particle affects the rate of adsorption since longer paths result in a longer time to equilibrium due to diffusion-limited pore transport (Pelekani and Snoeyink, 1999). Size has been shown to be an important factor in the adsorption kinetics of activated carbon, especially within the size range of PAC particles (Najm et al., 1990; Matsui et al., 2004). Size will be explored further in the next section on reduced size PAC.

Chemical Adsorption Parameters

Chemically, surface functional groups and their acid-base properties play a major role in the type of molecules that are preferentially adsorbed. Surface groups, which determine the adsorption affinity of the carbon, bond at the edges of the graphitic carbon plates (Boehm, 1994). Oxygen is chemisorbed most readily to activated carbon, and once on the surface, reacts to form carbon-oxygen functional groups (Boehm, 2002; Dabrowski et al., 2005). Activated carbon typically has oxygen content around 3–4%; those modified to increase oxygen-containing functional groups can have contents up to 10% (Li et al.,

2002; Apul et al., 2013). Modification of surface functional groups, and therefore adsorption properties, is controlled by chemical processing post-activation and even post-regeneration (Akmil Başar et al., 2003; Dastgheib et al., 2004; Liu et al., 2009). Oxidation of carbon results in increased adsorption of metal cations but decreased adsorption of phenolic compounds (Tessmer et al., 1997; Biniak et al., 1999; Jia and Thomas, 2000). While oxygen-containing functional groups can be acidic, neutral, or basic, most oxygen-containing groups found on activated carbon are acids since these are more prevalent on carbons exposed to oxygen at temperatures below 200°C (Dabrowski et al., 2005). Conversely, most base groups found on activated carbon are nitrogen-containing groups (Studebaker, 1957; Biniak et al., 1999).

By default, carbon is a hydrophobic material, which is beneficial towards the adsorption of non-polar molecules, such as aromatics (Zhang et al., 2011). Surface functionalization results in hydrophilicity and the formation of a water layer at the particle surface that increases resistance for the transfer of molecules to the surface (Müller and Gubbins, 1998; Li et al., 2002). While surface hydrophilicity increases adsorption affinity for polar compounds, the increased surface resistance negates the potential performance increase. A computational study found that even mild surface oxygenation resulted in heavy water adsorption (Müller and Gubbins, 1998). The sum of oxygen nitrogen content can be used as a surrogate measurement for sorbent polarity so carbons can be selected for low oxygen and nitrogen content to maintain sufficient hydrophobicity for carbon performance (Li et al., 2002).

Surface charge also affects adsorption; it is related to the surface functionalization but also a consequence of the bulk solution pH. A useful measurement is the point of zero charge, which determines the solution pH where the carbon is neutrally charged (Žalac and Kallay, 1992; Boehm, 2002). Above the point of zero charge, the particle will be negatively charged, and below it, the particle will be positively charged. The state of adsorbate ionization and subsequent dependency on a charged surface for adsorption are affected by solution pH as well so adsorption is an outcome of the adsorbate-adsorbent-solution system (Dabrowski et al., 2005). A detailed background on theories relating to surface charge, analytical measurement techniques, and particle stability are presented in the section on Colloidal Stability.

Equilibrium Models

The material adsorption capacity is a function of the bulk concentration. Isotherm models, called so because they are valid under constant temperature, describe capacity and are determined by measuring the equilibrium concentration resulting from several adsorbate to adsorbent ratios. The most common isotherm models for carbon adsorbents are the Langmuir model and the Freundlich model while other models include the Redlich-Petersen model and Tóth model (Chern and Chien, 2001).

The material adsorption capacity, q , is a function of the bulk concentration, C . The Langmuir model is theoretically derived and based on an adsorbed monolayer; the model fits q with the parameter q_{max} , which describes the maximum mass of adsorbed compound for the material, and the coefficient K_L (Equation 2.7). The Freundlich model is empirically

derived and gives the adsorption capacity, q , with the coefficient K_F and the exponent $1/n$ (Equation 2.8).

$$q = q_{max} \frac{K_L C}{1 + K_L C} \quad \text{Eq. 2.7}$$

$$q = K_F C^{\frac{1}{n}} \quad \text{Eq. 2.8}$$

The use of either Langmuir or Freundlich isotherms depends on which model is a better fit of the experimental isotherm data. Activated carbon is generally well described by the Freundlich isotherm, which is linearized by taking the natural log of both sides.

Reaction Models

Pseudo first-order and pseudo second-order models fit well to activated carbon adsorption data. The most popular first order form is the Lagergren equation (Equation 2.9) which uses the concentration at equilibrium, or in other words the adsorption capacity (Lagergren, 1898; Ho and McKay, 1999; Ho, 2004). Azizian (2004) developed a theoretical model of adsorption based on the adsorption capacity that produced a pseudo second-order model (Equation 2.10). Under certain conditions—when the initial adsorbate concentration is sufficiently higher than the adsorption capacity—the model reduced to the well-known Lagergren equation (Azizian, 2004). The pseudo second-order model applied when the initial concentration was not sufficiently large and the model must account for a changing driving force.

$$\ln\left(\frac{q_e - q}{q_e}\right) = -k_1 t \quad \text{Eq. 2.9}$$

$$\frac{t}{q} = \frac{1}{k_2 q_e^2} + \frac{1}{q_e} t \quad \text{Eq. 2.10}$$

Economic Considerations

Activated carbon is the most popular carbon-based adsorbant, but others also exist. Graphene and single- and multi-walled carbon nanotubes have been explored as adsorbants for water treatment applications (Ellerie et al., 2013; Apul and Karanfil, 2015). Single-walled nanotubes (SWCNT) have good adsorption properties but are more expensive to produce than multi-walled nanotubes (MWCNT) (Zhang et al., 2009). Graphene has high theoretical adsorption capacity due to high pore volume; however, its performance is comparable to PAC (Apul et al., 2013). Lastly, activated carbon can also be built from smaller molecule precursors, such as the carbonization of cellulose to produce activated carbon fibers (ACFs) (Li et al., 2002). The main benefits of these materials stem from homogeneity, whereas activated carbon is highly heterogenous due to natural material precursors. However, activated carbon is both cheap and reliable and thus is currently the most widely used adsorbent.

The economic trade-off between PAC and GAC depends on the carbon usage rate, which for PAC depends on dose and duration of application. PAC provides the benefit of flexibility since application does not require additional infrastructure, allowing for dosing only when additional removal of compounds is necessary. On the other hand, GAC contactors, which are deep bed filters, serve as both adsorptive media and filter media.

Also, since GAC is easier to handle than PAC, it can be transferred to a facility for thermal regeneration when capacity is exhausted, whereas PAC is removed via sedimentation and disposed along with settled sludge. In the next section, a new category of activated carbon is introduced that consists of particles much smaller than PAC. An economic picture of S-PAC is not complete since the material is still in the development. S-PAC removal is likely costlier than PAC removal, but a benefit could come from a reduced carbon usage rate due to faster adsorption.

Superfine Carbon

PAC with reduced sizes had been observed to have faster rates of adsorption than larger PAC sizes (Adham et al., 1991; Matsui et al., 2003). Much faster kinetics were then observed by PAC reduced to extremely small sizes. The first publication documenting superfine PAC was published in 2004 describing micro-ground powdered activated carbon, with following publications using the descriptor submicron-sized powdered activated carbon (Matsui et al., 2004, 2006, 2008; Heijman et al., 2009a). Since then, PAC with sizes slightly above one micron have been found to have the same property improvements over conventionally-sized PAC and the term submicron was dropped in favor of superfine.

S-PAC Adsorption Mechanisms

Matsui and colleagues speculated on the rapid adsorption mechanism of S-PAC in their earliest publication, where they observed faster adsorption of NOM and an increase in adsorption capacity for NOM and polystyrene sulfonate (PSS), though not for phenol (Matsui et al., 2004). Subsequent publications confirmed these results, particularly

increased adsorption capacity for the large molecules NOM and PSS, but not the small molecules geosmin and 2-methylisoborneol (2-MIB) (Matsui et al., 2005, 2009a; Ando et al., 2010). S-PAC was able to remove the taste and odor compounds geosmin and 2-MIB faster than PAC, especially in the presence of NOM (Matsui et al., 2009a, 2013). Additional observations include the rapid removal of free chlorine, dichloramine, and nitrogen trichloride (Matsui et al., 2008).

Small molecules are able to adsorb faster to smaller particles because transport within pores, which is a diffusion-limited process, has been shortened. (Pelekani and Snoeyink, 2000; Matsui et al., 2008; Ando et al., 2010; Ellerie et al., 2013). Molecules can adsorb and desorb along this pathway in a process termed surface diffusion, until they reach terminal adsorption sites within the narrowest pores where the overlap of adsorption potentials creates a strong adsorption bond (Li et al., 2002). Large molecules have unchanged adsorption kinetics with decreased particle size since these molecules only adsorb to external surfaces and large diameter macropores. Due to the difference in adsorption rates, under short contact times, the ratio of low to high molecular weight compounds adsorbed on a particle is higher for a smaller particle.

Since S-PAC has more surface area per mass than PAC, large molecules can exhibit higher adsorption capacities on S-PAC. Small molecules, which utilize more of the internal adsorption surface, do not exhibit these increases since the density of internal pathways does not change between PAC and S-PAC. Instances where small molecules have been observed to have increased adsorption capacity are attributed to the shell adsorption model (SAM); SAM postulates that only a certain penetration depth is reached in activated carbon

and when sizes are reduced, a larger percentage of the particle can be utilized (Matsui et al., 2011). SAM is discussed further in this chapter in the section on Adsorption Modeling.

S-PAC Production

S-PAC research has been limited to a small number of studies by a handful of researchers. A list of studies with S-PACs is found in Table 2.2; reporting of material parameters is limited with all publications reporting particle size, some reporting surface area and pore volume data, and few reporting the point of zero charge. A more detailed table of reported literature is published in chapter 4. Information regarding production parameters is also limited with researchers using only phrases such as wet grinding in a bead mill, pulverization in a ball mill, wet mill micro-grinding and micro-grinding in a wet bead mill to describe the production process, though all are wet milling techniques (Matsui et al., 2007; Heijman et al., 2009a; Ando et al., 2010; Ellerie et al., 2013).

Table 2.2. Summary of published literature regarding S-PAC. Size is reported in all studies but other properties are reported less frequently.

Carbon Name	Carbon Source Material	Particle Size (d-50, nm)	pH _{PZC}	Surface Area Data	Pore Volume Data	Publication
Calgon 6D	Coal	670	--	--	--	<i>Ando et al., 2010</i>
Calgon 6MD	Wood	660	--	--	--	<i>Ando et al., 2010</i>
Calgon F100-D	Coconut Shell	670	--	--	--	<i>Ando et al., 2010</i>
Calgon WPH	Coal	37000	6.1	x	x	<i>Ellerie et al., 2013</i>
	Coal	240	5.7	x	x	<i>Ellerie et al., 2013</i>
Norit SX Ultra	Peat	800	--	--	--	<i>Heijman et al., 2009</i>
Picahydro MP23	Wood	25000	--	x	x	<i>Matsui et al., 2014</i>
		680	--	--	--	<i>Ando et al., 2010</i>
		720	--	--	--	<i>Matsui et al., 2014</i>
		500	--	x	x	<i>Matsui et al., 2014</i>
Picahydro SP23	Coconut Shell	31000	--	x	x	<i>Matsui et al., 2014</i>
		650	--	--	--	<i>Ando et al., 2010</i>
		850	--	--	--	<i>Matsui et al., 2014</i>
		520	--	x	x	<i>Matsui et al., 2014</i>
Shirasagi	Wood	770	--	--	--	<i>Matsui et al., 2008</i>
Taikou-W	Wood	650	--	--	--	<i>Matsui et al., 2007</i>
		880	--	--	--	<i>Matsui et al., 2009</i>
		800	--	--	--	<i>Matsui et al., 2005</i>
		11800	--	x	--	<i>Matsui et al., 2013</i>
		725	--	x	x	<i>Ando et al., 2010;</i> <i>Matsui et al., 2013</i>
		13500	--	x	x	<i>Matsui et al., 2013;</i>
		857	--	x	--	<i>Matsui et al., 2013</i>
		19000	--	x	x	<i>Matsui et al., 2014</i>
		620	--	x	x	<i>Matsui et al., 2014</i>
Unknown	Coconut Shell	10000	9.6	x	x	<i>Dunn & Knappe, 2013</i>
		480	8.4	x	x	<i>Dunn & Knappe, 2013</i>
		430	7.8	x	x	<i>Dunn & Knappe, 2013</i>
Unknown	Lignite Coal	11000	10.7	x	x	<i>Dunn & Knappe, 2013</i>
		290	8.2	x	x	<i>Dunn & Knappe, 2013</i>
		180	8.5	x	x	<i>Dunn & Knappe, 2013</i>
Unknown	Wood	10000	10.7	x	x	<i>Dunn & Knappe, 2013</i>
		820	--	x	x	<i>Dunn & Knappe, 2013</i>
		210	7.9	x	x	<i>Dunn & Knappe, 2013</i>
Unknown	Wood	18000	4.9	x	x	<i>Dunn & Knappe, 2013</i>
		1200	5.9	x	x	<i>Dunn & Knappe, 2013</i>
		240	5.8	x	x	<i>Dunn & Knappe, 2013</i>
Unknown	Bituminous Coal	14000	6.2	x	x	<i>Dunn & Knappe, 2013</i>
		600	6.7	x	x	<i>Dunn & Knappe, 2013</i>
		540	6.3	x	X	<i>Dunn & Knappe, 2013</i>

Since S-PAC is not commercially available, consistency between batches of S-PAC is not expected. Additionally, details of the production process such as grinding media and contact time have rarely been reported. Differences in processing may in turn have impacts on adsorption characteristics. Particle size is the main driving force behind improved kinetics; however, changes in other physical and chemical properties can also impact adsorption performance. For example, it is possible for pulverization to shift the distribution of pore sizes by exposing smaller diameter pores, effectively resulting in larger diameter pores (Dunn and Knappe, 2013; Ellerie et al., 2013; Matsui et al., 2014)

Wet milling involves high velocity contact between grinding media and the product material—activated carbon in this case—that takes place in a solvent. While unstated in published literature, a reasonable assumption is that the solvent used was ultrapure water, due to the intended use of S-PAC for adsorption performance measurements. Grinding media can be made from a variety of materials, including steel and ceramics, and in a variety of sizes. Published studies have used generic descriptors such as “ball” and “bead” that likely refer to size ranges of the grinding media. The milling duration in combination with the loading of grinding media and the solids loading rate of the product all play into the milling outcome. Lastly, operation of the mill introduces a number of parameters, from mill rotational speed to recirculation rate and temperature.

Most recently, advances in technology have allowed for dry milling of particles to submicron sizes using steam as a carrying fluid. Compared to wet milling with water as a carrying fluid, steam based dry milling is faster and results in a compact product. One

study explored the use of dry milling and found the resulting particles to have diminished performance in comparison with wet milled particles (Pan et al., 2016). The dry milled particles were observed to aggregate more readily and even when disaggregated showed less adsorption capacity, potentially due to higher concentrations of oxygen on the particle surface introduced by the milling environment.

One example of S-PAC production for municipal use is the Kawai Water Purification Plant in Yokohama, Japan (Metawater Co Ltd, 2011). The plant is co-operated by the local municipality and Metawater Co, Ltd., a distributor of the ceramic membranes. An older conventional water treatment plant was replaced with two parallel lines of 0.1 μm pore size ceramic membranes for direct source water filtration. They have on-site capacity for S-PAC production and application for the removal of seasonal taste and odor compounds. The S-PAC is produced by one pass through a wet mill and stored as a slurry until needed. Pilot scale studies were used to determine the grinding parameters and it was found that one pass produced a mean size around 1 μm that was useful for both compound adsorption and application in conjunction with dead-end membrane filtration. The plant's first application of S-PAC occurred in August of 2016 during an algal bloom when the concentration of 2-MIB was elevated for 24 days. An S-PAC dose of 3 mg/L was used to bring concentrations from an influent as high as 9 ng/L to an effluent concentration below 2 ng/L.

Membrane Separations

Membranes are an extremely versatile technology for separation processes and are applicable to the removal of small particles that cannot be removed via sedimentation due

to the reduced settling rate of smaller particles. However, a consequence of particle rejection is the formation of a cake layer that causes additional flow resistance and a reduction in membrane flux. Microfiltration (MF) membranes, which would reject S-PAC particle sizes, are already common in many surface water plants.

MF units are often used as a polishing step after sedimentation to remove any remaining suspended solids. In the application method known as direct filtration where sedimentation is not used, all material is sent to the membrane. In this scenario, backwashing must be performed very often but the lack of a sedimentation basin greatly reduces the total plant footprint (Crittenden et al., 2012). The drawback is that even low-pressure membrane processes are more energy intensive than natural settling processes. An interesting outcome of combining activated carbon and microfiltration is that even coagulation and flocculation can be eliminated; an integrated PAC-MF system consisting of a PAC contactor followed by a microfiltration membrane removes soluble content via adsorption instead of coagulation and settling, and the membrane serves as both a treatment process and PAC separator (Thiruvengkatachari et al., 2004; Crittenden et al., 2012; Stoquart et al., 2012).

Filtration of Particles

S-PAC particles range from several hundred nanometers in diameter to near one micrometer and are rejected via size exclusion using membranes with nominal pore sizes smaller than the majority of particles (Matsui et al., 2006, 2007, 2009b; Hamad et al., 2008; Ellerie et al., 2013; Amaral et al., 2016). Membranes are used to remove S-PAC added to the bulk flow; Matsui et al. (2006, 2007, 2009) fed S-PAC ahead of a ceramic membrane

and successfully removed the rejected S-PAC via backwash with no loss of integrity. To date, only ceramic membranes have been tested for S-PAC direct filtration, that is, filtration without settling as pretreatment. In the section below on S-PAC membrane coatings, both ceramic and polymeric membranes have been used.

The build-up of particles on the membrane results in fouling and reduction in flux. Membrane flux, J , is dependent on the applied pressure, ΔP , the fluid viscosity, μ , and the resistance of the membrane plus any cake formed, $R_m + R_c$ (Equation 2.11). The total pressure drop over the cake layer and the membrane is the sum of the individual pressure drops. Fouling by individual solids is correlated to the size of the solids, with particles close to the membrane pore size resulting in the most fouling (Schäfer et al., 2000). Such observations were seen with S-PAC; particles with diameters near 200 nm caused marked flux decline on flat sheet membranes when compared to the particles with larger diameters (Amaral et al., 2016).

$$J = \frac{\Delta P}{\mu(R_m + R_c)} \quad \text{Eq. 2.11}$$

PAC has been examined in conjunction with membrane filtration for treatment of both drinking water and wastewater. Most cases have used a submerged membrane system with air sparging to keep PAC particles suspended (Kim et al., 2005; Stoquart et al., 2012; Vigneswaran et al., 2016). Direct filtration is a less common approach (Adham et al., 1991; Lee et al., 2007; Matsui et al., 2007). The large size of PAC particles combined with the

low pressure and air sparging within the membrane reactor minimize loss of flux due to PAC.

Two concerns associated with membrane filtration of particles is potential loss of membrane integrity due to abrasion and potential particle breakthrough. Abrasion is a concern from particles filtered onto on polymeric membrane fibers where fiber breakage can result in membrane failure; there is no concern for ceramic membranes since their material is harder than activated carbon (Stoquart et al., 2012). Particle breakthrough is an outcome of membrane failure, and particle detection can be used to monitor membrane integrity, but passage of fine particles through membranes is also a concern (Guo et al., 2009; Lipp et al., 2009; Ladner et al., 2012). Breakthrough of fines even without membrane failure is also a concern, particularly for S-PAC, where fines can be smaller than 100 nm. The effects of engineered nanoparticles on both human and environmental health are not yet fully understood, and introduction of nanoparticles in drinking water treatment is risky as municipal water has a direct route to consumers (Brar et al., 2009). While S-PAC sizes are not as small as nanoparticles, free particles may still result in adverse effects. However, membranes may be sufficient to retain particles, especially if fines adhere to polymeric fibers through adsorption. An idea that has been tested for the application of silver nanoparticles, which have known environmental toxicity effects, to drinking water filtration is to coat a foam with the particles, therefore, rendering the silver nanoparticles immobile (Jain and Pradeep, 2005). Such an approach can also be considered for S-PAC. In fact, a study found that S-PAC encapsulated in polystyrene and rendered immobile still had usable adsorption capacity (Apul et al., 2017).

Particle Configuration

Several layers of particles forming a cake on a membrane create a type of porous media or, in the case of activated carbon, a packed bed reactor. For nearly homogeneous particles, properties of the cake layer are predictable through the theory of random close pack (RCP). For spheres of uniform size in RCP, the maximum packing density is 64% (Scott and Kilgour, 1969).

Darcy's Law gives the flux through a porous medium of permeability, κ , and thickness, L (Equation 2.12). The equation for flow through porous media is very similar to the flow through a membrane. The membrane can be viewed as a porous media comprised of interwoven polymer threads while the particle cake layer is represented by an adjacent porous media of a different permeability. The interstitial velocity, u_i , is given by the bulk fluid velocity, u , divided by the void fraction, ε (Equation 2.13). Assuming RCP, the void fraction, ε , is 36% as the inverse of the packing efficiency. The permeability, k , of the packed media can be predicted from the particle size, d , via the Carman-Kozeny equation (Equation 2.14) (Waite et al., 1999; Rushton et al., 2008). The equation uses κ_z , the Kozeny constant, which depends on the geometry of the particles. For packed beds of identical spheres, κ_z is taken conventionally to be 5, which is the value reported by Carman; κ_z for packed beds has since been found to range in values near 5 (Carman, 1956; Heijs and Lowe, 1995; Xu and Yu, 2008).

$$J = \frac{-\kappa\Delta P}{\mu L} \quad \text{Eq. 2.12}$$

$$u_i = \frac{u}{\varepsilon} \quad \text{Eq. 2.13}$$

$$k = \frac{\varepsilon^3}{36\kappa_z(1 - \varepsilon)^2} d^2 \quad \text{Eq. 2.14}$$

Analytically, RCP is not easily interpreted as a geometric model since particles are not placed with certainty. Ordered packing schemes include hexagonal close pack (HCP) or face-centered cubic (FCC) packing. Both of these ordered packing configurations result in a packing density of 74%, which is higher than the packing efficiency of randomly ordered particles. While it is not expected that particles forming a cake layer or membrane coating will be packed in ordered forms, these schemes can be useful for analyzing localized phenomena (Suekane et al., 2003; Gunjal et al., 2005). Unlike RCP, ordered lattice structures can be generated via geometric relationships. An HCP lattice is constructed by stacking planes of spheres in a hexagonal arrangement where spheres in adjacent planes reside in the space between three touching spheres (Figure 2.1). If a centric sphere reside at (0, 0, 0) in Cartesian coordinates surrounded evenly by six spheres, then a

sphere in an adjacent plane and centered over the space between three touching spheres in the original plane will be at $\left(R, \frac{\sqrt{3}R}{3}, \frac{2\sqrt{6}R}{3}\right)$.

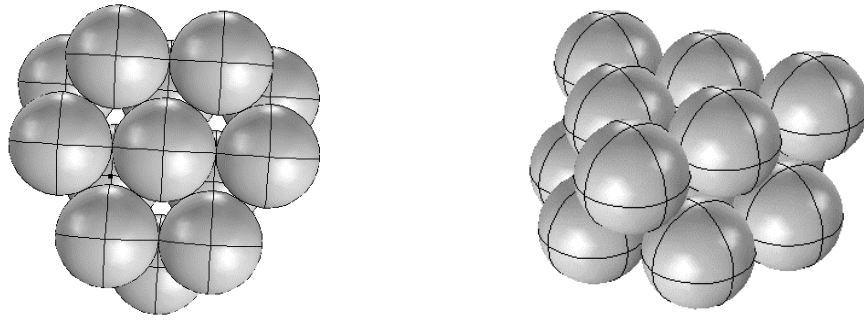


Figure 2.1. Two planes of uniform spheres in a hexagonal close packed arrangement. Left: The base layer demonstrates the hexagonal arrangement. Right: An isometric view shows that the next plane is offset from the first, but is also in hexagonal arrangement.

Membrane Coatings

Prefiltration of S-PAC onto a membrane with full particle rejection creates a coating of carbon that can be used to treat the entire volume of water filtered by the membrane. S-PAC coated on a flat sheet polymeric membrane in a dead-end configuration removed atrazine quickly and effectively (Heijman et al., 2009a; Ellerie et al., 2013; Amaral et al., 2016). However, pilot-scale application of an S-PAC coating on a tubular ceramic membrane was not as successful for atrazine removal due to difficulty in achieving an even coating. (Heijman et al., 2009a). Carbon membrane coatings have also been used on membranes to create gas separators, either through adsorption or through size exclusion by creating coatings with pore size less than 0.5 nm (Ismail and David, 2001). Carbon films can be fabricated onto numerous substrates, or even fabricated in an unsupported fashion,

but cracking of the film has posed an issue (Bird and Trimm, 1983; Ismail and David, 2001). One method of forming the carbon film is by coating a ceramic ultrafiltration membrane with a film containing carbon precursors and together they are heated for carbonization of the coating (Menendez and Fuerte, 2001; Saufi and Ismail, 2004). In an aging study, carbon films were found to lose removal efficiency faster when exposed to environments containing oxygen as compared to environments without oxygen (Menendez and Fuerte, 2001).

Filtration of Dissolved Fractions

While MF membranes contain physical pores that allow soluble constituents to pass through the membrane easily, dissolved fractions can still cause membrane fouling via adsorption within pores and onto pore openings or adsorption to solid foulants which obstruct flow and result in an increased cake resistivity (Huang et al., 2008). Dissolved NOM (DOM), for example, can adsorb strongly to membranes and other surfaces due to its high negative charge—it is often removed before membrane filtration via pretreatment due to its high fouling propensity. In conventional treatment, dissolved fractions must be converted into solids via coagulation and flocculation in order to be removed, even if removed by MF, but S-PAC has the potential to serve as a method of pretreatment to reduce the fouling caused by dissolved components (Carroll et al., 2000; Matsui et al., 2003). A pilot study found S-PAC to mitigate transmembrane pressure increase as compared to PAC due to increased adsorption of NOM components that contribute to membrane fouling (Matsui et al., 2007). When NOM is not present, S-PAC causes higher flux decline than PAC due to a higher cake resistance of smaller packed particles (Ellerie et al., 2013).

Colloidal Stability

A conclusion of particle-size dependent fouling is that particles that have aggregated to a larger effective particle size should result in less membrane fouling. Particles are stable in solution when electrostatic or osmotic forces override the difference between gravitational and buoyant forces on a particle, but can aggregate when stability is disrupted. Stability is reduced when the difference in electric potential between the particle surface, which depends on charges fixed to the particle surface as well as charges that adsorb and desorb, and the bulk fluid, which depends on the ionic strength, is reduced. The charges on the surface and a short distance above the surface comprise what is known as the Stern-Helmholtz layer, while charges further away from the surface all the way until concentrations match the bulk fluid comprise the diffuse layer; together, these layers form what is known as the electrical double layer (Israelachvili, 2011). Reduction in the double layer reduces repulsive forces, decreases stability, and increases propensity for aggregation.

Zeta Potential

Zeta potential is a useful measurement of stability; it measures the electric potential from the slipping plane, that is the point between the Stern-Helmholtz layer and the diffuse layer, to the particle surface and assumes the additional potential difference between the slipping plane and the bulk water is negligible (Berg, 2010). Bulk water parameters leading to zeta potentials between 0 and ± 5 typically indicate settling or aggregating conditions, and the boundary between stability and instability occurs at ± 30 (Malvern Instruments, no date).

Zeta potential is measured electrokinetically by running a current between two points in a sample and using optical measurements to determine the degree of resulting particle movement (Malvern Instruments, no date). The zeta potential changes as a function of pH since changes to pH affects the distribution of charges near the particle surface. The pH at which the charges in the bulk fluid are in equilibrium with the charges at the particle surface has a zeta potential of zero and is known as the isoelectric point; here, the diffuse layer has disappeared and the electric double layer is fully compressed. When measuring the zeta potential of activated carbon, only charges on the external surfaces are considered since it would take longer than the measurement duration for charges to diffuse to and from the surfaces of internal pores of porous materials such as activated carbon.

DLVO Theory

The interactions between particle surfaces and bulk fluids are described in Derjaguin-Landau-Verwey-Overbeek (DLVO) theory. Factors that affect stability such as particle concentration and ionic strength are inputs in the model. The interaction energy between two surfaces is a function of the separation distance and predicts the distance at which attractive forces exceed repulsive forces and aggregation can occur (Zhang et al., 2012). The DLVO interaction energy is the sum of attractive van der Waals forces (Equation 2.15) and repulsive electrostatic forces (Equation 2.16).

Interaction energy for two particles of radius r is a function of the separation distance, h ; here, the equations are simplified with the substitution of $u = \frac{h}{r}$. $K_B T$ is calculated from Boltzmann's constant multiplied by temperature in units of Kelvin; it is used as a thermal energy scale where interaction energies are normalized to $K_B T$. κ^{-1} is the

Debye-Huckel screening length, and can be found through the relation $\kappa^2 = 4\pi\lambda_{BN}$, where n is the concentration of monovalent ions in the solution. H is the Hamaker constant and is an intrinsic material property. It is calculated from the relative emissivities of the particle, A_p , and of the liquid, A_l (Equation 2.17). Equation 2.16 is obtained for spheres of equal size and relatively large radius (Gregory, 1975). The hyperbolic tangent term, sometimes also called γ , is comprised of the elementary charge, e_0 , and the surface potential, ψ . Here, the zeta potential, as an empirically determined value, is used as a substitute for surface potential.

$$U_{VDW}(h) = \left(-\frac{H}{6}\right) \left[\frac{2}{u^2 + 4u} + \frac{2}{(u + 2)^2} + \ln\left(\frac{u + 4u}{(u + 2)^2}\right) \right] \quad \text{Eq. 2.15}$$

$$U_{EL}(h) = k_B T \left(\frac{r^2}{u}\right) \left(\frac{128\pi n}{\kappa^2}\right) \tanh\left(\frac{e_0\psi}{4k_B T}\right) \exp(-\kappa h) \quad \text{Eq. 2.16}$$

$$H = \left(\sqrt{A_p} - \sqrt{A_l}\right) \quad \text{Eq. 2.17}$$

Under high ionic strength or high particle concentration, DLVO theory predicts that the interaction energy between two particles drops. The result is a compressed electric double layer and destabilized particles. The ratio of the DLVO interaction energy to the van der Waals interaction energy is known as the stability ratio, α . Under relatively high attractive van der Waals forces, stability goes to zero and particles tend to aggregate. The inverse of the stability ratio is known as the attachment efficiency and is obtained by integrating Equation 2.18 over distances of interest (Zhang et al., 2012). A correction factor, λ_u , is used according to Zhang et al. (2012): $\lambda_u = \frac{6u^2+13u+2}{6u^2+4u}$.

$$\alpha = \frac{\int_0^{\infty} \lambda(u) \frac{\exp\left(\frac{1}{K_B T} U_{VDW}(h)\right)}{(2+u)^2} du}{\int_0^{\infty} \lambda(u) \frac{\exp\left(\frac{1}{K_B T} U_{DLVO}(h)\right)}{(2+u)^2} du} \quad \text{Eq. 2.18}$$

An outcome of DLVO theory is the Schulze-Hardy rule, which says that the effect of an ion is proportional to its charge to the 6th power (Russel et al., 1992). Chemical coagulants, including metal salts, such as ferric chloride, aluminum sulfate, and polyaluminum choride (PACl), are often used to cause particles to destabilize and settle out of solution since the trivalent ions iron and aluminum contribute to positive charges adsorbed on particles which result in charge neutralization and a reduction in the zeta potential (Stumm and Morgan, 1942; Hendricks, 2006).

Adsorption Modeling

The last section discusses methods for modeling systems with adsorption. Mechanisms of activated carbon adsorption have been studied and modeled for a number of adsorbates. Adsorption onto PAC has been described well with a combination of film theory at the particle surface and diffusion-limited mass transfer into particle pores. However, models have been seen to break down as particle sizes reduce. Model modifications to address size effects are discussed.

Single Parameter Analytical Solutions (HSDM/PDM)

A common assumption made for adsorption into porous materials is that of homogenous surface or pore diffusion, which assumes that diffusive travel into the pore or along its surface occurs at the same rate throughout the particle. These models are termed the homogeneous surface diffusion model (HSDM) and pore diffusion model (PDM) respectively (Equations 2.19 and 2.20) (Roy et al., 1993). The rate term is the change in the solid-phase concentration, q , over time and as a function of the radius, r . HSDM is governed by a surface diffusion coefficient, D_s , while PDM is governed by a pore diffusion coefficient, D_p , and matched in dimension through the particle density, ρ . The only difference between HSDM and PDM is that HSDM uses the surface-phase concentration, c_s , as the variable, while PDM uses the liquid-phase concentration, c_l . Continuity may be assumed between the particle surface and the bulk concentration or a film transfer coefficient can be introduced into the mass balance and used as an additional fitting parameter.

Rapid small scale column tests (RSSCTs) which are used to model full-scale packed bed GAC reactors via a scaled-down column and scaled-down adsorbent material use PDM (Crittenden et al., 1991). S-PAC coatings can be viewed as very thin packed column reactors with a large diameter to height ratio. In RSSCTs, a proportional diffusivity model in place of a constant diffusivity model is used available when particle size effects are present. Application of HSDM to reactors is done by combining the intrapore transport with mass balance boundary equations; batch tests and RSSCTs are used to determine

diffusion coefficients that can then be applied to full reactor models (Crittenden et al., 1987; Roy et al., 1993; Cook et al., 2001).

$$\frac{dq}{dt} = D_s \frac{1}{r^2} \frac{\partial}{\partial r} \left(r^2 \frac{\partial c_s}{\partial r} \right) \quad \text{Eq. 2.19}$$

$$\frac{dq}{dt} = \frac{D_p}{\rho} \frac{1}{r^2} \frac{\partial}{\partial r} \left(r^2 \frac{\partial c_l}{\partial r} \right) \quad \text{Eq. 2.20}$$

A set of equations similar to HSDM/PDM is those based on the linear driving force (LDF) model. In HSDM/PDM, the radial diffusion equation results from solving the governing transport equation over spherical particles. In LDF, pores are assumed to be linear channels and movement follows a concentration gradient (Equation 2.21). The linear model is simpler than the radial diffusion model. LDF is solved from the driving force at the liquid-solid interface (Lua and Jia, 2009).

Two versions of this model can be used based on the limiting factor, whether it is surface diffusion as in the HSDM model or diffusion to the particle surface following film theory. The surface diffusion scenario model, termed LDFQ, can be fit either to a surface diffusion coefficient or a pore diffusion coefficient. The external mass transfer limited scenario model is termed LDFC. By applying both models to a data set, the rate-limiting mechanism can be identified.

$$\rho \frac{dq}{dt} = Ka(C - C^*) \quad \text{Eq. 2.21}$$

Using HSDM, different diffusion coefficients were needed to fit particles of different size from the same carbon (Najm et al., 1990; Matsui et al., 2009a; Ellerie, 2012). Since diffusion constants should not change as a function of particle size, it is clear that HSDM cannot accurately account for particle size as a variable and thus is not suitable for S-PAC modeling where particle size is the main factor behind a changing adsorption rate. Developers of RSSCT models also saw the breakdown of predictions at small particle sizes; the use of a variable diffusivity workaround in RSSCT models is useful for predictions but does not address why the model doesn't extend to small sizes.

Multiple Parameter Analytical Solutions (BPKM/SAM)

Models with more complexity address some of the shortcomings observed with simpler models. In the branched pore kinetic model (BPKM), which was particularly developed for activated carbon adsorption, two rates of internal transfer are proposed—one for movement through large pore diameters and one for smaller pore diameters (Peel et al., 1981). Thus, there are two distinct regions of molecular transport: radial transport through macropores (Equation 2.22), which is the same as HSDM/PDM equations, and linear transport through micropores (Equation 2.23), which is the same as the LDF equation. The three unknowns are surface diffusion, D_s , macropore-to-micropore transfer coefficient, k_B , and the fraction of adsorption capacity in macropores, φ . When φ is one, the micropore transport equation is negated and the equation reverts to HSDM/PDM radial diffusion. The third equation needed to solve for the three unknowns is formulated by equating the flux at two locations. A solution has been developed for BPKM in conjunction

with a film transfer coefficient, therefore not assuming concentration continuity at the particle surface, for a total of four fitting parameters (Ko et al., 2002).

$$\varphi \frac{\partial q_M}{\partial t} = \frac{\varphi}{r^2} \frac{d}{dr} \left\{ D_S r^2 \left[\frac{dq_M}{dr} \right] \right\} - k_B [q_M - q_B] \quad \text{Eq. 2.22}$$

$$[1 - \varphi] \frac{\partial q_B}{\partial t} = k_B [q_M - q_B] \quad \text{Eq. 2.23}$$

The results of previous studies by Matsui and colleagues correspond well with this model; in their first paper on S-PAC, they attributed the faster adsorption of NOM onto S-PAC to an increase in the mesoporous fraction as a result of milling (Matsui et al., 2004). While HSDM produces good fits with differing surface diffusion coefficients for PAC and S-PAC, good fits of both PAC and S-PAC data were achieved with BPKM using one set of values for the three fitting parameters (Matsui et al., 2009a). Additionally, they found that the S-PAC model was more dependent on diffusion through micropores, whereas the PAC model was more dependent on overall surface diffusion, which implies that small molecules arrive at the mesopore-micropore boundary faster in S-PAC than in PAC. Since the fitting parameters were the same in both cases, the data thus points to a longer distance traveled to micropores in the case of PAC and not faster surface diffusion nor slower micropore diffusion for S-PAC.

Another layer of complexity added to activated carbon modeling is the postulation that adsorption onto activated carbon is limited to a certain penetration depth that is a function of the adsorbate and the carbon material (Ando et al., 2011; Matsui et al., 2011, 2013). The result of this hypothesis is that the usable volume as dictated by the penetration

depth compared to the total particle volume is larger for smaller particles than larger particles; thus, smaller particles would have more utilizable capacity on a mass basis. The idea of a limited penetration depth is implemented in the Shell Adsorption Model (SAM), where penetration depth is represented by the variable δ (Equation 2.24) (Matsui et al., 2011).

As a model of adsorption equilibrium, SAM is an alternative to Freundlich and Langmuir isotherms and is akin to a modified Freundlich isotherm. SAM incorporates the Freundlich isotherm coefficient as K_o to describe maximum adsorption at the particle surface. The expression in straight brackets accounts for declining adsorption capacity from a maximum at the surface to a constant level p at penetration depth δ . The expression $f_R(R)$ is used to account for a distribution of particle sizes; if only one particle size is used, the integral becomes 1. However, there remains an R outside the integral as $1/R^3$ and it is not clear what value should be used there. SAM explained S-PAC behavior better than the Freundlich isotherm, while PAC behavior was still better fit with the Freundlich isotherm (Matsui et al., 2011).

$$q_E = C_E^n \frac{3K_o}{R^3} \int_0^\infty \left\{ \int_0^R \left[\max\left(\frac{r - R - \delta}{\delta}, 0\right) (1 - p) + p \right] r^2 dr \right\} f_R(R) dR \quad \text{Eq. 2.24}$$

SAM was applied in conjunction with the pore diffusion model (PDM) for the reason that PDM does not depend on the solid phase concentration (Matsui et al., 2011). SAM with PDM modeled a data set of PSS adsorption onto activated carbon better than the Freundlich isotherm with either HSDM or PDM; fitting parameters were determined

by optimizing the fit for data sets from multiple carbon sizes for each adsorbate (Matsui et al., 2011). The authors note briefly without data that BPKM described the PSS adsorption slightly better than HSDM and PDM; a subsequent study examines SAM and BPKM. For the adsorption of small molecules geosmin and 2-MIB, SAM was applied in conjunction with BPKM with good fitting results (Matsui et al., 2013). It is likely that BPKM would not have provided much improvement in modeling PSS adsorption since the large adsorbate size only requires the radial macropore diffusion component, which is effectively HSDM and which has limitations for small particle size. With small molecule adsorbates, the inclusion of two diffusion regions, as seen previously with BPKM with Freundlich modeling of geosmin adsorption, and a limitation on the depth of adsorption via SAM provide the complexity needed to describe the system; particularly, the penetration depth factor allowed for much better agreement for data sets spanning multiple carbon particle sizes, including PAC sizes (Matsui et al., 2013). A study on the use of spent GAC for S-PAC production further supports the theory of limited penetration depth since the S-PAC had nearly the same adsorption capacity as virgin materials (Pan et al., 2017).

Numerical Solving Techniques

To solve these analytical models, finite element modeling (FEM) techniques are used to solve the equations over smaller steps in time and space. The spatial domain consists of radial elements within the particle over which q is solved. Mass balances are used to determine changes in the system over each time step. FEM technique involves rewriting solution equations to replace continuous variables with discretized ones (Ervin, 2015). The subsequent equations can be represented in matrix form to facilitate solving for

the vector of q values. In the method used by Priscilla To to solve HSDM, a Thomas method is used to solve the tridiagonal solution matrix (To, 2008). In the work by Ko, Porter, and McKay, matrix inversion is used to solve for the next value of the variable (Ko et al., 2002).

Computational Solving Techniques

Where geometrical complexity makes it difficult to derive analytical models, computer-aided finite element modeling (FEM) is useful. In FEM, the governing differential equations are solved over small elements that are part of a mesh applied to the entire geometry. Essentially, CFD uses numerical finite element techniques in combination with high computational power to solve equations over a very large number of elements that are not necessarily ordered in any predictable fashion. Adding computational power to finite element analysis makes it possible to easily work in multiple dimensions and determine results over geometries such as surfaces and to present results along contours.

Computational fluid dynamics (CFD), an FEM tool for hydrodynamic modeling, has been used to model fixed bed reactors for the reasons that the assumption of homogeneity is not required and that CFD can make predictions regarding flows in particle interstices (Dixon and Nijemeisland, 2001). In the case of S-PAC coatings, the location of particles within the coating and the local fluid velocity around the particles both play important roles in determining the transport and adsorption of soluble contaminants.

The combined mass transport, reaction kinetics, and fluid dynamics poses a challenging problem because analysis needs to occur at both the macro scale and the micro scale. COMSOL Multiphysics, a software tool for computational FEM analysis, contains

a package called Reactive Pellet Bed to model reactions within pellets that comprise a porous media. Combining the Reactive Pellet Bed package, which models transport and reaction along with particle radius, with three dimensional flow allows for modeling of packed beds in a total of four dimensions.

CHAPTER THREE

MICROFILTRATION OF AGGREGATED S-PAC UNDER NATURAL AND CHEMICALLY ENHANCED COAGULATION

Motivation

Ellerie et al. (2013) showed that fully disaggregated S-PAC fed to a microfiltration membrane resulted in higher flux decline than PAC. The size of S-PAC particles plays a large role in membrane coatings; particles with diameters near 200 nm caused marked flux decline on flat sheet membranes when compared to the particles with larger diameters (Amaral et al., 2016). Flux is an important economic consideration, thus, aggregation is explored in this chapter to determine if small particles aggregated to form effectively larger particles will result in higher flux than small unaggregated particles.

Materials and Methods

Carbon

S-PAC was produced from a commercially available coal-based PAC, Watercarb 800 (Standard Purification, Florida, USA), using a wet bead mill (MiniCer, Netzsch Premier Technologies, Exton, PA, USA). The carbon was milled for 7 hours using 0.5 mm steel beads and has an average hydrodynamic diameter of 200 nm as measured by dynamic light scattering. Table 3.1 shows the distribution of the S-PAC particle size; S-PAC size was measured in dispersant (Darvan 821A, Vanderbilt Minerals, Norwalk, CT, USA) by Netzsch Technologies (Laser Diffraction Analyzer, Horiba, Kyoto, Japan).

Table 3.1. Particle size distribution of milled S-PAC

Hydrodynamic diameter (nm)	Fraction (%)	Hydrodynamic diameter (nm)	Fraction (%)
58	0.322	389	2.026
67	0.707	445	1.074
76	1.532	510	0.618
87	2.960	584	0.402
100	4.749	669	0.298
115	6.771	766	0.246
131	9.082	877	0.221
150	11.241	1005	0.203
172	12.656	1151	0.191
197	12.819	1318	0.175
226	11.586	1510	0.157
259	9.276	1729	0.136
296	6.510	1981	0.116
339	3.926		

Chemicals

Three chemical coagulants were tested: ferric chloride (FeCl_3), aluminum sulfate ($\text{Al}_2(\text{SO}_4)_3$), and polyaluminum chloride (PACl). Ferric chloride was obtained as a heptahydrate ($\text{FeCl}_3 \cdot 6\text{H}_2\text{O}$) and aluminum sulfate was obtained as an octadecahydrate ($\text{Al}_2(\text{SO}_4)_3 \cdot 18\text{H}_2\text{O}$). Commercially available PACl with 42% basicity was used (PAX-18, Kemira, Atlanta, GA, USA). Calcium content (CaCl_2) was also tested for its destabilizing properties.

Atrazine (ACROS Organics, Belgium) was used as a model small molecule contaminant. Radiolabeled (American Radiolabeled Chemicals, St. Louis, MO, USA) atrazine was used as a tracer for atrazine adsorption in a 1:300 ratio.

Particle Size Measurements

S-PAC was measured for size using the Zetasizer Nano ZS (Malvern, Worcestershire, UK) and checked with the Microtrac (Nikkiso Co., Ltd., Tokyo, Japan). The Zetasizer NS measures particle sizes of samples in cuvettes using dynamic light scattering (DLS) technology while the Microtrac uses laser light scattering (LLS) technology and a circulating flow measurement system. Surfactant was used to disperse particles before measurement (0.08% Triton X-100, Kanto Chemical Co., Inc., Tokyo, Japan). The fully dispersed carbon particles were 170 nm +/- 10 nm in diameter using DLS, and the corresponding size determined by LLS was 199 nm diameter.

Time resolved dynamic light scattering (TR-DLS) measurements were taken with the Zetasizer Nano ZS without surfactant. Attachment efficiencies were found experimentally from the rate of increase in measured particle sizes using the slope of the particle size measurements versus time, which were taken every 20 seconds for 30 minutes, and normalizing to the slope of the fastest aggregation condition. Slopes were taken after the particle increase rate had stabilized, which was approximately after a 30% increase in particle size (Zhang et al., 2012).

Membranes

S-PAC was filtered onto polymeric polyvinylidene fluoride (PVDF) membrane coupons with nominal pore size of 0.1 μm . Membrane coupons were soaked in distilled and deionized water before use in filtration experiments and discarded afterwards.

Bench-scale apparatus

Polymeric membrane coupons were housed in a plastic filtration cell of diameter 44.5 mm and volume 50 mL (Amicon, Millipore, Billerica, MA). The active diameter of the installed membrane was 39 mm. Experiments were performed at 10 psi pressure supplied by a nitrogen gas tank. Feed water was added to the pressure vessel ahead of the membrane cell and the permeate was collected in a beaker on a balance for calculation of flux via computer (Figure 3.1).

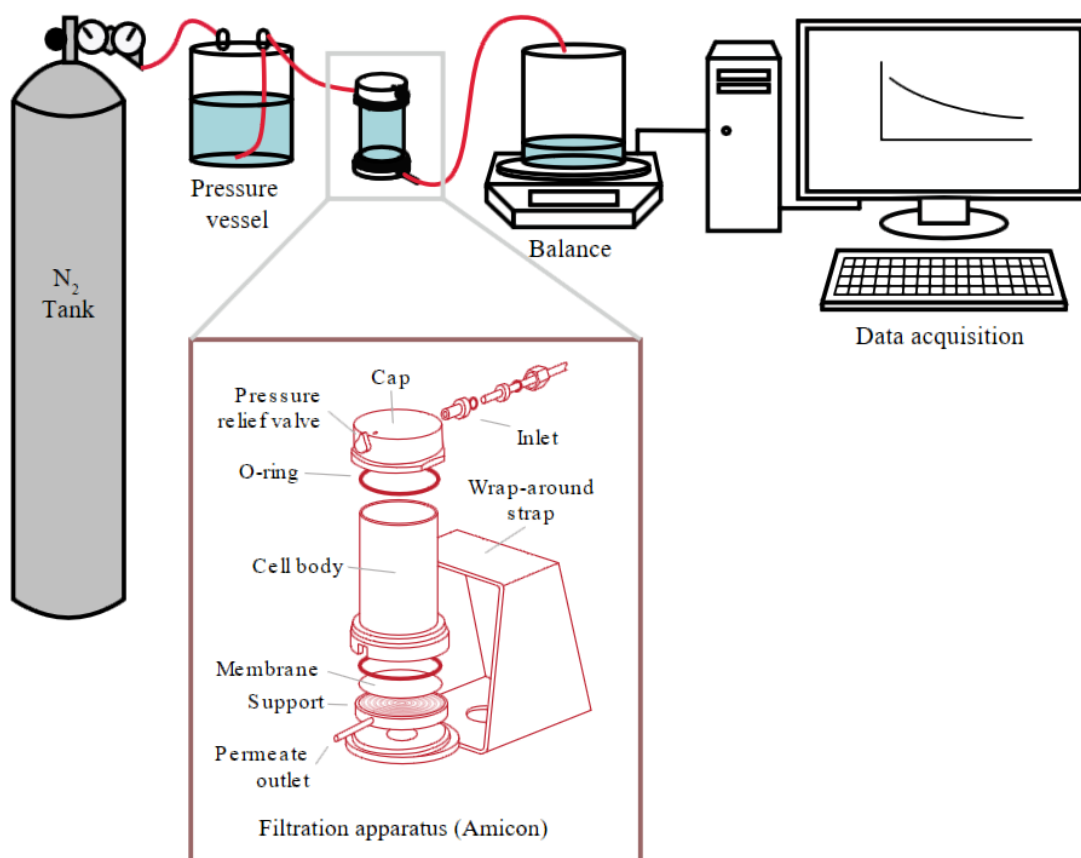


Figure 3.1. Benchscale filtration apparatus using Amicon dead-end filtration cell and operated by constant pressure from a gas cylinder. Data of permeate mass over time is collected by computer.

Water Composition

Feedwaters were prepared from laboratory grade reagents in distilled and deionized water (DDI). The type of chemical coagulant and the ionic composition were varied over the test matrix (Table 3.2). pH adjustment was made after the addition of stable components, including alkalinity, ionic content, and NOM, and before addition of carbon and chemical coagulants.

Table 3.2. Test matrix of feedwater composition. All trials used a carbon concentration of 5 mg/L. Ionic strength was held constant at 10 mM in trials containing ionic compounds.

Description	Coagulant Dose ($\mu\text{M Fe/Al}$)	pH	Alkalinity (mg/L as CaCO_3)	Carbon concentration (mg/L)	NaCl (mM)	CaCl₂ (mM)	NOM (mg/L)
Carbon only	0	7	6	5	0	0	0
Carbon only	0	7	6	5	10	0	0
Carbon only	0	6	6	5	0	0	4
Carbon only	0	7	6	5	0	0	4
Calcium	0	7	6	5	8	1	0
Ferric chloride	37	7	6	5	0	0	0
Ferric chloride	37	6	6	5	0	0	0
Ferric chloride	37	6	6	5	0	0	4
Ferric chloride	37	7	6	5	0	0	4
Ferric chloride after settling	37	7	6	5	0	0	0
Ferric chloride	37	7	6	5	10	0	0
Ferric chloride + calcium	37	7	6	5	8	1	0
Ferric chloride + calcium	37	7	6	5	8	1	0
Ferric chloride + calcium	37	7	6	5	8	1	0
Ferric chloride + calcium	37	7	6	5	8	1	4
Ferric chloride + calcium	37	7	6	5	8	1	4
Aluminum sulfate	37	7	6	5	10	0	0
Polyaluminum chloride	37	6	6	5	10	0	0

All tests used a carbon concentration of 5 mg/L. Aliquots of carbon were prepared by adding the total carbon mass to 50 mL of DDI water and sonicating at 50% power for one minute (S-4000, Qsonica, LLC) to fully disaggregate the carbon particles.

After formation of the carbon cake, some trials were tested for contaminant removal using atrazine. DDI water containing both radiolabeled and non-radiolabeled atrazine was prepared with the molecules in a 1:300 ratio for a total concentration of 15 ppb atrazine.

Filtration Method

A jar test apparatus with 2 liter square beakers and a flat paddle mixer was used to apply flash mix and flocculation conditions—rapid mixing at 100 rpm for 30 seconds and slow mixing at 15 rpm for 10 minutes—to the feedwaters (Phipps and Bird). Turbidity was measured immediately after slow mixing. Samples were also taken for floc imaging using the camera attachment of a drop analyzer (EasyDrop, Kruss USA, NC).

One liter of feedwater was taken from the sampling port of the square beaker and transferred to the pressure vessel for filtration. Post-filtration, a carbon cake is formed as all the carbon is rejected by the membrane. The carbon cake was used to test contaminant removal by passing atrazine in DDI through the membrane and collecting samples to monitor permeate concentrations. 450 mL of atrazine solution was passed through a carbon cake and 5 mL samples were collected after every 45 mL of permeate for a total of 9 samples. Atrazine was quantified via the radioactive decays per minute measured by LSC.

Preliminary Work

Some experiments were done before undertaking the methods described above in order to understand the behavior of S-PAC filtration in aggregated and disaggregated forms, and to explore how S-PAC becomes aggregated over time.

Dispersion Effects

Initial experimentation concerning S-PAC on flat sheet membranes as a carbon coating discovered high fouling associated with S-PAC. In her research thesis, Mengfei Li performed an experiment where she used sonication methods to control the level of S-PAC aggregation (Li, 2014). She compared the filtration of S-PAC that was fully dispersed using high powered probe sonication to S-PAC that was only partially dispersed using low power bath sonication. The parent PAC was also fully dispersed using probe sonication and filtered. The flux decline was least for the parent PAC followed by the bath sonicated S-PAC and was worst for the probe sonicated S-PAC (Figure 3.2). Since the same S-PAC was used in both trials, it is concluded that the larger effective particle size found in the less dispersed S-PAC sample results in less flux decline by the same mechanism which the larger actual particle size of the PAC results in less flux decline.

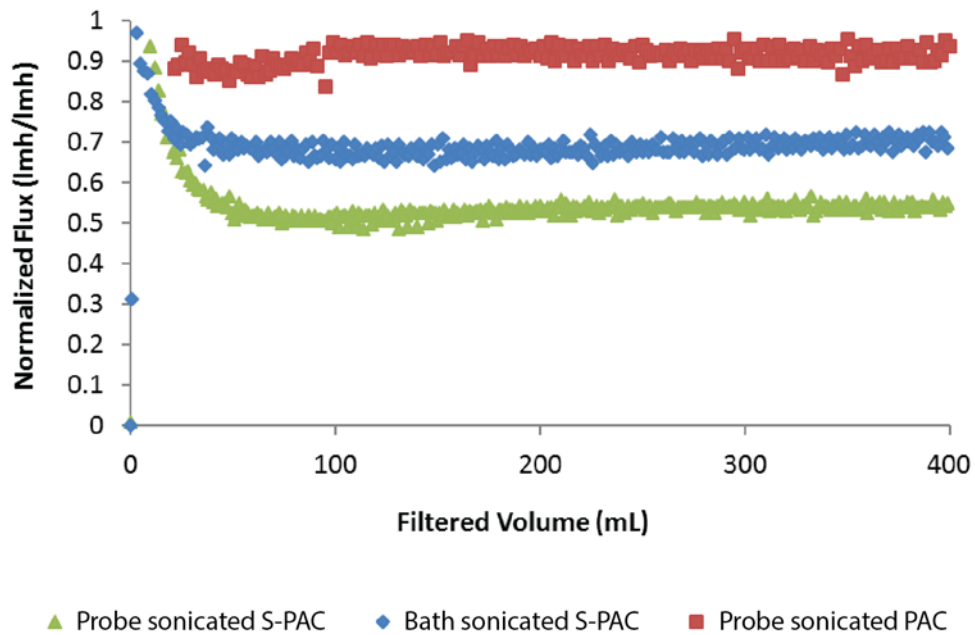


Figure 3.2. Membrane coating using activated carbon of three effective sizes. The largest size is the parent PAC, the smallest size is the fully dispersed probe sonicated S-PAC, and the bath sonicated S-PAC has an effective size between the two.

Fouling from a cake layer can be visualized in two ways: as flux decline or as resistance increase. By using Equation 2.11, the resistance associated with the cake layer was isolated from the constant membrane resistance, which is calculated from the clean water flux for each coupon. The fouling due to S-PAC is a direct function of carbon mass, therefore, the resistance associated with the carbon cake increases linearly with the mass of carbon fed to the membrane (Figure 3.3).

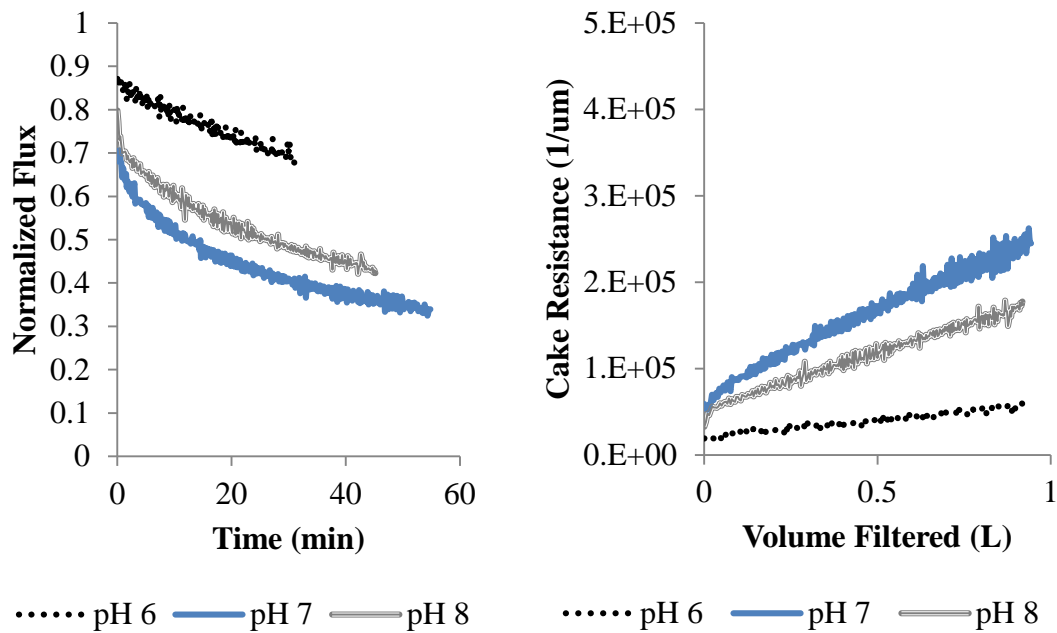


Figure 3.3. Left: Flux decline due to filtration of fully dispersed carbon at varied pH. Right: Translating flux decline into cake resistance reveals a linearly increasing resistance with increasing mass on the membrane.

Self-Aggregation

When particles were measured for effective size over time, particle aggregation was observed to be a function of the particle concentration. Fully dispersed carbon samples at 20 mg/L and 100 mg/L did not increase in size over the course of an hour, but the sample with 1000 mg/L increased continually over time (Figure 3.4). Subsequent filtration experiments were performed with a carbon concentration of 5 mg/L to avoid results from unaided aggregation.

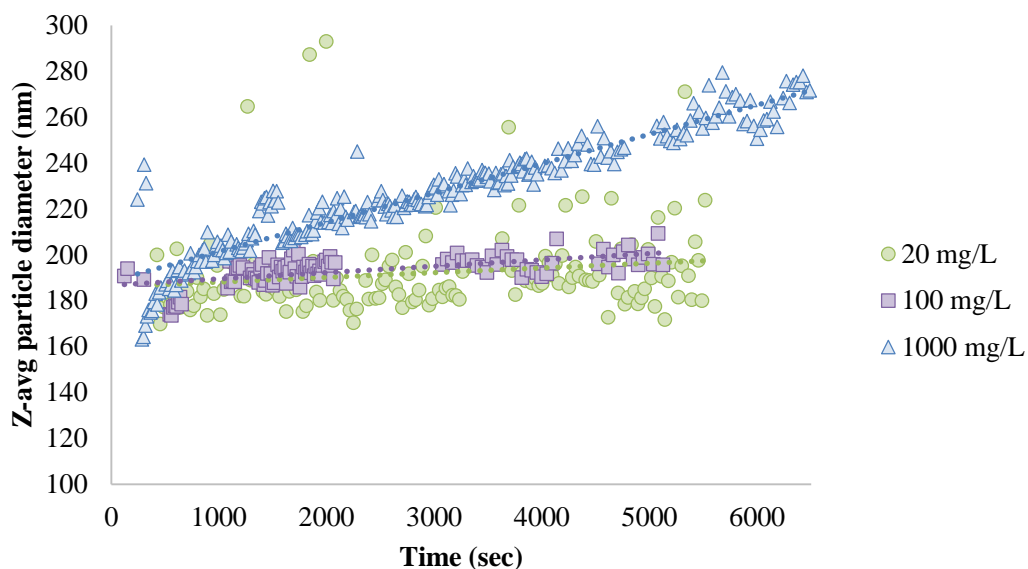


Figure 3.4. Increases in particle size over time as a result of natural aggregation processes is observable at a very high particle concentration of 1000 mg/L. Particle size increase at 20 mg/L and 100 mg/L are not observed over the measurement time frame. Linear fit lines of particle size increase after an initial 30% increase are used as an indicator of aggregation rate.

Results

Ionic Strength Effects

To examine the effect of ionic content on aggregation, concentrated salt solutions were dosed into fully dispersed carbon. Measurements of particle size over time were taken in triplicate for NaCl, KCl, and CaCl₂ over a range of ionic strength values (Figure 3.5). CaCl₂ resulted in much faster particle aggregation than KCl or NaCl, and KCl resulted in slightly faster aggregation than NaCl at the same concentrations. Effects from calcium are predicted by the Schulze-Hardy rule, which says that the effect of charge on particle interactions is proportional to the charge to the sixth power.

DLVO theory was applied to the data after normalizing each measurement to the fastest particle growth observed for that salt. Particle size contributions were weighted according to the size distribution of the S-PAC (Table 3.1). NaCl and KCl show similar trends from low to high salt concentrations. Since DLVO predicts high interaction energy as a result of the concentration of monovalent ions, S-PAC appears to follow DLVO theory with aggregation induced by increased monovalent salt concentrations. Increases in CaCl₂ concentration do not greatly affect aggregation—high aggregation effects are seen at even low concentrations (Figure 3.6). Calcium causes destabilization resulting in particle size increase partially through ionic strength but more prominently through divalent bonding. Therefore, aggregation due to calcium is not expected to be modeled well with DLVO theory.

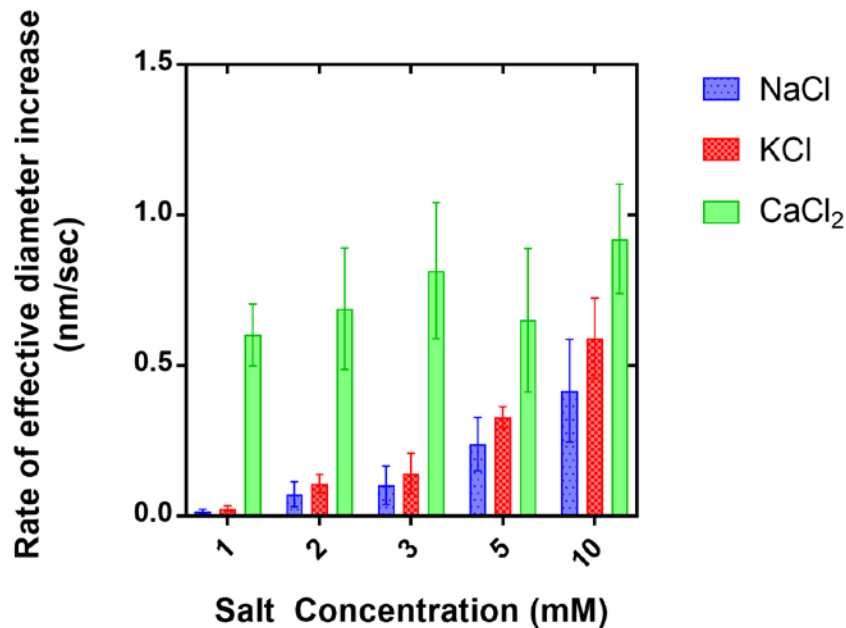


Figure 3.5. Particle size increase as a result of ionic strength. CaCl₂ ions resulted in much faster aggregation than NaCl or KCl at the same concentrations.

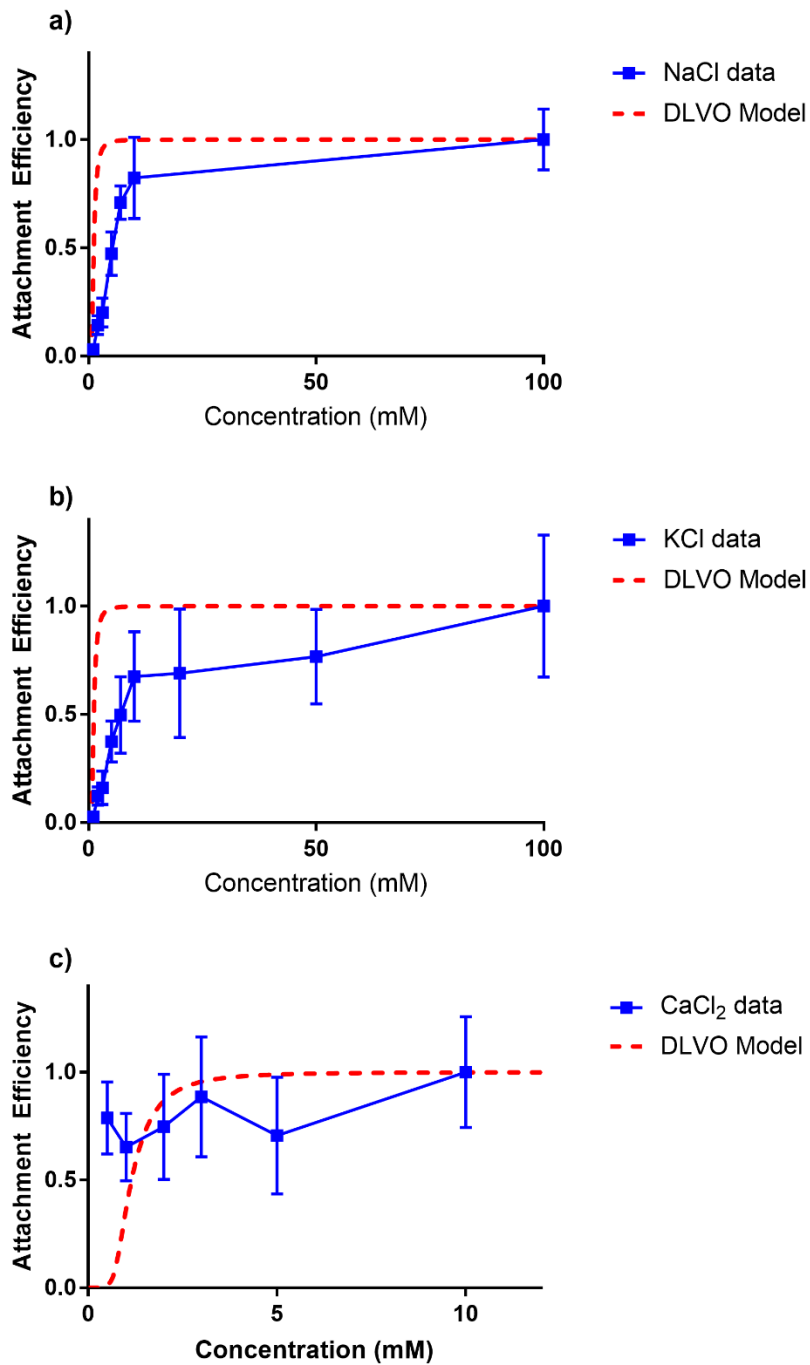


Figure 3.6. Normalized attachment efficiencies as a result of monovalent Na^+ , Cl^- , and K^+ ions, and divalent Ca^{2+} ions. a) Particles in NaCl up to 100 mM, b) Particles in KCl up to 100 mM, c) Particles in CaCl_2 up to 10 mM. DLVO models for each salt are shown as red dashed lines.

Chemical Coagulant Effects

Three chemical coagulants were measured for their ability to reduce fouling through effective particle size increase: aluminum sulfate, ferric chloride, and polyaluminum chloride. All chemical coagulants were dosed at $37 \mu\text{M}$ as either Fe or Al, which is equivalent to 10 mg/L of ferric chloride heptahydrate. Dosing was determined via jar testing and the amount of coagulant was chosen as the minimum dose necessary to produce visible flocs. The flocs produced by the chemical coagulants were large, as seen through optical imaging (Figure 3.7).

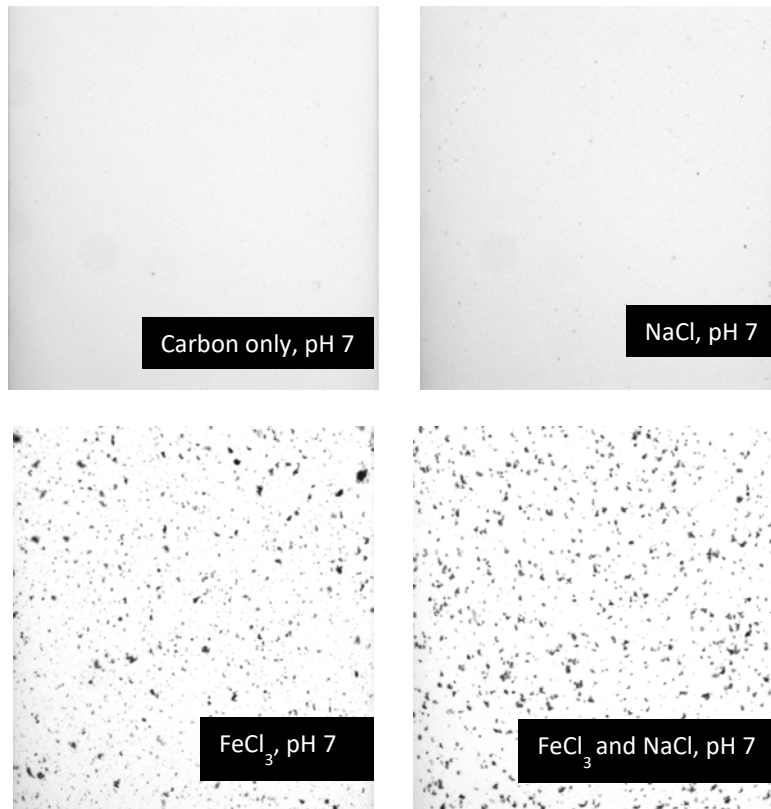


Figure 3.7. Visual observation of samples from jar tests after slow mixing. Image width is 10 mm. Clockwise from top left: carbon only in DDI at pH 7, carbon in 10 mM NaCl at pH 7, carbon in ferric chloride and DDI at pH 7, carbon in ferric chloride, 10 mM NaCl and DDI at pH 7.

No particles were observable in the carbon only test case, which supports unaided aggregation results that do not show effective particle size increase at low concentrations of carbon without added ionic strength. 10 mM NaCl produced scattered pinpoint floc that did not settle, while ferric chloride in DDI produced large flocs that were capable of settling.

Filtration of flocs transferred from the jar test to the filtration pressure vessel revealed whether floc production resulted in flux enhancement. Over the course of filtration, the build-up of rejected material forms a cake layer on the membrane that continually increases the resistance to flow. When the cake resistance is plotted against the amount of carbon that comprises the cake layer on the membrane, which is determined by assuming carbon has a uniform concentration in the volume of water sent to the membrane, the nearly linear slope reveals that the cake layer has a constant permeability. The difference in slopes reveals different permeabilities in the cakes formed by various jar test trials.

With only the addition of 10 mM NaCl, increase in cake resistance is nearly the same as the DDI trial, but the inclusion of 0.5 mM calcium with 8 mM NaCl improved flux performance (Figure 3.8). Ferric chloride at pH 7 slightly improved the flux as compared to carbon only, however, ferric chloride at pH 6 resulted in a much higher cake resistance. Alum and PACl, at their optimal pH of 7 and 6 respectively, also resulted in higher cake resistance than the carbon only case (Figure 3.9).

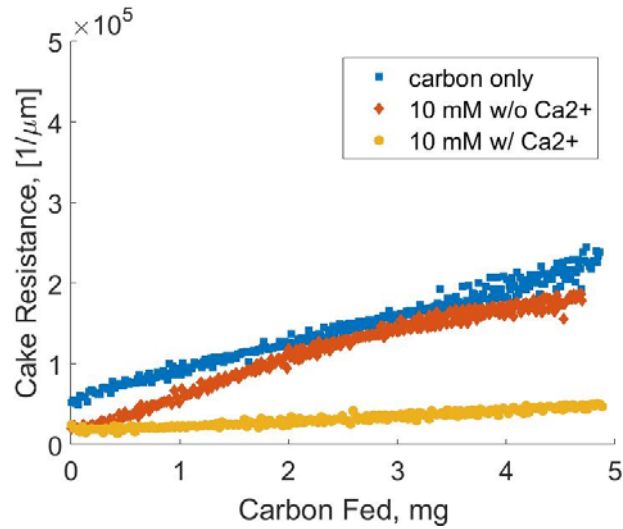


Figure 3.8. Growth in cake resistance associated with carbon fed to the membrane at pH 7 under no ionic strength, 10 mM NaCl, and 0.5 mM CaCl₂ + 8 mM NaCl.

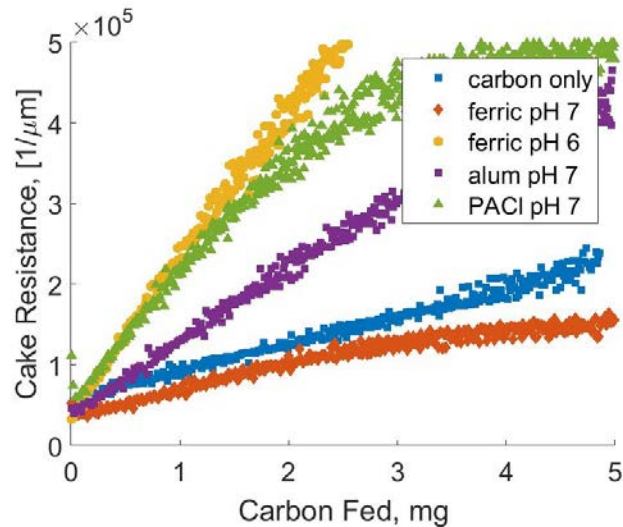


Figure 3.9. Growth in cake resistance associated with carbon fed to the membrane using ferric chloride at pH 6 and pH 7, alum at pH 7, and PACl at pH 7.

Chemical coagulants performed the same or better with background ionic strength of 10 mM NaCl (Figure 3.10). Ferric chloride with NaCl resulted in a much lower flux resistance at both pH 6 and pH 7 than either NaCl or ferric chloride alone. PACl performed

similarly with the ionic strength only trial. Interestingly, when ferric chloride was used in conjunction with NaCl and calcium, the flux resistance returned to the original value, even though calcium alone as well as ferric chloride with NaCl both individually resulted in flux improvement (Figure 3.11).

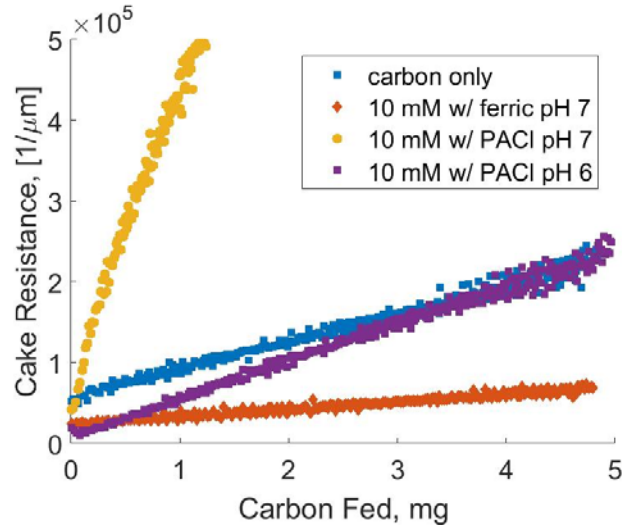


Figure 3.10. Growth in cake resistance associated with carbon fed to the membrane with NaCl using ferric chloride at pH 7 and PACl at pH 6 and pH 7.

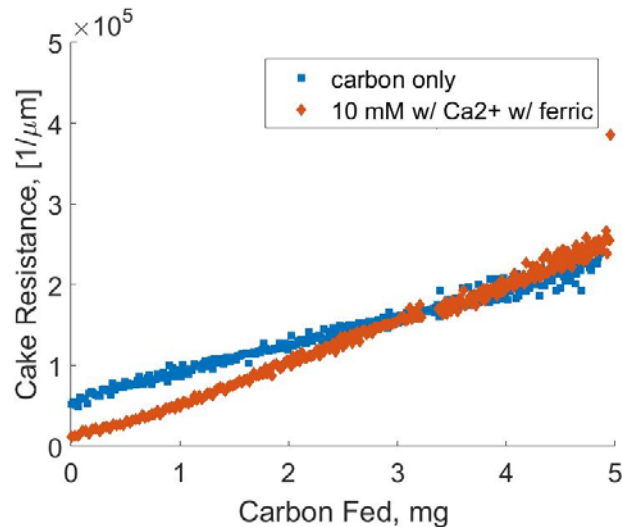


Figure 3.11. Growth in cake resistance associated with carbon fed to the membrane with NaCl and Ca²⁺ using ferric chloride at pH 7.

Lastly, filtrations were performed with one liter of supernatant resulting from 20 minutes of settling in contrast to the direct filtration method. One liter was drawn from the jar test beaker sampling port after coagulation, flocculation, and settling. Note that the true amount of carbon is unknown for this test, but the volume filtered can be expressed as equivalent carbon dosed, since 5 mg/L of carbon was used in all tests. Despite the reduction in total mass sent to the membrane, the cake resistance is nearly the same as the carbon only case (Figure 3.12). The ferric chloride trial with settling used the exact same recipe as the ferric chloride trial that resulted in less fouling than the carbon only case. Therefore, the particulates causing fouling in the settling trial should also have been present in the non-settling trial. The reason for the different filtration performance is that the small particles alone created a denser and less permeable cake layer, albeit a thin layer, than the small particles in conjunction with larger particles. The small particles can possibly also adsorb within membrane pore channels and cause fouling through pore width restriction.

Poor filtration performance occurred with supernatant of both ferric chloride and alum trials despite lower turbidity. There was no correlation found between turbidity of the flocculated water and filtration performance for either settled or non-settled trials (Figure 3.13). In fact, the trials with the smallest cake resistance slope had medium to high turbidities.

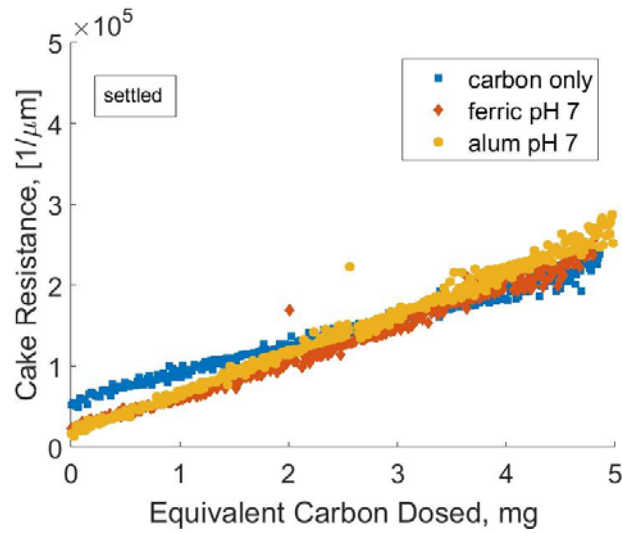


Figure 3.12. Growth in cake resistance from supernatant of ferric chloride and alum coagulation at pH 7 after settling for 20 minutes. Equivalent carbon dosed refers to the carbon used to treat the volume filtered, but not necessarily the carbon mass filtered.

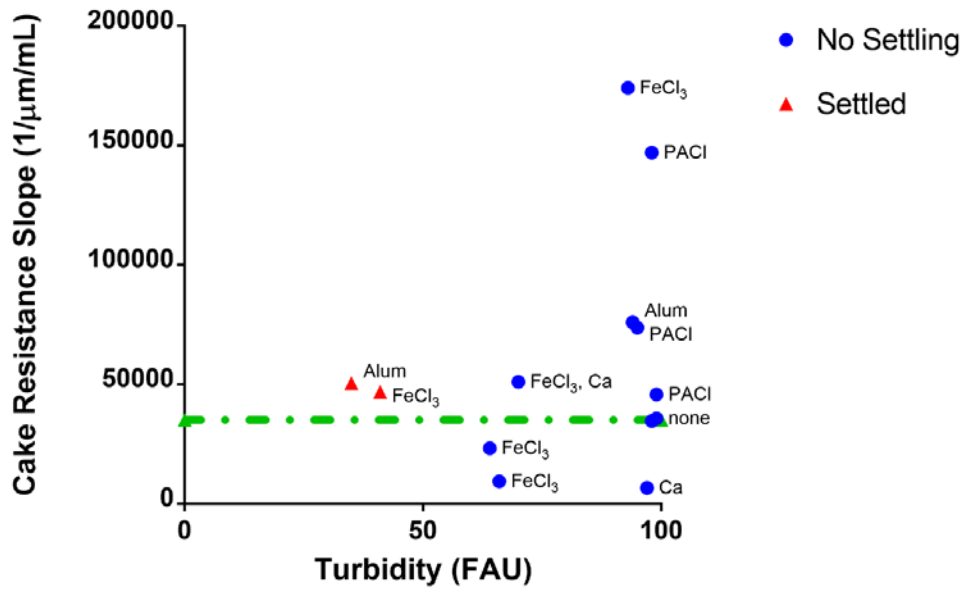


Figure 3.13. Turbidity was not a good predictor of filtration performance. Tests with settling had low turbidity, as expected, but tests without settling performed even better.

The trivalent nature of aluminum and iron ions leads to the prediction that higher valency will lead to more destabilization, following the Schulze-Hardy rule. However, none of the chemical coagulants performed as well as calcium, which is divalent, for improving filtration performance in terms of the rate of cake resistance increase (Figure 3.14).. Some trials with ferric chloride and polyaluminum chloride did result in less flux decline than the carbon alone, but on average the coagulants did not perform statistically different than the carbon only case. The reason for highly variable performance with chemical coagulants is likely related to the high fouling material observed in the settling trials. The variability could be explained by error introduced by the jar test apparatus, which could cause slight differences in the mixing patterns, or by the formation of high fouling particulates through a stochastic mechanism. Repeats of the settling experiments may provide information on the origin of high fouling, non-settling particulates.

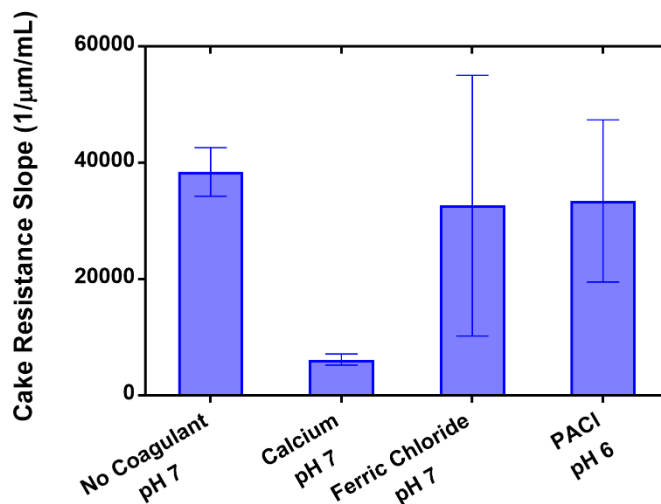


Figure 3.14. Replicates of filtration performance for four filtration scenarios: carbon in 10 mM NaCl, carbon in 0.5 mM CaCl₂ and 8 mM NaCl, carbon with 37 μM ferric chloride in 10 mM NaCl, and carbon in 37 μM aluminum via PACl.

Aggregation Effects on Contaminant Removal

Atrazine prepared in a 1:300 ratio of radiolabeled to unlabeled compounds was filtered through the aggregated carbon after one liter had been filtered onto the membrane. Approximately 5 mg of carbon is loaded onto the membrane as a result of filtering one liter, however, heterogeneity in the distribution of flocculated material makes the true mass of carbon unknown. The concentration of atrazine in samples taken from the permeate is shown in Figure 3.15. Cakes formed from carbon in DDI or with background ionic strength removed all atrazine from the volume filtered. However, carbon aggregated with ferric chloride did not fully remove atrazine and all trials with ferric chloride had non-zero measurements of atrazine.

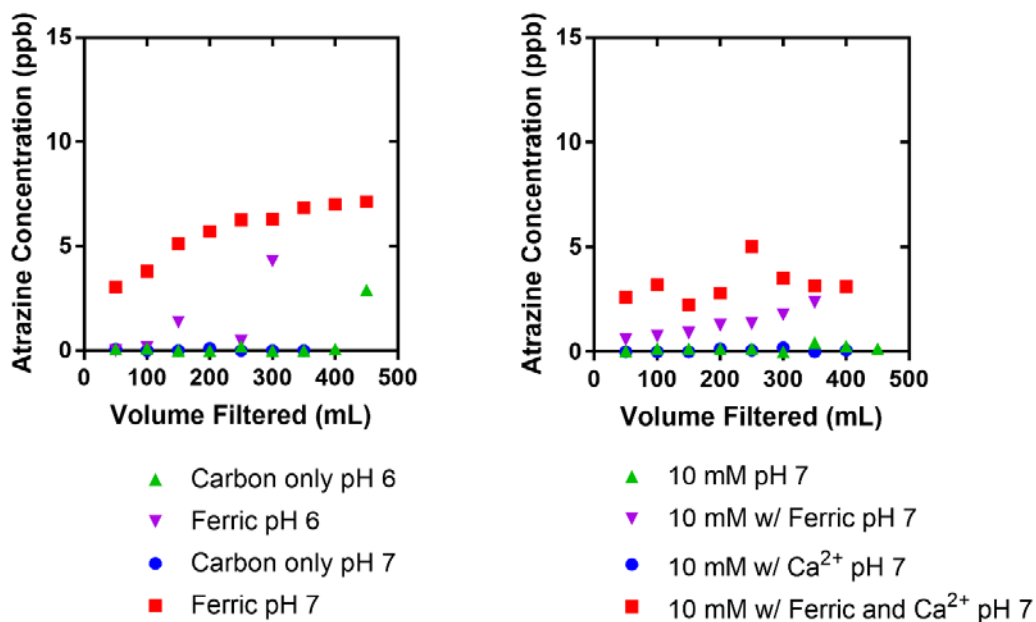


Figure 3.15. Atrazine concentrations in the permeate from 15 ppb atrazine in DDI filtered through carbon cakes formed from aggregated carbon. All trials with ferric chloride resulted in breakthrough, whereas trials without ferric chloride did not see breakthrough.

Flux and Adsorption Trade-off

A series of trials was performed with varied ferric chloride doses to examine how atrazine adsorption and filtration flux are affected by dose. Four parameters were measured: pH after coagulant addition, slope of cake resistance over time, turbidity after flocculation and without settling, and percent removal of atrazine using the carbon cake (Table 3.3). The pH after coagulation decreased with increasing ferric chloride dose, but the change in pH did not correlate with performance factors. Doses higher than 10 mg/L resulted in higher flux than the no dose case, while 5 mg/L resulted in the least fouling (Figure 3.16). The turbidity does not correlate significantly with filtration performance results. Atrazine removal is plotted against cake resistance increase in Figure 3.17. The trial without ferric chloride removed 100% of atrazine, while all trials with ferric chloride impacted atrazine removal to some extent. Most doses did not significantly impact removal, with doses of 5–20 mg/L removing over 90% of atrazine, but a dose of 40 mg/L only removed 68% of atrazine.

Table 3.3. Trials with varied ferric chloride dose resulted in trends in slope increase and atrazine removal. The pH correlated directly with the ferric chloride dose and did not affect performance. Neither was turbidity an indicator of performance.

Ferric Dose (mg/L)	pH after dose	Slope (1/μm/mL)	Turbidity (FAU)	ATZ Removal
0	7.03	3.70×10^4	105	100%
5	6.89	3.26×10^4	100	93%
10	6.71	5.39×10^4	75	93%
15	6.68	6.76×10^4	60	97%
20	6.57	7.47×10^4	60	96%
40	6.09	1.05×10^4	70	68%

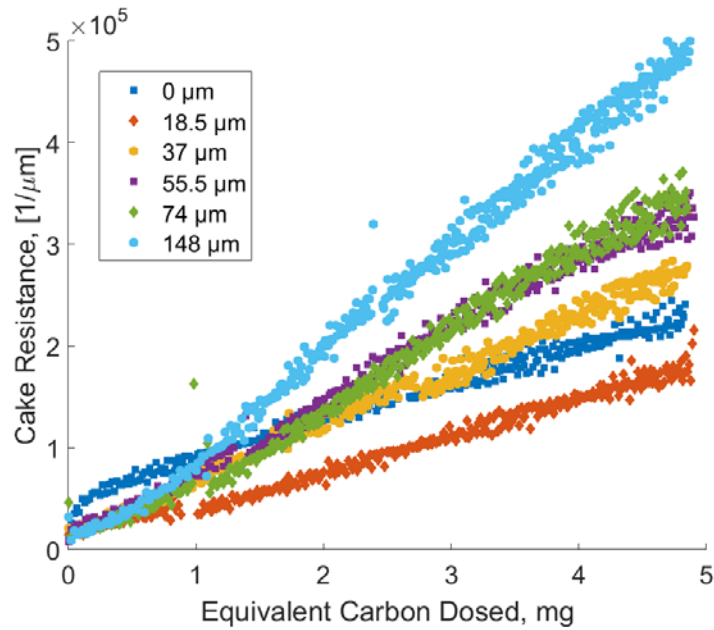


Figure 3.16. Growth in cake resistance associated with carbon aggregated with varied doses of ferric chloride. All trials include 60 mg/L of alkalinity as CaCO₃ and 10 mM ionic strength as NaCl.

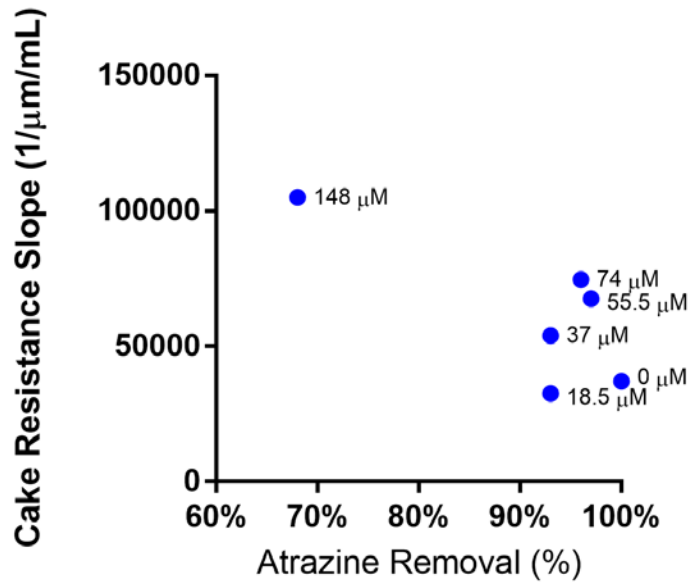


Figure 3.17. Atrazine removal is not heavily impacted by ferric dose, noted by data label, until very high doses. Moderate doses removed over 90% of atrazine, while no dose resulted in 100% atrazine removal.

Aggregation with NOM

NOM results in high membrane fouling even without the presence of carbon. Trials revealed that direct filtration of NOM and carbon aggregated with a chemical coagulant do not result in improved performance (Figure 3.18). Additionally, inclusion of ferric chloride negatively impacted atrazine removal, even though the presence of NOM did not affect atrazine removal (Figure 3.19). The structure of flocs formed from NOM with ferric chloride are large and therefore well suited to settling prior to filtration, but are not suited to membrane filtration. In a previous study, S-PAC was shown to alleviate membrane fouling due to NOM; it is likely that these results differ due to the minimal contact time between S-PAC and NOM prior to coagulant addition (Matsui et al., 2006).

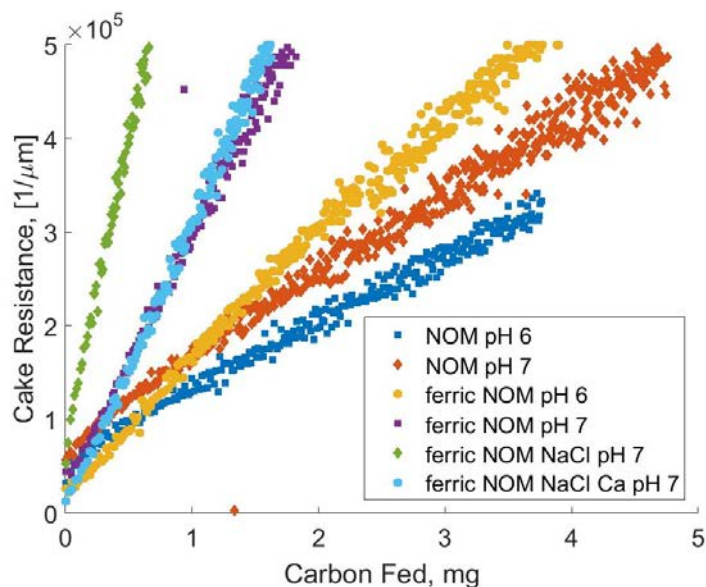


Figure 3.18. Addition of ferric chloride to direct filtration schemes containing NOM do not result in improved filtration performance.

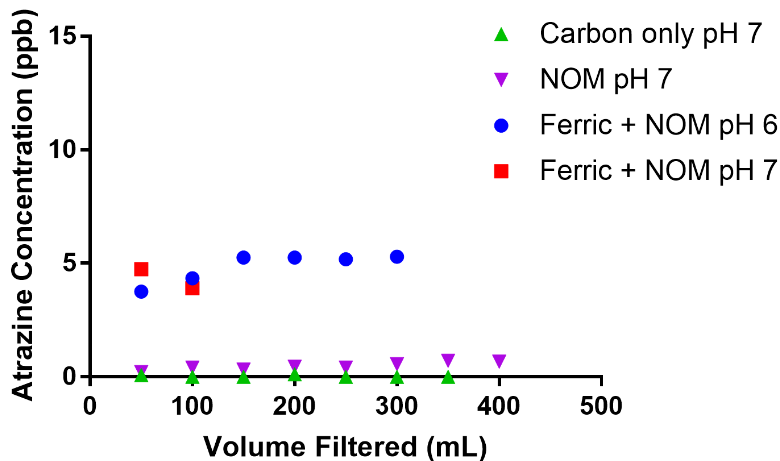


Figure 3.19. Atrazine is removed well by carbon alone and even carbon with NOM, however, the addition of ferric chloride negatively impacts atrazine removal.

Discussion

Chemical coagulants resulted in highly varied filtration performances. Mixed results have also been reported regarding the effect of coagulant use on membrane flux. One study found direct filtration of flocculated dissolved components using aluminum based coagulants led to high flux decline on 0.22 μm polymeric membranes (Wang et al., 2008), while another study found direct filtration with aluminum sulfate on a polymeric membrane did not result in fouling because stirring was incorporated (Lee et al., 2007). Another study using alum found that low doses, that is, less than required for enhanced coagulation, resulted in higher fouling than no dose at all (Howe and Clark, 2006). A comparative study examining ferric chloride, ferric sulfate, polyaluminum chloride, and aluminum sulfate found that aluminum sulfate resulted in the least flux decline

(Pikkarainen et al., 2004). The results here are in line with previous findings since no chemical coagulant performed consistently better than the case without coagulant.

A reason for poor filtration after floc formation can be attributed to a few possible mechanisms. The use of chemical coagulants introduces more mass into the cake layer so the resulting cake after flocculation must have a much higher permeability than the case without coagulant to result in less flux decline. Aggregates or flocs result in less predictable fouling than individual particles. If the flocs have a loose formation, they may compact during filtration to create a more resistant cake layer than the carbon alone. Flocs with a lower fractal dimension, that is, a less complex shape closer to a sphere, result in higher permeability as a cake than flocs with a higher fractal dimension, which have a higher porosity but intermesh to create a less permeable cake (Chellam and Wiesner, 1993; Waite et al., 1999). Fractal dimension has been evaluated previously with computational analysis of high contrast imaging; another analytical method utilizes a confocal scanning laser microscope which is able to image cross-sections through a volume (Thill et al., 1998; Chakraborti et al., 2000). Properties of flocs are a function of water quality, coagulant dose, and shear rate, in addition to parameters of the aggregated material.

Floc strength is a factor due to the turbulence introduced by the filtration system. Flocs with low strength may not withstand the shear stresses introduced filtration. Once broken apart, the flocs no longer have achieved the intention of increased effective particle size. One option to avoid turbulence in the system and avoid floc degradation is to filter under negative pressure through a submerged membrane.

The contribution of chemical coagulants to the formation of high fouling components is unclear. Settling tests revealed that non-settling components severely fouled the membrane. The particles may be precipitates from excess coagulant. The particle size of ferric hydroxides can range from half a micrometer to a few micrometers in diameter, which are on the order of size of carbon particles and larger than the membrane pore size (Hove et al., 2007). A trial with only coagulant and without carbon would reveal whether enough precipitation to cause membrane fouling would occur under the experimental conditions.

Another possible reason for high fouling when coagulant is used is that carbon cannot effectively use all of the coagulant dosed since carbon is denser than typical flocs produced by water treatment. In that case, NOM should utilize excess coagulant and prevent the formation of small particulates that can foul the membrane, as demonstrated through the settling tests. The initial results presented here do not support the idea that coagulant can improve filtration of a system with NOM and carbon, but not all factors are considered. While dosing was optimized to produce visible flocs with the least coagulant, flocculation in a system containing NOM may require other optimization such as the duration and intensity of mixing for coagulation and flocculation.

Conclusions

- The addition of coagulants to increase particle aggregation and reduce fouling was not successful in all cases. It appears the coagulant itself contributed to fouling.
- One contributor to fouling is small, non-settling particles. the formation unflocculated metal precipitates that adsorb to the membrane surface and pore

channels. In settled experiments, fouling was nearly as high as disaggregated particle despite much less mass being filtered. Therefore, small suspended material after flocculation are higher contributors to fouling than the carbon particles themselves.

- Another contributor is interparticle bridging between metals and particles that result in less permeable meshes when compacted on the membrane. Tests with calcium showed that particle aggregation in the absence of metal precipitates did not result in high fouling. Therefore, in the absence of interparticle bridging but still with a larger effective particle size, fouling was mitigated.
- The next step is to evaluate the ability to backwash S-PAC from a membrane with and without chemical coagulants. Precise dosing to reduce fouling is likely extremely difficult, but there may be a trade-off in the ability to remove the S-PAC from the membrane after filtration.

CHAPTER FOUR

EFFECT OF BEAD MILLING ON CHEMICAL AND PHYSICAL CHARACTERISTICS OF S-PAC

Motivation

To date, there has been only a small number of studies on S-PAC, each with limited reporting of material parameters. With a limited data set, using material parameters to understand S-PAC performance is difficult. Additionally, the conditions of S-PAC production in published research are not reported in great detail, which discourages data aggregation and analysis. This study systematically examines a number of carbon types under varying degrees of milling in order to elucidate specific effects of wet milling on the chemical and physical characteristics of activated carbons.

Materials and Methods

Activated Carbon

Activated carbon materials were obtained from several commercial sources and chosen to cover a range of source materials and characteristics. Seven commercial carbons were used with variation in specific surface area, pore volume, and pH_{PZC} : Watercarb-800 (bituminous coal, Standard Purification), Filtrasorb 400 (bituminous coal, Calgon), PAC 20 B (bituminous coal, Norit), Hydrodarco 3000 (lignite coal, Norit), Hydrodarco B (lignite coal, Norit), Aqua Nuchar (wood, Mead Westvaco), and Aquacarb 1230C (coconut shell, Siemens). The carbons are labeled as BC1, BC2, BC3, LC1, LC2, WD, and CS, respectively (Table 4.1). BC1, BC3, LC2, and WD were received as PAC, and they were sufficiently small to pass the 200 μm mesh screen within the bead mill. LC1, BC2, and CS

were received as GAC, and they were processed using a coffee grinder and sieved through a #100 screen (150 μm openings) to isolate the smaller particles for milling.

Table 4.1. Measured characteristics of parent PAC materials: specific surface area, total pore volume, and point of zero charge (pH_{PZC}). Seven PACs were milled including coal, wood, and coconut shell based materials.

Origin Material	Label	Product Name	PAC Size (μm)	Specific Surface Area (m^2/g)	Specific Pore Volume (cm^3/g)	pH_{PZC}
Bituminous Coal	BC1	Watercarb-800	12.3	644	0.35	10.37
Bituminous Coal	BC2	Filtrisorb 400	11.3	1038	0.67	8.65
Bituminous Coal	BC3	PAC 20 B	13.6	880	0.48	9.79
Wood	WD	Aqua Nuchar	11.3	1676	0.89	6.20
Coconut Shell	CS	Aquacarb 1230C	11.3	1027	0.72	10.79
Lignite Coal	LC1	Hydrodarco 3000	12.8	660	0.61	5.39
Lignite Coal	LC2	Hydrodarco B	13.5	505	0.39	11.40

Wet Milling Procedure

PAC was pulverized to S-PAC using a bead mill (MiniCer, Netzsch Premier Technologies, Exton, PA, USA) containing 0.3–0.5 mm yttrium-stabilized zirconium oxide ceramic beads. The mill was operated at 85% loading capacity; 120 mL of beads were measured with a graduated cylinder and added to the 140 mL mill. Thus, the design mill void was 20 mL, but the total mill void was 50 mL after accounting for void space when measuring the beads. The 120 mL loading volume corresponds to approximately 2 million beads. PAC was added to the mill as a slurry comprised of 24 grams of dry carbon in 300 mL of distilled and deionized water (DDI) with 18 $\text{M}\Omega$ resistivity, yielding a percent solids concentration of approximately 6–7%. The slurry was kept chilled at 10 $^{\circ}\text{C}$ during milling.

It is common in milling applications to use a dispersant to aid the milling process. Without dispersants the breakup of particles results in an increase in solution viscosity;

dispersants help maintain fluidity and decrease pumping energy. One dispersant type (Reax, Mead Westvaco) was tested to evaluate its effects on carbon milling; however, all of the samples used for further characterization were milled with no dispersant addition.

Characterization Methods

Milled and unmilled carbons were analyzed for physical and chemical parameters. Elemental analysis, measuring weight percent compositions of carbon, oxygen, hydrogen, and nitrogen, was performed using a Flash Elemental Analyzer 1112 series (Thermo Electron Corporation). Sizes for particles less than 6 μm in diameter were measured using dynamic light scattering (DLS) with a Zetasizer NanoZS (Malvern, Worcestershire, UK). Readings were taken in distilled water after bath sonication and Z-avg hydrodynamic diameters are reported. Particles larger than 6 μm were measured by optical microscopy imaging using a Zeiss Axioskop 2 Plus optical microscope with a Zeiss AxioCam MRc5 camera attachment running AxioVision AC version 4.2 software. Particles were sonicated in DDI before imaging and Zeiss Immersionsol 518C immersion oil was used to view the particles at 40x magnification. The images were processed using ImageJ software to determine the average Feret diameter of the particles and the particle size distribution. Particles were also visually observed with scanning electron microscopy (SEM, Hitachi SU6600) of uncoated dry carbons. Nitrogen gas adsorption was performed at 77 K with an ASAP 2020 analyzer (Micromeritics Instrument Corp. U.S.) and pore size distributions were determined using density functional theory (DFT) and calculated surface area from the Brunauer-Emmett-Teller (BET) equation. The DFT model allows for categorization of pore volumes into micropore (< 2 nm), mesopore (2–50 nm), and macropore (> 50 nm)

fractions. pH_{PZC} in the bulk material was measured by a pH drift method where the point of zero charge is defined as the pH where no drift occurs after 48 hours (Lopez-Ramon et al., 1999; Dastgheib et al., 2004). For each pH point and carbon, 100 mg of dry carbon were added to 20 mL of pH adjusted 0.1 M NaCl in a CO_2 -free atmosphere. After a minimum of 48 hours on a shaker table, pH was measured in each vial and compared to a no carbon blank. The isoelectric point (pH_{IEP}) of the carbon was determined by measuring the zeta potential of S-PACs using the Zetasizer NanoZS (Malvern, Worcestershire, UK) and observing the pH that produced a zeta potential reading of zero. Samples were prepared by probe sonication in DDI and manually titrated for pH adjustment.

Results and Discussion

All S-PAC samples were produced using the same flow rate, mill loading, and mill rotational speed; thus, the rate of energy transfer to the carbon particles was kept constant through all tests. Total energy applied was varied by changing the total milling time, which varied from one pass through the mill to six hours. In the one pass scenario carbon was fed into the mill and then collected as product in the output. This was repeated once more for the two-pass scenario. Each pass took approximately 45 seconds. In all other millings, the carbon slurry was recirculated through the system by connecting the output line back to the feed tank.

Each pass through the mill corresponded with approximately 5 seconds of contact time through the 50 mL mill void. A milling time of 30 minutes corresponded to approximately 40 passes through the mill based on average residence time; due to short circuiting and dead zones, the true number of passes was likely higher for some particles

and lower for others. Additionally, viscosity increased at different rates for each carbon, so the number of passes made by one carbon may differ slightly from the number made by a different carbon due to a changing flow rate. DDI was added as needed to allow for complete mixing, but kept to a minimum. To examine the effect of dispersant on milling, WD was milled with varying dispersant concentrations. Dispersant mitigated viscosity increase, reducing the need to add DDI, and did not affect the particle size reduction. Notably, the coconut shell-based carbon, CS, did not noticeably increase in viscosity though no dispersant was added. As mentioned previously, none of the samples milled with dispersants were used for further characterization in this study.

Particle Size Effects

PAC particle sizes were very similar among carbons, with median sizes ranging from 11 to 14 μm (Table 4.1). Milling times as brief as one pass through the mill resulted in particle sizes near or below one micrometer and subsequent milling further reduced median particle sizes but with diminishing returns (Figure 4.1). Due to the different analytical measurements for determining particle size above and below 6 micrometers—DLS for smaller particles and visible-light microscope image analysis for larger ones—comparison of S-PAC size with parent PAC is indirect. The hydrodynamic diameter measurements from DLS are found using models that assume spherical shape. The spherical assumption is supported by SEM images, especially for particles milled for longer times, but particles milled for shorter times have more angularity. SEM also qualitatively supports Z-avg particle size measurements with observable declines in particle size as milling time increases. Images of PAC and all S-PACs from BC1 taken by SEM at 10,000

times magnification reveal the range of particle sizes from large PAC and 1 pass particles to small particles after 6 hrs that have a tendency to aggregate (Figure 4.2). The smallest particles—after 1 hr, 2 hrs, and 6 hrs—were also imaged at 20,000 times magnification where individual particles are more clearly identifiable (Figure 4.3).

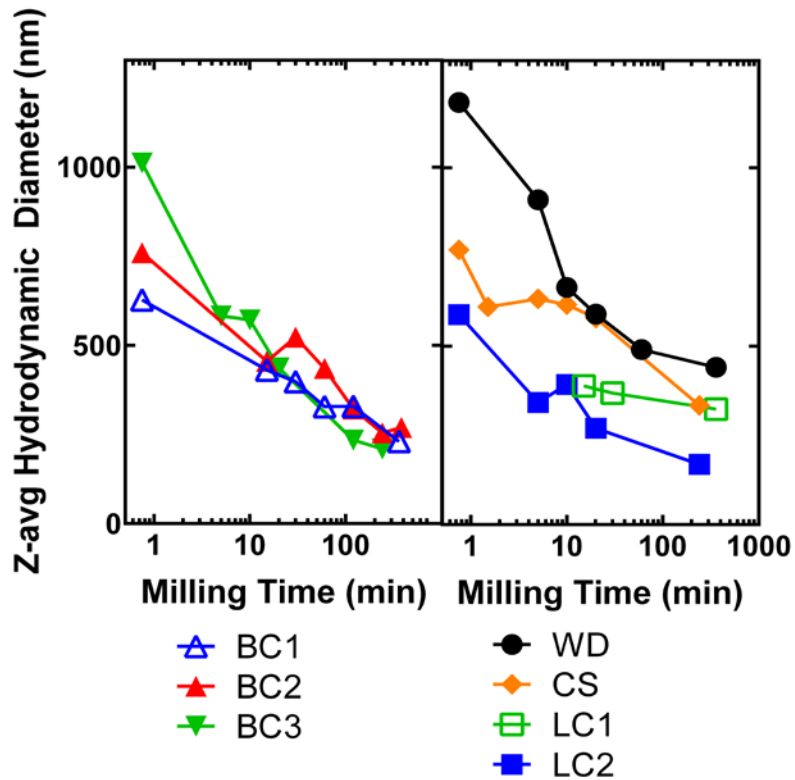


Figure 4.1. Particle size of milled carbons with milling times varied from one pass through the mill to 6.3 hours. Data is split into two panes to avoid excessive overlap.

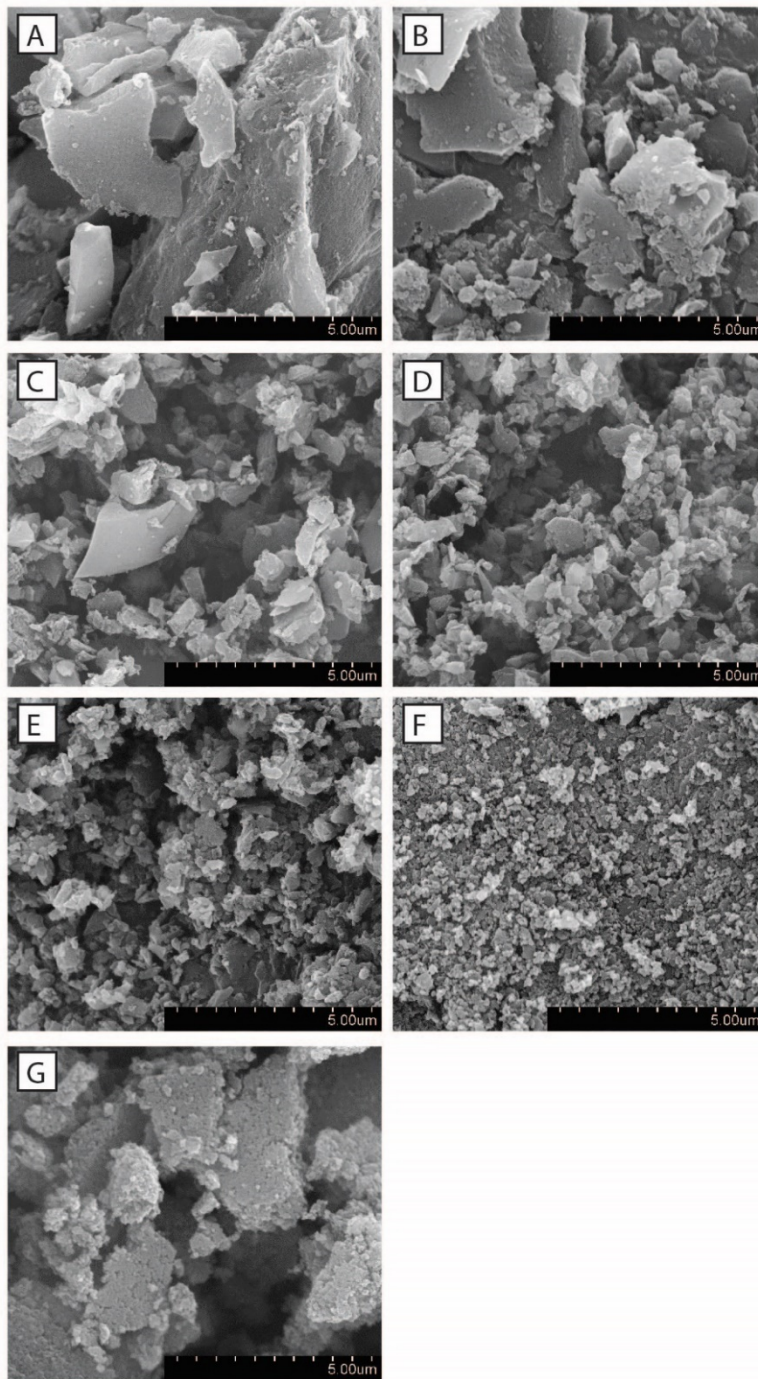


Figure 4.2. Scanning electron microscopy images (10K magnification) of all forms of BC1, including PAC (A) and all S-PACs. Particles visibly decrease in size as milling increases from 1 pass (B) to 15 min (C), 30 min (D), 1 hr (E), 2 hrs (F), and 6 hrs (G).

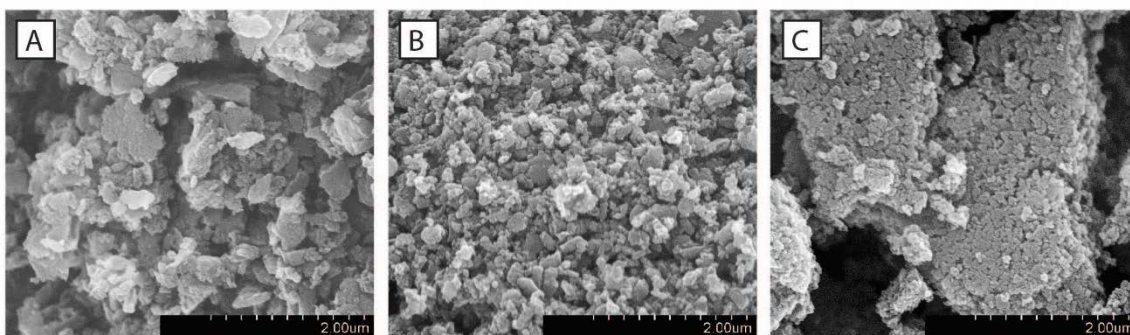


Figure 4.3. Scanning electron microscopy images (20K magnification) of BC1 after milling for 1 hr (A), 2 hrs (B), and 6 hrs (C). Particle size differences are apparent.

The longest milling times resulted in the smallest particle sizes for each carbon. Most carbons reduced to median particle sizes of 200–400 nm; the largest size was 440 nm for WD after 6 hours of milling and the smallest was LC2 at 170 nm after 4 hours of milling (Figure 4.1). In addition to producing the smallest S-PAC, LC2 also had the largest reduction in size in the shortest time; particles had a median size of 342 nm after 5 minutes and 270 nm after 20 minutes. The second lignite-based carbon, LC1, also exhibited relatively fast size reduction resulting in a median size of 390 nm after 15 minutes; however, it did not continue decreasing in size with further milling, with a size of 324 nm after 6 hours. WD, BC2, and CS had little particle breakdown under short milling times, with median sizes above 700 nm and up to 1000 nm in the case of WD after one pass through the mill.

Overall, CS and WD were the slowest to decrease in size during milling, as seen by a low slope in its concentration over milling time (Figure 4.4). Concentration was calculated from measured average particle sizes and conservation of mass; a decreased average particle size corresponds to an increase in the number of particles. Most carbons

exhibited nearly linear trends of increase in particle concentration; LC2 had the fastest breakdown, followed by BC3. BC1 and BC2 had similar rates. WD and LC1 had nonlinear trends with rates that leveled off after reaching a minimum particle size.

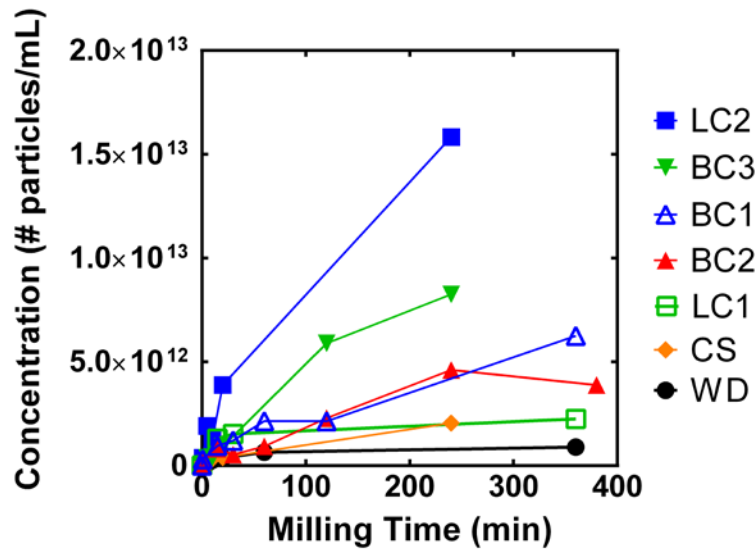


Figure 4.4. Concentration of particles increases as particle size decreases. Concentrations were calculated from measured average particle sizes and conservation of mass.

The particle size results indicate that the same milling energy has different results for different carbons. The three bituminous coals exhibited similar milling responses. The lignite coals acted similarly at first, but one continued to decrease in particle size while the other leveled off. Both WD and CS remained as large particles after initial milling, though CS responded to continued milling while WD did not. Thus, the rates of particle breakdown as well as the minimum achievable particle size were highly specific to each carbon and generalizations based on material are difficult to draw.

Carbon Chemical Properties

Carbons were measured for elemental composition, surface charge via pH, surface charge via electrokinetics, and ash content. Milling did not result in changes to the percent content of carbon, hydrogen, and nitrogen in any of the samples (Table 4.2). Similarly, the ash content did not change significantly as a result of milling (Figure 4.5). Therefore, inert materials are not susceptible to alternation within the milling environment.

Table 4.2. Elemental analysis of PAC and S-PAC for four carbons in terms of carbon content, hydrogen content, and nitrogen content by weight percent.

Carbon	Carbon Content (%)	Hydrogen Content (%)	Nitrogen Content (%)	Carbon	Carbon Content (%)	Hydrogen Content (%)	Nitrogen Content (%)
BC1				WD			
PAC	77.09	0.34	0.48	PAC	84.45	1.03	0.40
1 pass	77.88	0.48	0.39	1 pass	85.20	0.97	0.46
15 min	75.96	0.32	0.19	5 min	84.91	1.05	0.51
30 min	75.78	0.29	0.27	10 min	84.44	1.06	0.54
1 hr	73.65	0.57	0.15	20 min	84.01	1.11	0.48
2 hrs	73.67	0.74	0.40	1 hr	82.92	0.83	0.85
6 hrs	67.48	0.88	0.23	6 hrs	80.84	1.13	0.85
BC2				CS			
PAC	89.06	0.00	0.10	PAC	90.94	0.00	0.01
1 pass	84.35	0.08	0.22	1 pass	97.06	0.20	0.01
15 min	85.70	0.00	0.18	2 pass	94.29	0.06	0.01
30 min	84.85	0.02	0.18	5 min	80.42	0.22	0.01
1 hr	84.06	0.03	0.23	10 min	91.56	0.06	0.01
2 hrs	82.30	0.08	0.22	20 min	90.95	0.05	0.03
4 hrs	82.45	0.09	0.23	4 hrs	87.11	0.13	0.05
6.33 hrs	79.59	0.05	0.23				

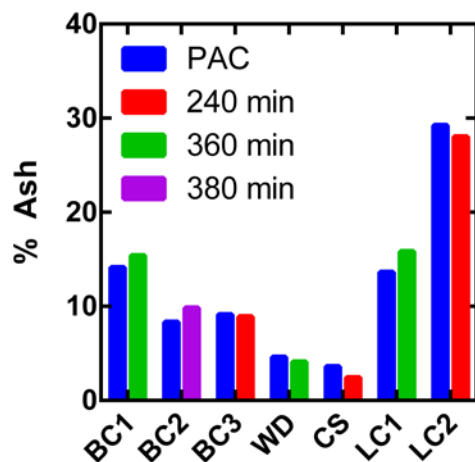


Figure 4.5. Ash content of PAC and S-PAC with the longest milling time for each carbon. Milling times are denoted by color. No trends are seen in changes between PAC and S-PAC.

The majority of PACs had a basic pH_{PZC} , though WD was neutral and LC1 had an acidic pH_{PZC} . As milling time increased, the pH_{PZC} of all carbons decreased and the oxygen content of all carbons increased (Table 4.3). LC1 and LC2 had the least observed pH_{PZC} change, shifting down about half a pH point, while the other carbons dropped approximately two pH points over the longest milling times. BC1, BC2, and BC3 had similar PAC oxygen content around 2%, and increased to 4.87%, 6.45%, and 7.86%, respectively. WD had the highest initial oxygen content, 7.14%, as well as the highest final oxygen content, 10.50%. CS experienced the smallest increase in oxygen content from 3.38% to 5.38%. pH_{PZC} values were inversely correlated with oxygen content (Figure 4.6). CS, BC2, and BC3 correlated with an R^2 above 0.95 while WD and BC1 had R^2 values of 0.90 and 0.83, respectively. A decrease in pH_{PZC} and an increase in oxygen content as a result of milling have been reported previously (Dunn and Knappe,

2013). The data shown here for several milling times provide convincing evidence that these changes are directly caused by milling.

Table 4.3. Surface charge properties measured by point of zero charge, isoelectric point, and percent oxygen content. The difference between pH_{PZC} and pH_{IEP} is shown as ΔpH . Carbons are distinguished by material and milling time. Dashed lines indicate that measurements were not taken.

Carbon	pH_{PZC}	pH_{IEP}	ΔpH	Oxygen Content (w/w%)	Carbon	pH_{PZC}	pH_{IEP}	ΔpH	Oxygen Content (w/w%)
BC1					WD				
PAC	10.37	--	--	2.41	PAC	6.20	--	--	7.14
1 pass	9.31	3.27	6.04	2.79	1 pass	6.25	2.48	3.77	7.25
15 min	9.09	2.92	6.17	3.51	5 min	6.03	2.78	3.25	7.80
30 min	8.92	2.71	6.21	4.19	10 min	5.72	2.87	2.85	7.85
1 hr	8.07	2.57	5.50	5.23	20 min	5.82	3.06	2.76	8.30
2 hrs	8.10	4.17	3.93	5.87	1 hr	5.11	2.67	2.44	9.15
6 hrs	7.75	2.64	5.11	7.86	6 hrs	4.95	2.84	2.11	10.50
BC2					CS				
PAC	8.65	--	--	2.29	PAC	10.79	--	--	3.38
1 pass	8.62	3.32	5.30	2.34	1 pass	10.73	2.39	8.34	3.71
15 min	8.65	3.85	4.80	2.82	2 pass	10.44	2.86	7.58	3.84
30 min	8.25	3.91	4.34	3.28	5 min	10.57	3.15	7.42	3.91
1 hr	6.78	3.86	2.92	3.95	10 min	10.47	3.09	7.38	3.99
2 hrs	6.7	3.71	2.99	5.29	20 min	10.33	2.75	7.58	4.06
4 hrs	6.42	3.87	2.55	5.34	4 hrs	8.00	3.39	4.61	5.38
6.33 hrs	5.74	4.36	1.38	6.45	LC1				
BC3					PAC	5.39	--	--	3.42
PAC	9.79	--	--	1.6	15 min	5.52	--	--	--
1 pass	9.37	--	--	2.23	30 min	5.55	--	--	--
5 min	9.00	--	--	2.44	6 hrs	4.85	--	--	6.76
10 min	8.72	--	--	2.94	LC2				
20 min	8.50	--	--	3.44	PAC	11.58	--	--	5.52
2 hrs	7.38	--	--	4.85	1 pass	9.55	--	--	--
4 hrs	7.05	--	--	4.87	5 min	9.39	--	--	--
					10 min	9.28	--	--	--
					20 min	9.22	--	--	--
					4 hrs	9.01	--	--	9.49

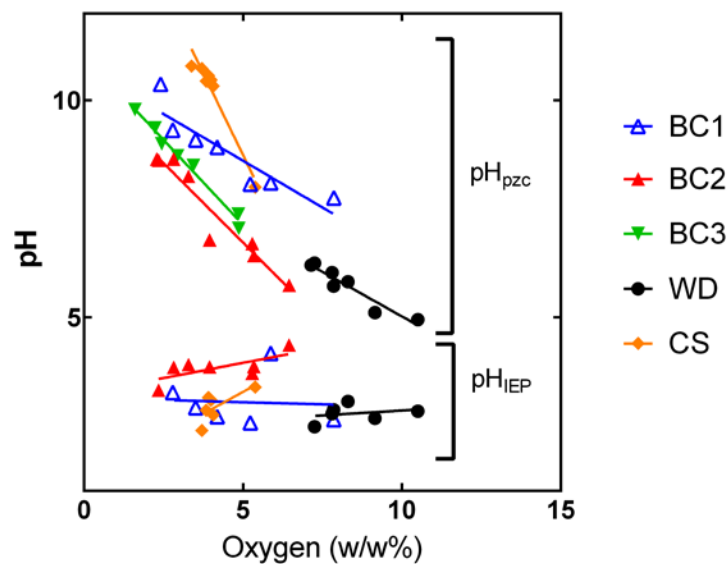


Figure 4.6. Decreases in pH_{PZC} correlated strongly with increases in weight percent of oxygen while pH_{IEP} measurements did not correlate with oxygen. Linear regression of pH_{PZC} data found R^2 values of 0.83, 0.93, 0.98, 0.95, and 0.90 for BC1, BC2, BC3, WD, and CS, respectively. Linear regression of pH_{IEP} data found R^2 values of 0.00, 0.49, 0.07, and 0.50 for BC1, BC2, WD, and CS, respectively.

With two measures of pH, pH_{IEP} values could be expected to decrease following pH_{PZC} values. Interestingly, pH_{IEP} did not change appreciably with milling time, and thus also did not correlate with oxygen increases. Additionally, the values were notably lower than pH_{PZC} values, ranging from approximately 2.4 to 4.2 for the S-PAC of four carbons. The pH_{IEP} of PAC could not be measured using the electrophoretic mobility technique since the PAC particles settled too quickly, thus, while it is clear that pH_{IEP} remained unchanged among S-PAC, it is unclear whether the pH_{IEP} changed during the initial pass of PAC through the mill.

The difference in pH_{PZC} and pH_{IEP} is a result of the qualities measured by each technique. The pH drift method for pH_{PZC} utilized in this study used a 48-hour equilibration time, thus allowing for complete diffusion of solutes into and out of carbon pores. The pH_{PZC} is thus a measure of acidity throughout the carbon material. pH_{IEP} measurements are based on electrophoretic movement which is affected only by charges on the outer surface of the carbon; charged functional groups within the pores should have little or no effect on pH_{IEP} . There are two possible mechanisms for a decreasing pH_{PZC} and unchanging pH_{IEP} : either chemical changes are only occurring at internal sites, which are measured by pH_{PZC} but not pH_{IEP} , or chemical changes are happening rapidly at external sites, wherein all S-PAC have the same external condition and the average pH value decreases as particle size decreases and total external surface area increases. The second scenario is consistent with previous work in activated carbon where it has been reported that incomplete oxidation results in preferential oxidation on the external surface, and can be indicated by measuring both pH_{IEP} and pH_{PZC} (Menendez et al., 1995). The low and unchanging pH_{IEP} values imply that there are similar external surface charge densities of an acidic nature on all S-PAC, regardless of milling time. Correlation between pH shifts and specific external surface area, calculated from particle size measurements, reveal that the second mechanism is more likely; the difference between pH_{PZC} and pH_{IEP} is used as the correlating pH factor here and is termed ΔpH (Figure 4.7). WD, CS, and BC2 had R^2 values above 0.90 while BC1 had a poor correlation due to an outlier point. Oxygen increases also correlated strongly with specific external surface area, which is consistent with the idea that oxidation is happening primarily on the external surfaces (Figure 4.8). The concept of an easily

oxidized surface, once exposed to the abrasive milling environment, is sketched in Figure 4.9 and shows 1) the initial surface oxygen groups 2) the breakup of particles to create new external surface area, and 3) the subsequent oxidation of those new surfaces.

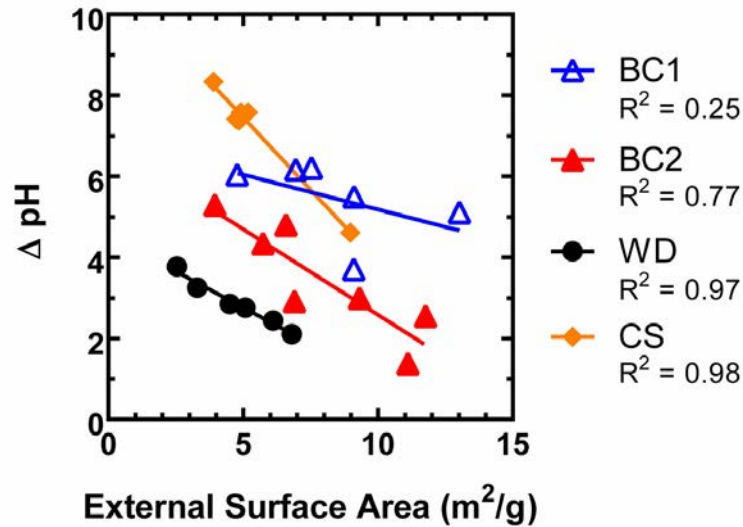


Figure 4.7. The difference between pH measured using the pH_{PZC} method and the electrokinetic measurement of the isoelectric point is correlated with the S-PAC external surface area, which increases as particle size decreases.

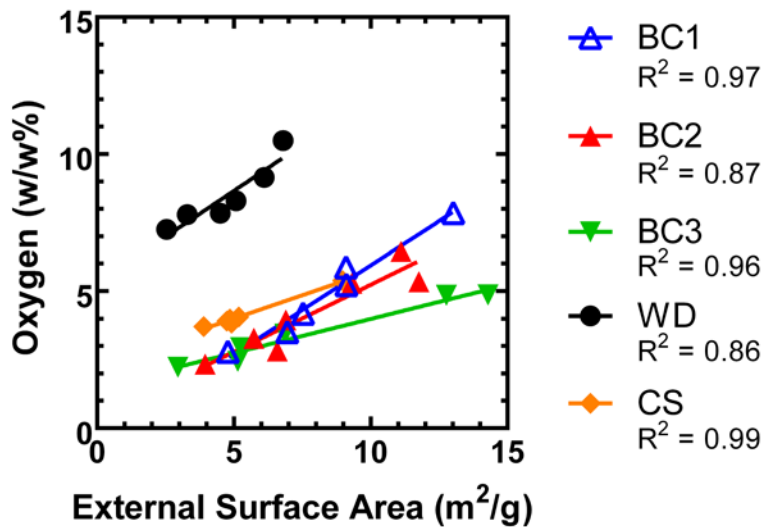


Figure 4.8. Oxygen increased with newly revealed surface area as a result of milling. External surface area was calculated from Z-avg particle size measurements.

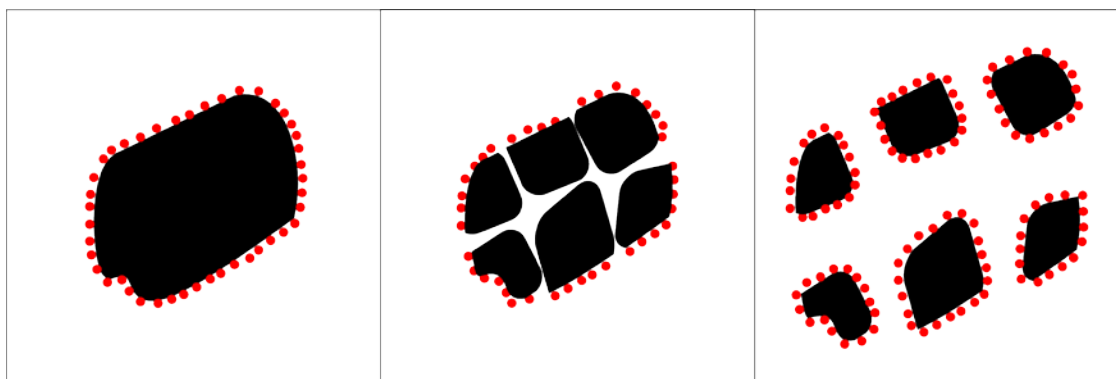


Figure 4.9. Illustration of PAC pulverization into S-PAC with proposed rapid surface oxidation.

Manifestation of oxygen on the outer surfaces occurs in multiple ways, such as through the formation of organic surface functional groups, or through inorganic oxidation. The variety of oxygen-containing surface functional groups that can occur at graphite edges in activated carbon have been documented (Boehm, 1994; Biniak et al., 2007). Based on the approximate mass of oxygen attached to S-PAC as a result of milling—2–5% by weight, or 0.13–0.31 mmol of oxygen per gram of carbon—the external surface concentration of oxygen-containing functional groups is on the order of 0.02 mmol/m². Percent oxygen increase between PAC and S-PAC correlated well with total ash content, and even better when only considering potentially reactive elements: Ca, Mg, Zn, Cu, Mn, Fe, and Al (Figure 4.10). The high correlation is likely the result of thorough surface oxidation on elements evenly distributed throughout the carbon matrix, however, its contribution is limited: for a concentration of divalent elements of approximately 10 mmol per gram of carbon, it is likely that only 1% of those elements would be accessible on external surfaces for oxidation, or 0.01 mmol/m².

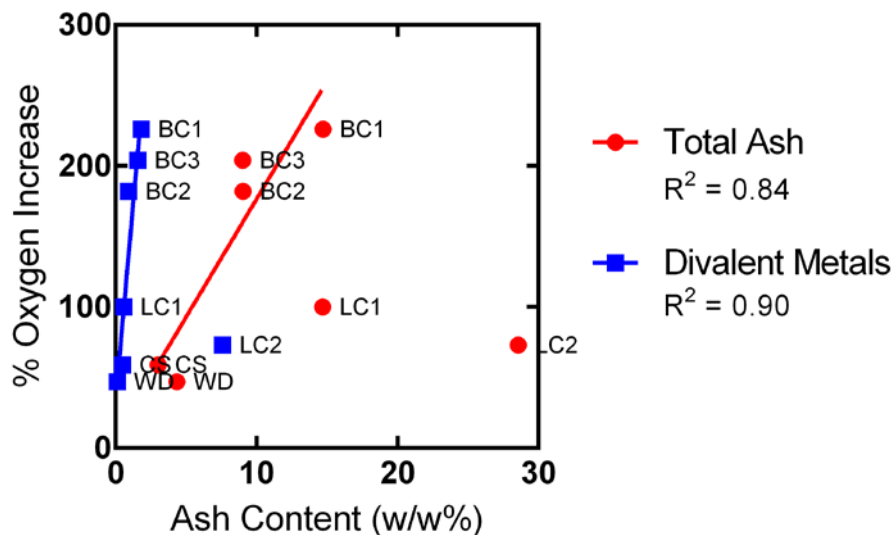


Figure 4.10. Oxygen increases correlated with the content of select metals in the carbons, averaged between PAC and the longest milled S-PAC. Linear regression was performed without the outlier LC2 for divalent elements, and without the outliers LC1 and LC2 for total ash.

Carbon Physical Properties

Total pore volume and distributions of volume to micropores, mesopores, and macropores shifted slightly as a result of milling (Table 4.4). BC1, BC2, BC3 and CS increased in the mesoporous fraction. BC2 increased in its macroporous fraction as well. WD had a decreased mesoporous fraction and an increased macroporous fraction. Primary and sub- microporous fractions—pores with diameters less than 1 nm (10 angstroms) and from 1 nm to 2 nm, respectively— were also examined due to their importance in adsorption of small molecules; however, there was little difference observed with respect to increased milling time (Stoeckli et al., 1993).

Table 4.4. Surface area and pore volume measurements for seven activated carbons.

Carbon	Specific Surface Area (m ² /g)	Total Pore Volume (cm ³ /g)	Macropore Volume (cm ³ /g)	Mesopore Volume (cm ³ /g)	Sub-micropore Volume (cm ³ /g)	Primary Micropore Volume (cm ³ /g)
BC1						
PAC	644	0.35	0.04	0.09	0.08	0.14
1 pass	777	0.44	0.05	0.13	0.08	0.18
15 min	786	0.32	0.07	0.07	0.13	0.05
30 min	857	0.49	0.07	0.13	0.09	0.20
1 hr	872	0.35	0.10	0.09	0.12	0.04
2 hrs	642	0.53	0.23	0.15	0.13	0.03
6 hrs	762	0.69	0.11	0.33	0.10	0.15
BC2						
PAC	991	0.50	0.04	0.10	0.15	0.21
1 pass	917	0.46	0.03	0.11	0.16	0.16
15 min	1019	0.54	0.07	0.12	0.17	0.19
30 min	1179	0.67	0.10	0.19	0.20	0.18
1 hr	1047	0.58	0.09	0.15	0.16	0.18
2 hrs	1010	0.56	0.12	0.13	0.15	0.15
4 hrs	997	0.56	0.14	0.14	0.10	0.15
6.33 hrs	872	0.69	0.17	0.28	0.12	0.13
BC3						
PAC	890	0.48	0.03	0.14	0.11	0.20
1 pass	931	0.56	0.08	0.16	0.15	0.18
5 min	802	0.43	0.05	0.12	0.12	0.15
10 min	881	0.47	0.05	0.14	0.13	0.15
20 min	895	0.51	0.07	0.16	0.13	0.16
2 hrs	890	1.04	0.42	0.37	0.14	0.11
4 hrs	798	0.73	0.19	0.28	0.10	0.15
WD						
PAC	1676	0.89	0.03	0.49	0.37	0.00
1 pass	1642	1.05	0.05	0.68	0.32	0.00
5 min	1575	0.99	0.06	0.63	0.31	0.00
10 min	1542	0.96	0.07	0.60	0.30	0.00
20 min	1521	0.91	0.06	0.55	0.29	0.02
1 hr	1269	0.89	0.13	0.45	0.23	0.09
6 hrs	1008	0.84	0.28	0.29	0.25	0.02
CS						
PAC	906	0.47	0.12	0.00	0.09	0.26
1 pass	1134	0.49	0.04	0.01	0.15	0.28
2 pass	895	0.39	0.03	0.02	0.12	0.23
5 min	932	0.42	0.04	0.02	0.13	0.23
10 min	938	0.42	0.05	0.01	0.14	0.23
20 min	1047	0.46	0.08	0.00	0.16	0.22
4 hrs	1050	0.50	0.09	0.09	0.17	0.15
LC1						
PAC	660	0.61	0.08	0.36	0.05	0.12
15 min	--	--	--	--	--	--
30 min	--	--	--	--	--	--
6 hrs	713	0.69	0.12	0.40	0.06	0.12
LC2						
PAC	505	0.39	0.05	0.19	0.04	0.11
1 pass	--	--	--	--	--	--
5 min	--	--	--	--	--	--
10 min	--	--	--	--	--	--
20 min	--	--	--	--	--	--
4 hrs	555	0.56	0.14	0.33	0.08	0.01

Macropore (> 50 nm); mesopore (2–50 nm); submicropore (1–2 nm); primary micropore (> 1 nm)

Changes to pore volumes were not a distinct function of milling time, though it is reasonable that shifts in pore volume distributions following milling will trend towards increases in meso- and macroporous fractions as internal pores are opened. Most notable is the development of a mesoporous fraction in the longest milled S-PAC of CS where previously there was none. Typically—and CS PAC was no exception—coconut-shell based activated carbons are microporous upon activation (Crittenden et al., 2005). Thus, despite a lack of direct correlation between milling and physical changes to the carbons, changes were observed that may still have an impact on adsorption performance.

Surface areas were also generally unchanged, with the exception of WD, which decreased from over 1500 m²/g to 1000 m²/g. It is likely that WD had thinner pore walls than other carbons, as indicated by a high specific surface area, and thus had channels that were easily crushed during milling. In practice it may be possible to avoid crushing pore channels by optimizing milling conditions, including reduction of milling time, operation at lower mill power, or processing at a lower percent solids content.

Comparison with S-PAC in Literature

A handful of publications over the past decade have explored milled carbon for use as an adsorbent; however, since most of these studies focus on adsorption performance, few have reported detailed physical and chemical carbon characteristics differences (Matsui et al., 2005, 2007, 2008, 2009a, 2013, 2014; Heijman et al., 2009b; Ando et al., 2010; Dunn and Knappe, 2013; Ellerie et al., 2013). Available characterization data was extracted from those publications and is presented in Table 4.5. Here we consider all reported carbons with sizes under one micrometer. All studies reported particle size, which

have been measured by various techniques, including dynamic light scattering (DLS), laser light scattering (LLS), laser diffraction, LED measurement, and optical and scanning electron microscopy. After particle size, surface area, as measured by nitrogen adsorption, was the next most common parameter reported. Since particle size and surface area are two characteristics often used to describe performance of PAC, reporting of these parameters is logical. Some papers have reported carbon characteristics not examined in this study, including uniformity coefficient and geometric standard deviation as related to particle size. The next most commonly reported parameters regard micropore fractions and mesopore fractions, though reporting is inconsistent; some studies report the volume of the pore fraction while others report the surface area of the pore fraction. The total pore volume is rarely reported. Lastly, pH_{PZC} has only been reported by Ellerie et al. (2013) and Dunn and Knappe (2013). Notably, only Dunn and Knappe (2013) have reported oxygen content (not included in the table). It is clear that data gaps exist for an analysis of S-PAC beyond particle size and select physical characteristics.

Another data gap lies in the reporting of milling parameters. No paper has discussed the details of milling beyond a description of the grinding media and, in one case, the milling duration. It is clear from the number of variables present in wet milling, and the variety of carbons produced in this study, that processing details are important to reproducible data. For this reason, grinding is often viewed as an art, rather than a science. The most critical information to be reported relate to the transfer of energy: mill speed, milling duration, grinding media characteristics (size, composition, and loading rate), grinding solvent plus dispersants used, and carbon loading rate (percent solids

content). However, it is likely that all process variables play some role or another towards the final outcome, thus it is recommended that as many details be reported as possible, including such parameters as mill configuration, rate of flow, and temperature of milling.

The studies in Table 4.5 have found S-PAC to perform well, despite having unknown parameters. It is understood that the improved rate of small molecular adsorption is governed by the path length, which is determined by particle size, a parameter that is reported in each study. However, the changes to chemical and physical characteristics observed in this study, and which likely have also occurred in carbons produced for previous studies, are known to have effects on adsorption. The increasingly negative surface charges observed could result in shifts in the adsorption affinity for hydrophobic compounds. Increases in the mesoporous and macroporous fractions would increase the adsorption capacity for lower molecular weight NOM. Lastly, optimization of S-PAC production is an important consideration. Between highly variable grinding procedures and the heterogeneity of activated carbon, an S-PAC with particular characteristics is produced. Additionally, extended milling yielded diminishing returns, thus there is a tradeoff between energy input and production of a useful S-PAC. Material choice is another major design consideration; for example, the lignite coals in this study reached small sizes very quickly, but the bituminous coals were more predictable in breakdown. An understanding of the grinding parameters and parent PAC that produce certain S-PAC types will result in the ability to fine tune the process for creating an S-PAC with certain desired characteristics.

Table 4.5. Characteristics for S-PAC reported in literature.

Carbon Name	Origin Material	Particle Size (d-50, nm)	Size Measurement Technique	pH _{PZC}	Surface Area (m ² /g)	Total Pore Volume (cm ³ /g)	Micropore Volume (cm ³ /g)	Micropore Surface Area (m ² /g)	Mesopore Volume (cm ³ /g)	Mesopore Surface Area (m ² /g)	Publication	
Calgon 6D	Coal	670	Seishin LMS	--	--	--	--	--	--	--	<i>Ando et al., 2010</i>	
Calgon 6MD	Wood	660	Seishin LMS	--	--	--	--	--	--	--	<i>Ando et al., 2010</i>	
Calgon F100-D	Coconut Shell	670	Seishin LMS	--	--	--	--	--	--	--	<i>Ando et al., 2010</i>	
Calgon WPH	Coal	37000	Optical Microscopy	6.1	900	0.46	0.70	--	0.01	--	<i>Ellerie et al., 2013</i>	
Norit SX Ultra	Coal	240	Zetasizer DLS	5.7	773	1.01	0.27	--	0.29	--	<i>Ellerie et al., 2013</i>	
Picahydro MP23	Peat	800	Coulter LS	--	--	--	--	--	--	--	<i>Heijman et al., 2009</i>	
Picahydro MP23	Wood	25000	Microtrac LLS	--	1320	--	--	1020	--	92	<i>Matsui et al., 2014</i>	
		680	Seishin LMS	--	--	--	--	--	--	--	<i>Ando et al., 2010</i>	
		720	Microtrac LLS	--	--	--	--	--	--	--	<i>Matsui et al., 2014</i>	
		500	Microtrac LLS	--	1220	--	--	1020	--	79	<i>Matsui et al., 2014</i>	
Picahydro SP23	Coconut Shell	31000	Microtrac LLS	--	1020	--	--	810	--	132	<i>Matsui et al., 2014</i>	
		650	Seishin LMS	--	--	--	--	--	--	--	<i>Ando et al., 2010</i>	
		850	Microtrac LLS	--	--	--	--	--	--	--	<i>Matsui et al., 2014</i>	
		520	Microtrac LLS	--	1150	--	--	920	--	138	<i>Matsui et al., 2014</i>	
Shirasagi	Wood	770	Seishin LMS	--	--	--	--	--	--	<i>Matsui et al., 2008</i>		
Taikou-W	Wood	650	Seishin LMS	--	--	--	--	--	--	--	<i>Matsui et al., 2007</i>	
		880	Seishin LMS	--	--	--	--	--	--	--	<i>Matsui et al., 2009</i>	
		800	Seishin LMS	--	--	--	--	--	--	--	<i>Matsui et al., 2005</i>	
		11800 ^a	Horiba LLS	--	1170	--	--	--	--	--	<i>Matsui et al., 2013</i>	
		^a 725	Horiba LLS	--	1110	0.62	--	--	--	--	--	<i>Ando et al., 2010; Matsui et al., 2013</i>
		13500 ^b	Horiba LLS	--	1070	--	--	--	--	--	--	<i>Matsui et al., 2013;</i>
		^b 857	Horiba LLS	--	1130	--	--	--	--	--	--	<i>Matsui et al., 2013</i>
19000 ^c	Microtrac LLS	--	1070	--	--	990	--	124	<i>Matsui et al., 2014</i>			

		°620	Microtrac LLS	--	1130	--	--	920	--	116	<i>Matsui et al., 2014</i>
Unknown	Coconut Shell	10000	SEM Analysis	9.6	1070	--	0.395	--	0.072	--	<i>Dunn & Knappe, 2013</i>
		480	SEM Analysis	8.4	1090	--	0.378	--	0.343	--	<i>Dunn & Knappe, 2013</i>
		430	SEM Analysis	7.8	1120	--	0.396	--	0.438	--	<i>Dunn & Knappe, 2013</i>
Unknown	Lignite Coal	11000	SEM Analysis	10.7	507	--	0.140	--	0.386	--	<i>Dunn & Knappe, 2013</i>
		290	SEM Analysis	8.2	595	--	0.164	--	0.629	--	<i>Dunn & Knappe, 2013</i>
		180	SEM Analysis	8.5	607	--	0.175	--	0.514	--	<i>Dunn & Knappe, 2013</i>
Unknown	Wood	10000	SEM Analysis	10.7	912	--	0.313	--	0.225	--	<i>Dunn & Knappe, 2013</i>
		820	SEM Analysis	--	950	--	0.323	--	0.339	--	<i>Dunn & Knappe, 2013</i>
		210	SEM Analysis	7.9	917	--	0.294	--	0.565	--	<i>Dunn & Knappe, 2013</i>
Unknown	Wood	18000	SEM Analysis	4.9	1460	--	0.390	--	0.807	--	<i>Dunn & Knappe, 2013</i>
		1200	SEM Analysis	5.9	1400	--	0.393	--	0.742	--	<i>Dunn & Knappe, 2013</i>
		240	SEM Analysis	5.8	1270	--	0.370	--	0.675	--	<i>Dunn & Knappe, 2013</i>
Unknown	Bituminous Coal	14000	SEM Analysis	6.2	901	--	0.317	--	0.140	--	<i>Dunn & Knappe, 2013</i>
		600	SEM Analysis	6.7	879	--	0.300	--	0.251	--	<i>Dunn & Knappe, 2013</i>
		540	SEM Analysis	6.3	888	--	0.292	--	0.438	--	<i>Dunn & Knappe, 2013</i>

LMS = LED Measurement System; LLS = Laser Light Scattering; Coulter LS uses Laser Diffraction method; SEM = Scanning Electron Microscopy

Conclusions

The primary conclusions from this study are as follows:

- Pulverization of activated carbon by bead milling predictably reduces the mean particle size. Ability to reduce in size was generally related to the carbon precursor material; lignite coals reached a similar final size, and bituminous coals reached a similar final size. Successful pulverization in all carbon types supports the potential of S-PAC technology for application.
- Chemical property measurements led to discovery of an oxidative process occurring during bead milling. The extent of oxidation appears to be limited to external surfaces and generally unaffected by milling duration. Since surface charge is known to affect adsorption processes, oxidation due to bead milling may affect S-PAC performance in relation to its parent PAC.
- Pore volume and surface area changes were not a direct function of milling time. However, observed differences are likely significant enough to affect adsorption performance.
- Material reporting is lacking among S-PAC studies. Improved reporting of material processing and characteristics would improve the ability to design future S-PAC processes.

CHAPTER FIVE

S-PAC MEMBRANE COATING ANALYSIS VIA MODELING

Motivation

S-PAC adsorption, whether in batch reactors or as a membrane coating, has not been modeled well with conventional analytical models. The models break down for small size particles but the reason for model failure is unknown. The S-PACs produced in-house and described in the previous chapter provide an ideal data set for exploring parameters regarding adsorption. Both analytical models and computational models are used here to determine how S-PAC adsorption mechanisms differ from PAC adsorption mechanisms.

Experimental Data Set

Amaral et al. (2016) used the WC800 bituminous coal PAC and S-PACs (denoted in the previous chapter as BC1) as microfiltration membrane coatings for the adsorption of atrazine. The data set includes flux data and atrazine adsorption data from filtration tests and atrazine data from batch kinetics experiments in continuously mixed reactors. In this chapter, the BC1 designation is dropped since it is the only carbon discussed.

Batch Kinetics

Batch adsorption kinetics were measured with an atrazine concentration of 15 ppb and a carbon concentration of 2.5 mg/L by weight after dried using a vacuum pump. Vials were tumbled for continuous mixing. Samples were withdrawn via pipette and filtered to remove the carbon before measuring atrazine via LSC. The filter retained less than 2% of atrazine. The batch kinetics data are presented in Table 5.1.

Table 5.1. Batch kinetics data for 15 ppb of atrazine in DDI onto 2.5 mg/L of each milled carbon.

Time (min)	Atrazine Concentration (ppb)						
	PAC	1 Pass	15 min	30 min	1 hour	2 hours	6 hours
0	15.0	15.0	15.0	15.0	15.0	15.0	15.0
1	10.0	8.58	2.09	0.426	0.263	3.08	0.521
5	5.89	4.02	0.245	0.170	0.075	0.113	0.313
10	5.70	3.24	0.122	0.0426	0.0375	0.0375	0.313
15	5.84	2.27	0.163	0.0426	0.0375	0.0375	0.0521
20	4.14	2.03	0.0408	0.0852	0.0375	0.0375	0.104
25	4.19	1.29	0.0815	0.0426	0.0375	0.225	0.0521
30	4.72	1.35	0.0408	0.0852	0.0375	0.1125	0.0521
60	3.60	0.781	0.0408	0.0852	0.0375	0.0375	0.0521
90	2.79	0.625	0.0408	0.0426	0.0375	0.0375	0.0521
120	1.81	0.625	0.0815	0.0426	0.0375	0.0750	0.0521
150	1.27	0.365	0.0408	0.0426	0.0375	0.0375	0.208
180	1.61	0.469	0.0408	0.0426	0.0375	0.0375	0.0521
210	1.21	0.469	0.0408	0.0426	0.0375	0.075	0.156
240	1.07	0.260	0.0408	0.0426	0.0375	0.0375	0.0521

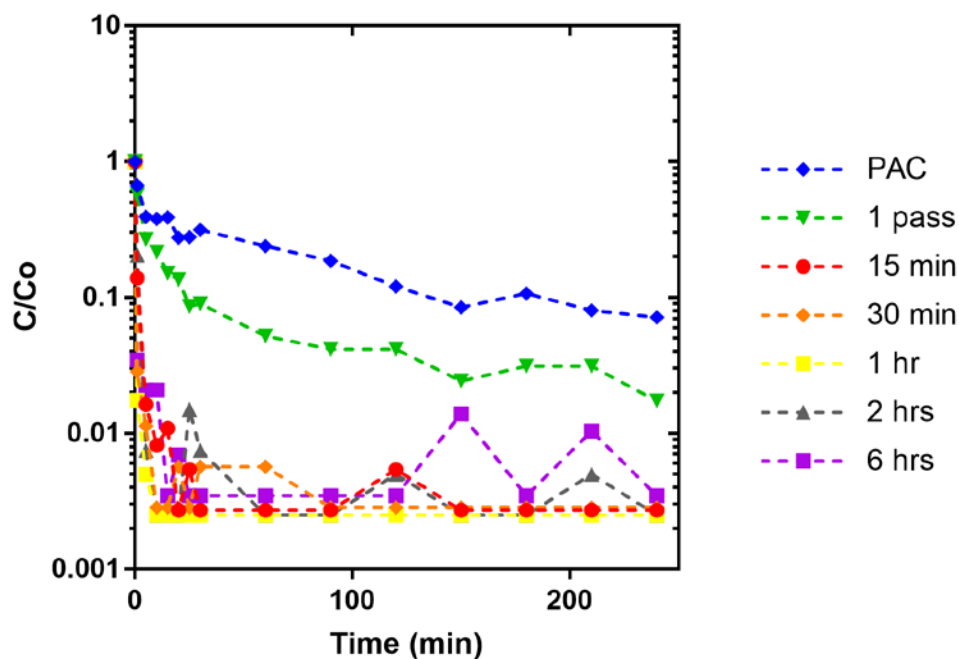


Figure 5.1. Normalized concentration in the liquid phase from batch adsorption kinetics experiments. 2.5 mg/L of carbon and 15 ppb of atrazine was used in each experiment.

Filtration Adsorption

15 mL aliquots containing 1 mg of carbon were prepared by probe sonication at 50% power for one minute to fully disperse the particles (S-4000, Qsonica, LLC, Newtown, CT, USA). The aliquot was added to the body of the membrane cell while 400 mL of DDI water containing 15 ppb of atrazine was added to a feed tank. Samples of the permeate were collected every 40 mL and measured via LSC for atrazine presence. The carbon cake filtration data are presented in Table 5.2 and plotted in Figure 5.2. Breakthrough occurred immediately with the PAC membrane coating, meaning that atrazine was measured in the permeate soon after filtration began. Atrazine broke through the 1-pass S-PAC layer after about 150 mL filtered, while no breakthrough was seen in other S-PACs except for the last sample of the 2-hour S-PAC. While each trial filtered the same total volume, due to differences in the permeability of each cake, the time elapsed during filtration varied. When atrazine concentration is plotted versus time, 6-hours is revealed to take the longest time to filter while the other trials are more similar in the time elapsed (Figure 5.3).

The overall removals of atrazine are calculated through integration over the total volume filtered. Total atrazine adsorption is presented in Table 5.3 along with the flux resulting from each carbon cake normalized to the clean water flux for each membrane coupon. Both results correlate somewhat with the particle size, more so for fouling. The flux values also provide verification that a Darcy's Law assumption is valid for the system. The Reynolds number ranges from 3.2×10^{-4} for 1-pass S-PAC to 4.7×10^{-5} for 6-hours S-PAC, keeping the system in range for Darcy's Law and laminar flow (Zeng and Grigg, 2006).

Table 5.2. Atrazine permeated through carbon cakes formed from 1 mg of carbon on a microfiltration membrane. S-PACs are labeled according to their extent of milling. Non-milled PAC and a no carbon condition were used for comparison.

Volume Permeated (mL)	Atrazine Concentration (ppb)							
	No Carbon	PAC	1 Pass	15 min	30 min	1 hour	2 hours	6 hours
40	12.7	1.15	0.469	0.0893	0.134	0.331	0.0375	0.0391
80	12.8	3.11	0.597	0.0893	0.0446	0.190	0.150	0.0781
120	13.2	4.98	0.341	0.0446	0.0893	0.0938	0.150	0.0391
160	13.6	5.98	0.682	0.134	0.0446	0.0469	0.188	0.0391
200	13.5	7.54	1.11	0.134	0.0893	0.0469	0.150	0.0391
240	13.0	8.49	1.41	0.0893	0.134	0.0469	0.300	0.0391
280	13.3	9.18	1.92	0.0893	0.0446	0.0469	0.338	0.0391
320	13.4	10.4	2.41	0.134	0.0446	0.0469	0.450	0.0391
360	12.7	11.2	2.46	0.134	0.0446	0.141	0.413	0.0781
400	13.5	12.7	3.17	0.179	0.0446	0.141	1.03	0.0391

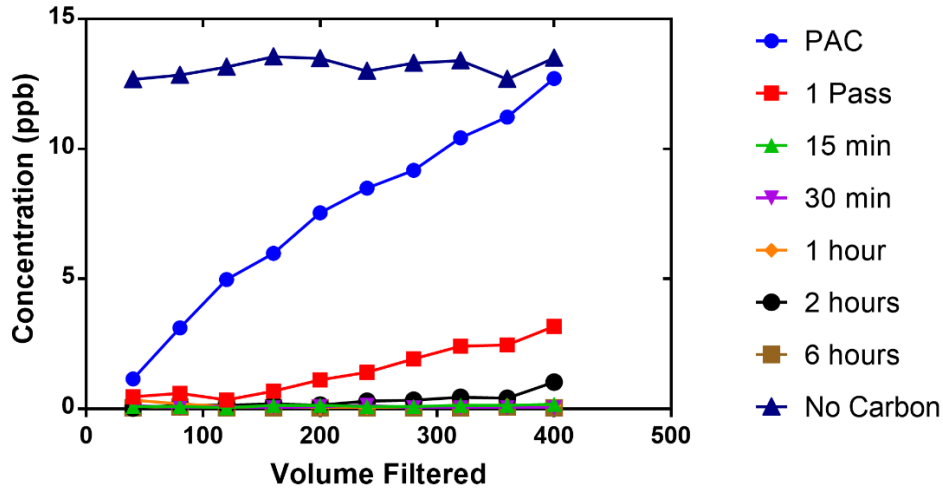


Figure 5.2. Permeate concentration as a function of the volume filtered. Minimum adsorption occurred through the membrane, as seen by the No Carbon data. Breakthrough occurred immediately and consistently through the PAC layer, while S-PACs provided higher removals. Breakthrough is seen partway through in 1-pass carbon and at the end for 2-hours carbon.

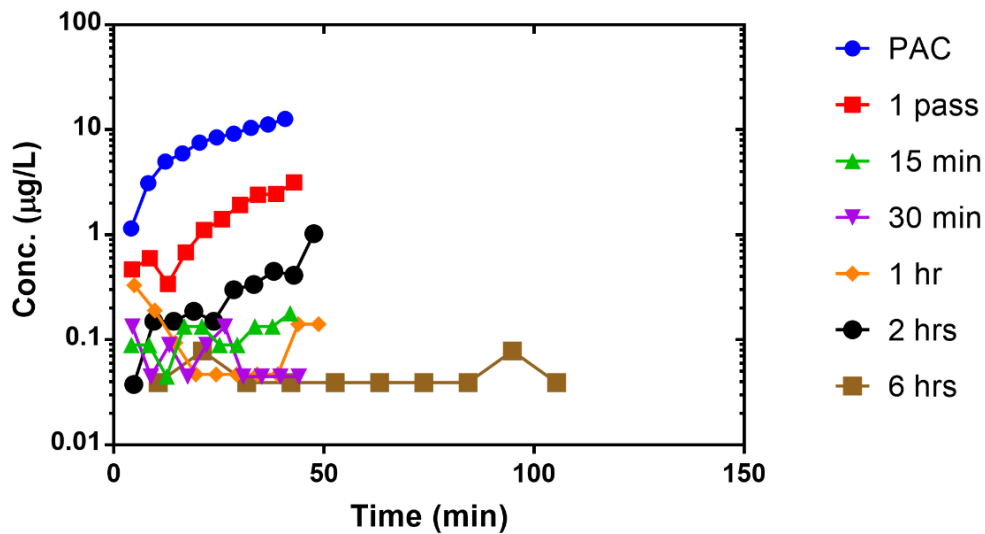


Figure 5.3. Permeate concentration as a function of time. A log y-axis is used to show S-PAC data more clearly. The flux through the 6-hours carbon cake was significantly lower than the other cakes and the filtration took more than twice as long.

Table 5.3. The normalized flux and total atrazine removal resulting from each carbon cake. Both correlate slightly with the particle size.

Carbon	Particle Size (µm)	Normalized Flux	Atrazine Removal (%)
PAC	12.3	0.94	6.67
1 Pass	0.628	0.90	24.3
15 min	0.432	0.92	60.6
30 min	0.398	0.87	67.5
1 hour	0.329	0.79	75.5
2 hours	0.330	0.81	80.6
6 hours	0.230	0.37	61.0

Adsorbent Property Correlations

The properties of the carbons measured in the previous chapter can be used to provide insights into the mechanisms of adsorption and membrane fouling. The flux

correlated strongly with the milling time, with a statistically significant ($p < 0.0001$) relationship of $0.93 - 1.52 \times 10^{-3} \cdot t$ where t is the milling time in minutes. However, correlation with milling time does not reveal any information as to the cause of flux decline. In fact, flux decline in general did not correlate well with particle size, but correlated significantly with oxygen content ($p = 0.006$) with relationship of $1.23 - 0.094 \cdot c_{oxy}$ where oxygen content (c_{oxy}) is measured in weight percent oxygen. Intuitively, particle size should have an impact on fouling, and it appears that flux decline has two trends related to particle size. Above a certain size, the fouling due to the carbon is independent of particle size and causes similar nominal amounts of flux decline. The 1-pass carbon and 15-minute carbon were both above this particle size and resulted in less than 10% flux decline. Below these particle sizes, flux decline correlated somewhat according to particle size with $R^2 = 0.86$, and was most strongly correlated ($p = 0.0029$) to external surface area (SA_{ext}) in m^2/g with $R^2 = 0.96$ and equation $1.59 - 0.092 \cdot SA_{ext}$ (Figure 5.4).

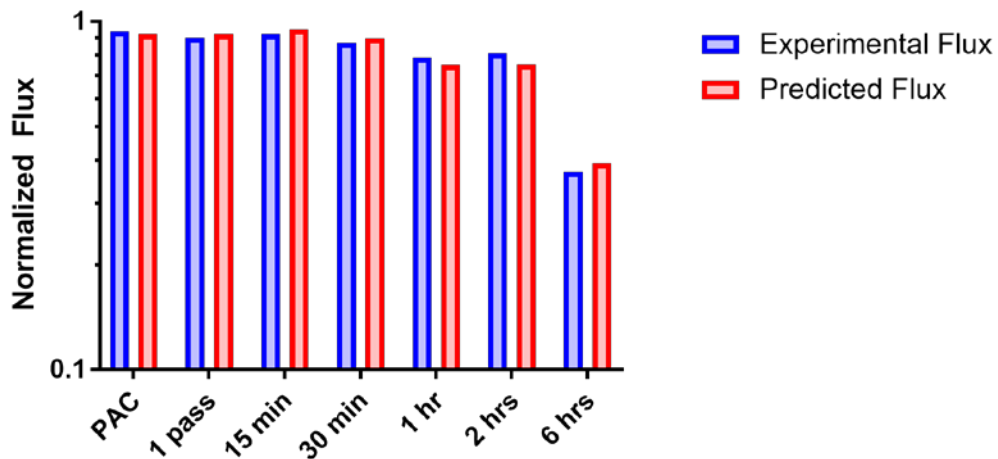


Figure 5.4. Flux values measured experimentally compared with predicted flux values. PAC and 1-pass S-PAC are predicted independent of other parameters, while all other carbon fluxes are predicted from their specific external surface area.

Atrazine removal was found to correlate to a combination of the specific external surface area and the particle oxygen content. A significant ($p < 0.0001$) regression equation was found with $R^2 = 0.734$ and equation $15.89 + 0.04 \cdot c_{oxy} + 5.98 \cdot SA_{ext} - 1.26(c_{oxy} - 5.62)(SA_{ext} - 5.34)$. All trials except for PAC filtration were modeled well with this equation (Figure 5.5)

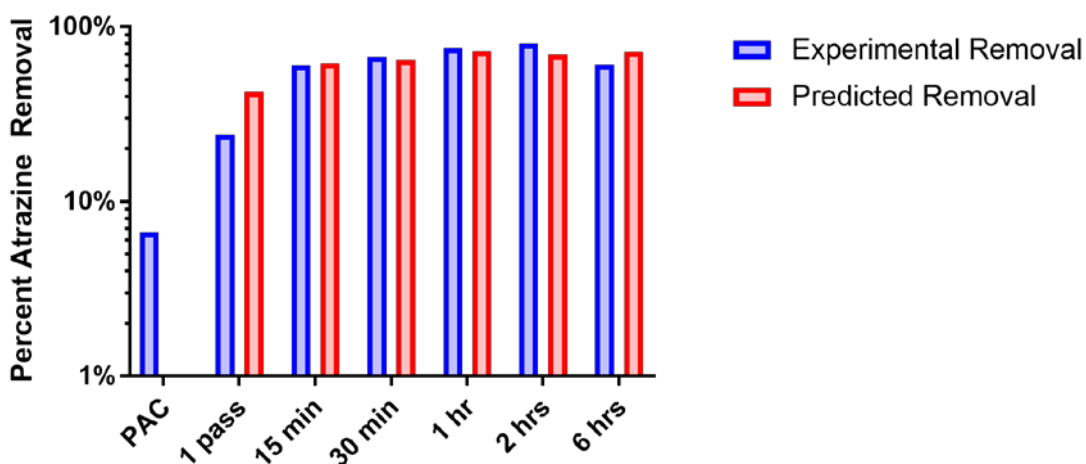


Figure 5.5. Percent of atrazine removed as measured experimentally and predicted from the specific external surface area and oxygen content of each carbon.

These regression models give an idea of the parameters that may govern each experimental outcome, however, there are other parameters not considered in these measurements. Only parameters of individual particles have been measured, but qualities regarding the carbon coating on the membrane have not. For instance, since flux only varies according to particle size after a threshold, flux likely correlates to a variable related to particle size in a coating context, such as the tortuosity of the packed layer. Additionally, the material parameters of the particle are non-independent of each other, since oxygen content was found to correlate with specific external surface area. Therefore, the

correlation found between atrazine removal and the combination of oxygen content and specific external surface area is not highly valid, but it is still indicative that surface groups and surface area are relevant to the mechanism of S-PAC adsorption in addition to other yet unknown parameters.

Homogeneous Surface Diffusion Model

HSDM has been successfully used in modeling PAC and GAC adsorption. The core of HSDM describes radial diffusion into a sphere. HSDM has been interpreted via mass balances into models of both batch reactors and column reactors. HSDM is applied here to batch kinetics data for PAC and all S-PACs.

Method

HSDM model scripts written by Priscilla To to model desorption from activated carbon are modified to take the batch kinetics data as inputs (Appendix A) (To, 2008). To calculate the movement of adsorbate between radial points, a finite difference approximation was applied. The finite difference approximation uses the difference between immediately adjacent elements to linearize the differential equation and solve it in conjunction with a boundary value (Ervin 2015). To solve the set of linear equations, the equations are arranged into a matrix comprised of a tridiagonal constant matrix multiplied by a variable matrix to produce a solution matrix. The matrix is solved at each time step and for each radial element using the Thomas algorithm, which solves a tridiagonal matrix through variable substitution (Thomas, 1995). Lastly, the solid phase concentration in the particle is integrated over the radial axis to determine the total mass of

adsorbate in the particle at each time step. A mass balance is used to determine the concentration in the bulk fluid as a function of time, which is the output of the model. The input parameters to the model are listed in Table 5.4.

Table 5.4. Input parameters for HSDM model.

Parameter	Variable	Units
Initial bulk concentration	C_o	$\mu\text{g/L}$
Initial solid phase concentration	q_o	$\mu\text{g /mg}$
Carbon concentration	C_c	mg/L
Carbon particle radius	R	μm
Number of radial elements	nr	-
Total run time	tf	min
Time step	dt	min
Fruendlich coefficient	K_F	$\mu\text{g /mg}*(\text{L}/\mu\text{g})^{1/n}$
Fruendlich exponent	$1/n$	-
Surface diffusion coefficient	D_s	cm^2/min

Method Verification

A study on the adsorption of arsenate onto granular ferric hydroxide was used to verify model outputs (Badruzzaman et al., 2004). In these experiments, different sieved fractions of GFH were contacted with arsenate in a flowing batch reactor. Two of the sieved fractions—the smallest sieved size corresponding to a mean 64 μm particle size and the largest size corresponding to a mean 650 μm particle size—were modeled with HSDM in the paper. Batch contactor data was manually extracted from the published figure and used as inputs to verify the HSDM model developed here.

The batch contactor was filled with 10 mg/L of GFH in each study, designed to result in moderate arsenate removal over the course of the experiment using isotherm data as a guideline. The isotherm data were fit to the Freundlich isotherm with the parameters

$K_F = 4 (\mu\text{g}/\text{mg})(L/\mu\text{g})^{1/n}$ and $1/n = 0.3$. Using the developed script for finding an optimized surface diffusion coefficient through error minimization resulted in $D_s = 2.12 \times 10^{-10} \text{ cm}^2/\text{min}$ for the 64 μm particles and $D_s = 4.81 \times 10^{-9} \text{ cm}^2/\text{min}$ for the 650 μm particles (Figure 5.6). Comparatively, the paper reported D_s fit values of $D_s = 1.79 \times 10^{-10} \text{ cm}^2/\text{min}$ for the 64 μm particles and $D_s = 3.84 \times 10^{-9} \text{ cm}^2/\text{min}$ for the 650 μm particles. The small difference between the values arrived using the developed HSDM model and the reported values from the paper confirm that the developed model is sufficiently accurate.

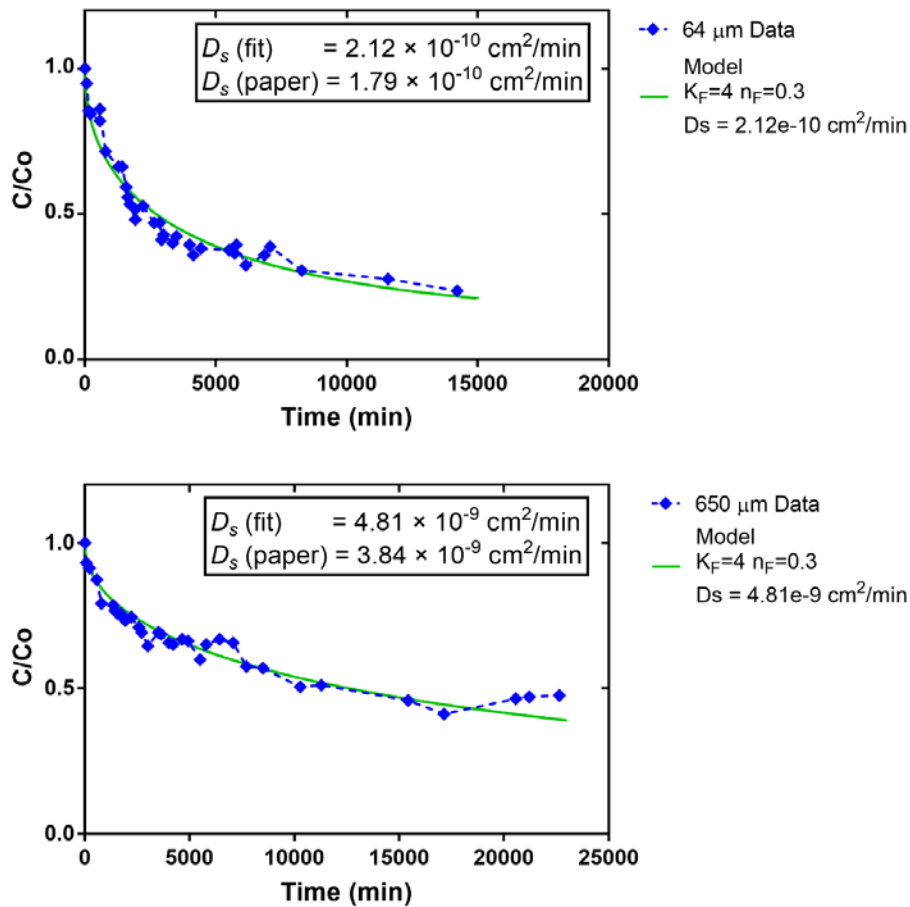


Figure 5.6. Literature data fit with the developed HSDM model (Badruzzaman et al., 2004). Error minimized surface diffusion coefficients are similar to reported fitted values.

HSDM Results

The surface diffusion coefficient, Freundlich coefficient, and Freundlich exponent were varied to find a best fit model to the experimental data from batch kinetics experiments. Bulk concentration in $\mu\text{g/L}$ over time was used as the data input to a search function for optimization of the surface diffusion coefficient value. Measured Freundlich parameters for WC800 PAC and a WC800 S-PAC milled for seven hours were as follows: K_F (PAC) = $0.24 (\mu\text{g/mg})(\text{L}/\mu\text{g})^{1/n}$, $1/n$ (PAC) = 0.88, K_F (S-PAC) = $0.09 (\mu\text{g/mg})(\text{L}/\mu\text{g})^{1/n}$, $1/n$ (S-PAC) = 0.46 (Bakkaloglu, 2014). Using the combined data set, an isotherm parameter set of $K_F = 0.15 (\mu\text{g/mg})(\text{L}/\mu\text{g})^{1/n}$ and $1/n = 0.67$ was obtained and used in the HSDM model for the in-house milled S-PACs (Table 5.5). A search method using iterative error minimization, where error is in the form of the sum of squared normalized residuals, was used to determine the value of D_s . The error associated with the best fit diffusion coefficient using the measured Freundlich parameters was very high. Plotting the predicted concentrations revealed that the combination of measured Freundlich parameters and best fit diffusion coefficient resulted in a final concentration of only 75% of the initial concentration over all of the carbons (Figures 5.7–5.13); the experimental PAC data show final concentrations below 10% and S-PAC data has final concentrations in the range of 0.3% of the initial concentration, so the HSDM model did not fit the data.

Using a trial and error method, the Freundlich parameters were altered and combined with the search method for the best fit diffusion coefficient to produce a model with minimal error when compared to the data set. Highly fitting models were found and the resulting parameters are presented on the right side of Table 5.6. The models are plotted

along with experimental data in Figures 5.7–5.13. A single set of isotherm parameters was not able to describe all of the data sets, but the set of $K_F = 11 (\mu\text{g}/\text{mg})(\text{L}/\mu\text{g})^{1/n}$ and $1/n = 0.4$ described all S-PACs well except 1 pass. The resulting D_s values with the artificial isotherm parameters are lower than the values arrived at using the measured isotherm parameters. Since the models resulting from the measured isotherm parameters were not able to recreate the high extent of removals observed in experiments, it is likely that the search function returned higher D_s values to compensate for the removal limitation. Therefore, by removing the limits on equilibrium value, the resulting D_s values are likely more true to actual values. The D_s values resulting from the best fit isotherm vary between two orders of magnitude with an average value of $1.2 \times 10^{-11} \text{ cm}^2/\text{min}$ and there is no trend according to particle size. Ideally, the diffusion coefficient is only a function of the material, adsorbate, and solvent and therefore one coefficient should describe all data sets.

Table 5.5. Diffusion coefficients determined using minimization of error (sum of squared normalized residuals) to best describe each data set.

Carbon	Size (μm)	WC800 isotherm data				Best Fit Isotherm			
		K_F ($\mu\text{g}/\text{mg})(\text{L}/\mu\text{g})^{1/n}$	$1/n$ (dim)	D_s (cm^2/min)	Error (cm^2/min) ²	K_F ($\mu\text{g}/\text{mg})(\text{L}/\mu\text{g})^{1/n}$	$1/n$ (dim)	D_s (cm^2/min)	Error (cm^2/min) ²
PAC	12.3	0.15	0.67	1.00×10^{-9}	1180	6.00	0.8	4.23×10^{-11}	6.73
1 pass	0.6281	0.15	0.67	9.99×10^{-10}	1280	6.00	0.4	2.00×10^{-12}	3.06
15 min	0.4315	0.15	0.67	1.00×10^{-9}	1690	11.00	0.4	4.64×10^{-12}	0.141
30 min	0.3982	0.15	0.67	1.00×10^{-9}	1730	11.00	0.4	1.42×10^{-11}	0.0161
1 hr	0.3290	0.15	0.67	9.96×10^{-10}	1740	11.00	0.4	1.48×10^{-11}	0.000666
2 hrs	0.3295	0.15	0.67	9.94×10^{-10}	1670	11.00	0.4	3.05×10^{-12}	2.51
6 hrs	0.2304	0.15	0.67	8.73×10^{-10}	1710	11.00	0.4	3.19×10^{-12}	0.160
AVG				9.80×10^{-10}				1.20×10^{-11}	
STD. DEV.				4.39×10^{-11}				1.33×10^{-11}	

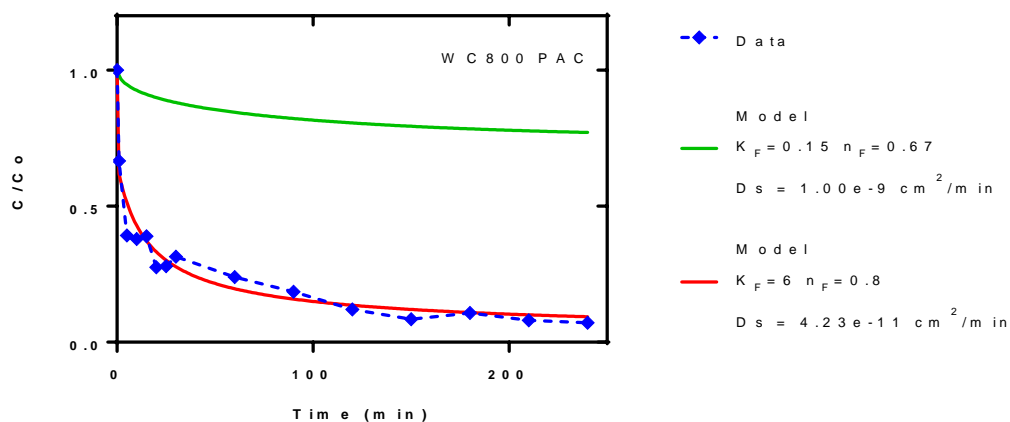


Figure 5.7. PAC modeled with HSDM using the measured Freundlich parameters and parameters chosen to best fit the experimental data.

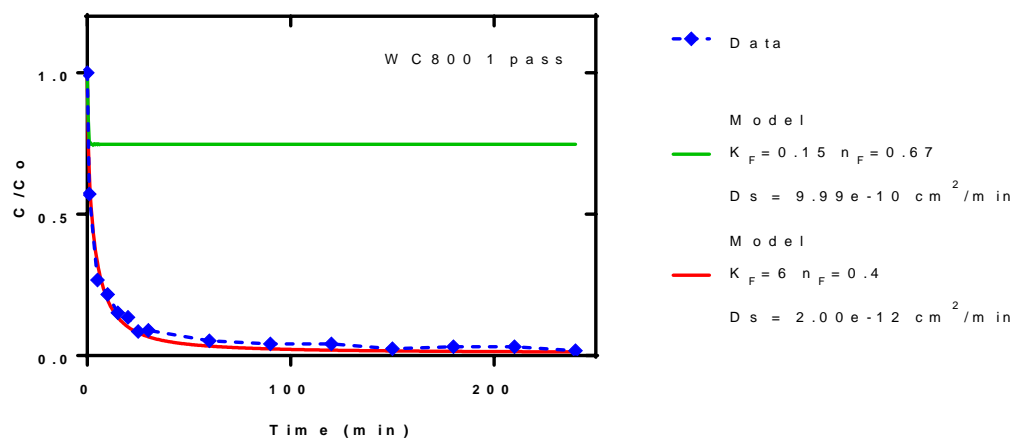


Figure 5.8. 1 pass S-PAC modeled with HSDM using the measured Freundlich parameters and parameters chosen to best fit the experimental data.

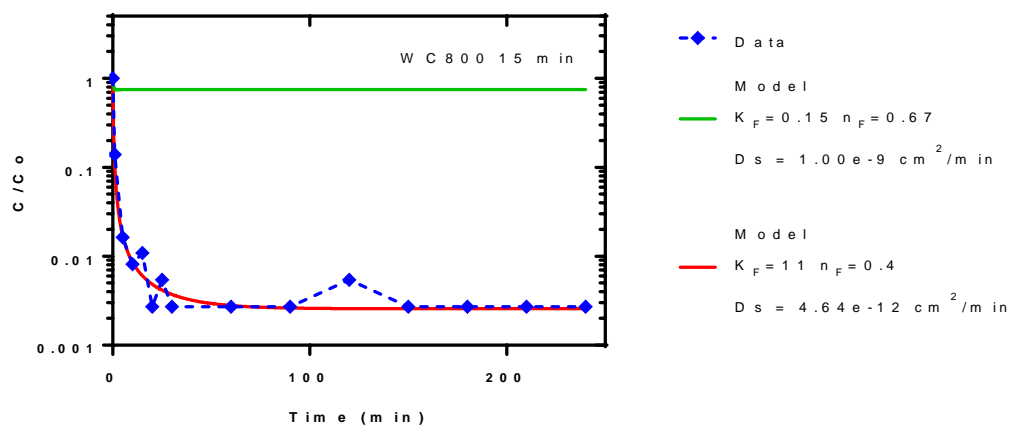


Figure 5.9. 15 min S-PAC modeled with HSDM using the measured Freundlich parameters and parameters chosen to best fit the experimental data.

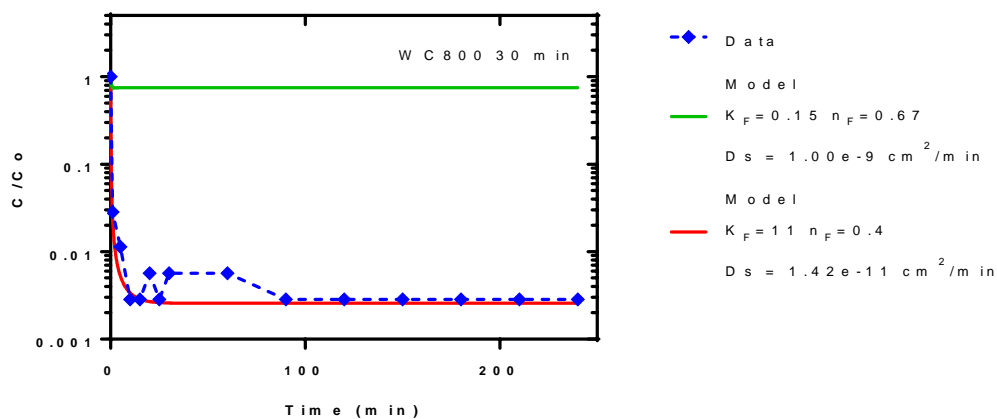


Figure 5.10. 30 min S-PAC modeled with HSDM using the measured Freundlich parameters and parameters chosen to best fit the experimental data.

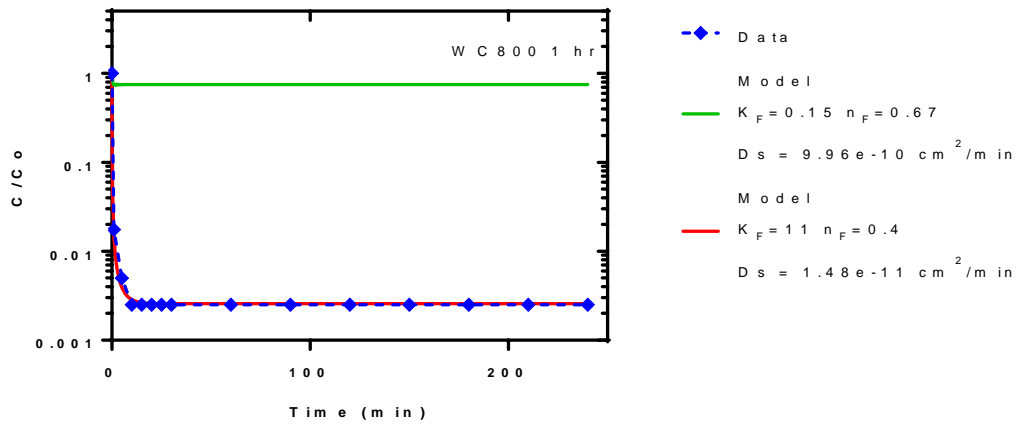


Figure 5.11. 1 hr S-PAC modeled with HSDM using the measured Freundlich parameters and parameters chosen to best fit the experimental data.

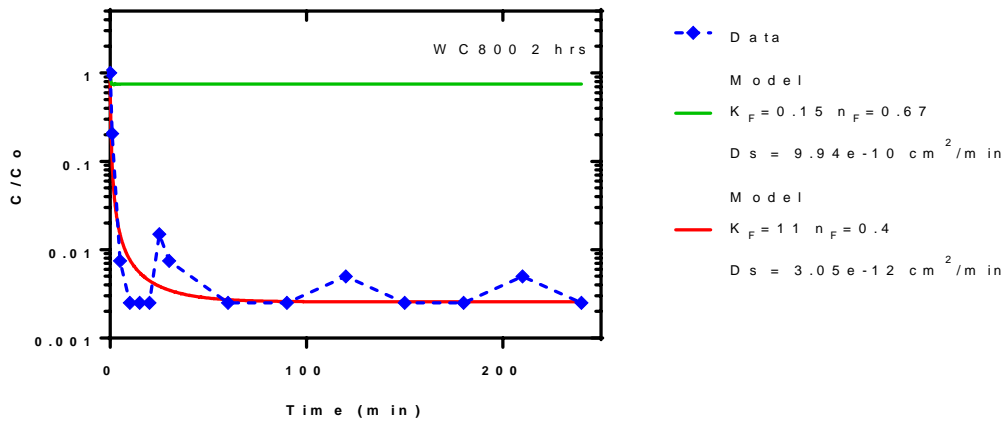


Figure 5.12. 2 hrs S-PAC modeled with HSDM using the measured Freundlich parameters and parameters chosen to best fit the experimental data.

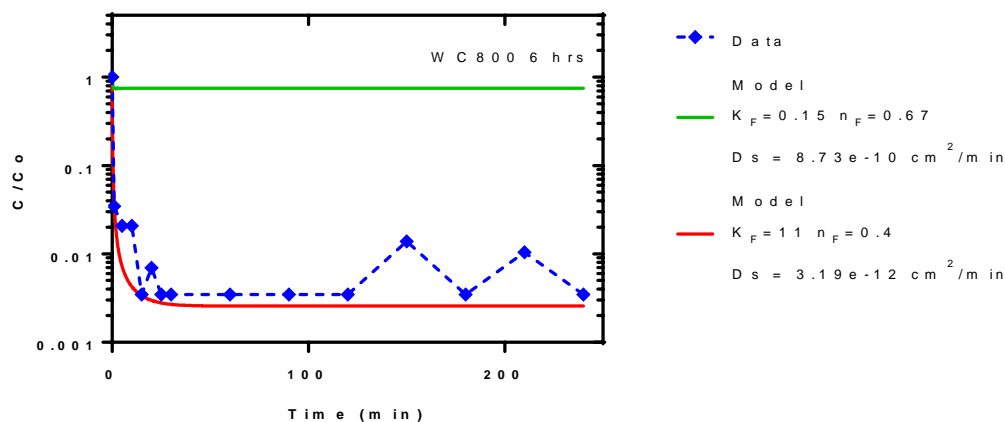


Figure 5.13. 6 hrs S-PAC modeled with HSDM using the measured Freundlich parameters and parameters chosen to best fit the experimental data.

The shape of the atrazine decline curve was modeled reasonably well with the HSDM, however, the higher equilibrium concentration required to fit the data is not explained by the modeling results. The poor fit of the measured Freundlich parameters can be potentially attributed to experimental error. In that case, the next best estimate of isotherm parameter values for the system of WC800 carbon and atrazine in DDI water are the best fit values using PAC data since HSDM is expected and verified to describe PAC adsorption well. With this assumption, the best fit values for S-PAC adsorption are close to the values for PAC adsorption, but the data sets are certainly not described by a unified parameter set.

In a previous study of S-PAC adsorption of atrazine, Freundlich parameters were $K_F = 2.06 (\mu\text{g}/\text{mg})(\text{L}/\mu\text{g})^{1/n}$ and $1/n = 0.59$ for the milled carbon and $K_F = 2.83 (\mu\text{g}/\text{mg})(\text{L}/\mu\text{g})^{1/n}$ and $1/n = 0.65$ for the parent carbon (Ellerie et al., 2013). Other studies

that have measured isotherm parameters for the adsorption of atrazine in pure water onto PAC have found values such as $K_F = 1.48 (\mu\text{g}/\text{mg})(\text{L}/\mu\text{g})^{1/n}$ and $1/n = 0.648$ (Knappe et al., 1998), $K_F = 9.76 (\mu\text{g}/\text{mg})(\text{L}/\mu\text{g})^{1/n}$ and $1/n = 0.56$ (Adams and Watson, 1996), and finally, $K_F = 0.0268 (\mu\text{g}/\text{mg})(\text{L}/\mu\text{g})^{1/n}$ and $1/n = 0.600$ for adsorption on activated carbon made from jack fruit peel (Jain et al., 2009). For studies of activated carbons smaller than one micrometer that use an adsorbate other than atrazine, Freundlich parameters of $K_F = 1.714 (\mu\text{g}/\text{mg})(\text{L}/\mu\text{g})^{1/n}$ and $1/n = 0.466$ were found for the adsorption of 2-MIB (Matsui et al., 2012) and $K_F = 0.26 (\mu\text{g}/\text{mg})(\text{L}/\mu\text{g})^{1/n}$ and $1/n = 1.77$ for the adsorption of geosmin (Matsui et al., 2009a). When using HSDM to model 2-MIB and geosmin adsorption onto S-PAC, a single diffusion coefficient was also not able to model both PAC and S-PAC batch adsorption results (Matsui et al., 2009a). None of the literature values for adsorption isotherm parameters are as high as the ones found here when fitting the HSDM model to the batch kinetics data. Values in this range have been measured for small size contaminant adsorption to other carbon adsorbents, such as activated carbon fiber and carbon nanotubes (Pelekani and Snoeyink, 2000; Yan et al., 2008).

The branched pore kinetic model (BPKM) has been able to fit S-PAC data well; however, BPKM uses three fitting parameters which fits by nature of having more degrees of freedom. Effectively, degrees of freedom are also increased in the HSDM approach taken here since the two Freundlich parameters are varied, thus adding two degrees of freedom. Some modelers have used HSDM with a film transfer resistance in the mass balance. It is possible that the increased specific external surface area of S-PAC makes film transfer a larger component of S-PAC adsorption as compared to PAC adsorption.

CFD Packed Bed Reactor Model

CFD offers an advantage in solving geometrically dependent processes and systems without analytical solutions. Here, S-PAC coatings are modeled as a packed bed reactor using the CFD software COMSOL Multiphysics 5.2. Transport of water and a chemical species is governed by Darcy's Law through a packed bed modeled as porous media. Adsorption is defined as a reaction of species A to species AS where species A is the species dissolved in the liquid phase and AS is the species adsorbed to the solid phase. The reaction occurs within a derived extra dimension that is created using the Reactive Pellet Bed package. The result is 3-D variation of species concentration, pressure, and velocity along the packed column and one dimensional variation of species concentration along the particle radial axis.

Model Geometry

A cylindrical section of a carbon cake was modeled via a revolved 2D cross-section. Since concentration changes over the height of the carbon cake, it is necessary to model the full height, but it is not necessary to extend the radius of the carbon cake to the full extent of the membrane size since minimal net transfer occurs in the radial direction. The height of the cake was estimated from scanning electron microscope (SEM) images taken of carbon that was formed into a cake on a membrane as a result of filtration. 4 mg of WC800 6-hour milled carbon was filtered onto a 21 mm membrane and the height of the cake was approximately 8–10 μm , as shown in Figure 5.14. The image also shows the carbon cake detaching from the membrane surface as a result of desiccation prior to imaging, so it is likely that the cake was slightly more compacted than its hydrated version.

The membrane coating data were taken using 1 mg of carbon filtered onto a 21 mm membrane, thus, the computer model used a conservative estimate of a 3 μm cake thickness with a radius of 3 μm to produce a cylindrical geometry (Figure 5.15). Lastly, a 0.1 μm layer was appended to the outflow of the carbon cake to represent resistance to flow due to the membrane.

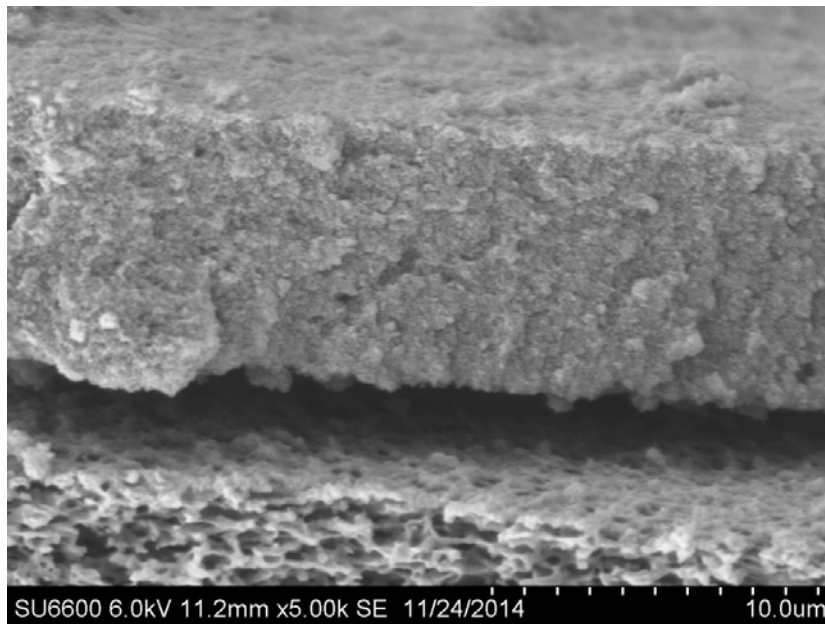


Figure 5.14. Scanning electron microscopy (SEM) image of 4 mg of WC800 6 hour milled carbon on a 21 mm diameter microfiltration membrane.

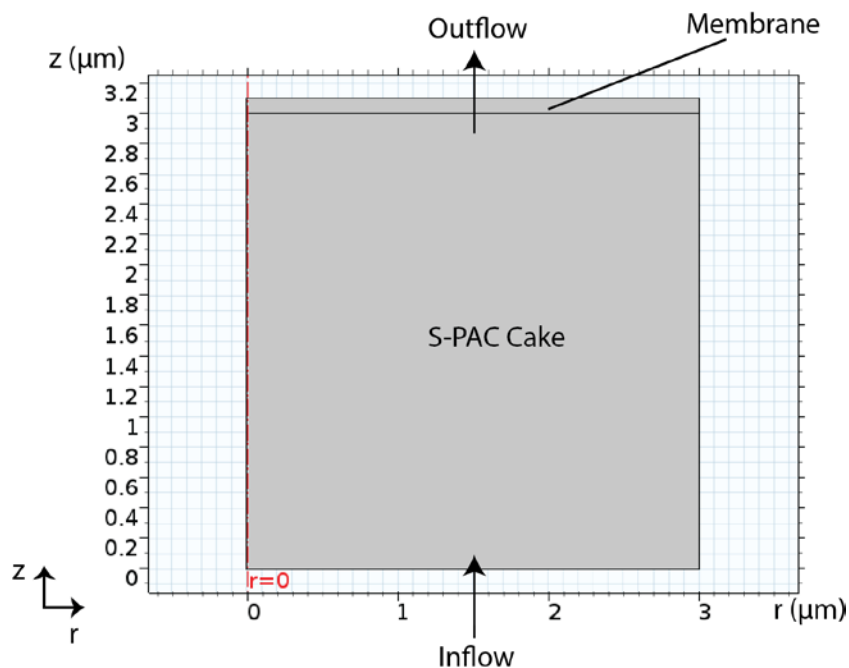


Figure 5.15. Representation of a slice of a column section of a packed bed reactor created in COMSOL Multiphysics 5.2. The column is 3 μm in height with a radius of 3 μm . The membrane layer is modeled with a 0.1 μm thickness.

Model Parameters

The packed bed reactor was defined with parameters relating to both the bed and the reactive pellets, such as density and porosity of both the pellets and the packed bed. A full list of parameter inputs required for the COMSOL model, including variables calculated by expression inputs, is found in Table 5.6.

Activated carbon has a density of approximately 2.0 g/cm^3 and this value was used for the pellet density. (The density of the specific carbon used in the experiments is unknown). The density of the bed was estimated from the assumption that particles are arranged in random close pack with a 64% packing efficiency, giving an estimated bed density of 1.28 g/cm^3 . The porosity of activated carbon was estimated from measurements

of pore volume using nitrogen gas adsorption and analysis with BET theory, reported in Table 4.4. An average value of $0.45 \text{ cm}^3/\text{g}$ was used in conjunction with the density of activated carbon to produce a dimensionless porosity, that is void volume divided by particle volume, of 0.9. Lastly, the active surface area of the pellet was obtained from measured data reported in chapter 4; an average surface area of all WC800 S-PACs was used. The concentration of surface sites—that is, the maximum absorbed mass of adsorbate per mass of carbon—was calculated from the surface area and the equilibrium surface concentration.

Parameters regarding the molecular species, such as molar mass, were based on atrazine properties. The experimental inlet concentration of $15 \text{ }\mu\text{g}/\text{L}$ of atrazine translates into $7 \times 10^{-6} \text{ mol}/\text{m}^3$, which was the unit used in the model. The diffusivity of atrazine in water is $6.70 \times 10^{-6} \text{ cm}^2/\text{s}$ (EPA, 2006). Inside the pellet, the diffusivity is a surface diffusion coefficient instead of a liquid diffusion coefficient and so that value was different. The outcome of HSDM modeling was used as a starting point for the value of the surface diffusion coefficient within the pellet.

COMSOL uses adsorption equilibrium parameters in mole fraction units so the Freundlich isotherm coefficient was accordingly converted from mass units to mole fraction units (Bowman, 1982). Liquid phase concentration was converted from $\mu\text{g}/\text{L}$ to mol/mol by dividing by the ratio of the contaminant molecular weight to the solvent molecular weight and converting to the proper units with the solvent density. Solid phase concentration was converted from mg/g to mol/kg by multiplying by the carbon concentration and dividing by the contaminant molecular weight. The exponent remains

unchanged in this conversion; however, the exponent affects the value of the converted coefficient. For example, a Freundlich coefficient of 4.0 ($\mu\text{g}/\text{mg})(\text{L}/\mu\text{g})^{1/n}$ converts to 1.0 mol/kg for an exponent of 0.4, 103.29 mol/kg for an exponent of 0.6, and 10706.9 mol/kg for an exponent of 0.8.

Table 5.6. Parameter inputs to the COMSOL model.

Parameter	Value [unit]	Description
d_pe	0.628[um]	Pellet diameter
r_pe	d_pe/2	Pellet radius
rho_b	1.28[g/cm^3]	Density of bed
rho_pe	2.0[g/cm^3]	Density individual pellet
epsilon_b	1-rho_b/rho_pe	Porosity of bed
epsilon_pe	0.90[1]	Porosity of pellet
DA	6.70e-6[cm^2/s]	Diffusion coefficient in bed
DAP	5e-10[cm^2/min]	Diffusion coefficient in pellet
Kfl	1e-1[cm/s]	Film transfer coefficient
CA_in	7e-5[mol/m^3]	Inlet concentration
p_Darcy	10[psi]	Inlet pressure
L_h	3[um]	Cake height
Rm	1.38E11[1/m]	Membrane resistance
L_mem	0.1[um]	Membrane height
kappa_mem	L_mem/Rm	Membrane permeability
kappa_cake	$(\epsilon_b^3 \cdot (d_{pe})^2) / (36 \cdot 10 \cdot (1 - \epsilon_b)^2)$	Cake permeability
MW_water	18.02[g/mol]	MW of water
mu	1e-3[N*s/m^2]	Viscosity of water
rho_water	1[g/cm^3]	Density of water
Mn_A	0.2156[kg/mol]	Molar mass
Kf	20[mol/kg]	Fruendlich coefficient
nf	0.15[1]	Fruendlich exponent
qe	$Kf \cdot (CA_{in} \cdot MW_{water} / \rho_{water})^{nf}$	Max equilibrium concentration
k_ads	100[m^3/mol/s]	Adsorption reaction coefficient
SA	800[m^2/g]	Total surface area of particle
theta_surf	qe/SA	Concentration of surface sites

Permeability of the packed bed and of the membrane were calculated from other parameter inputs. The membrane permeability was based on measurement of clean water flux through a bare membrane (see Equation 2.11, page 29), which had a resistance of $1.38 \times 10^{11} \text{ m}^{-1}$. Then, the permeability is calculated by the membrane thickness divided by the membrane resistance. The permeability of the carbon cake can be calculated similarly. In this case, the resistance of the combined cake layer and membrane is determined from the flux measurement and the cake layer resistance is found by subtracting out the membrane resistance. Using the Carman-Kozeny equation (Equation 2.14, page 32), permeability of a packed bed can be predicted from the particle size. The Kozeny constant has been measured for packed beds of uniform spherical pellets with results near 5; the Kozeny constant correlates with porosity, decreasing for lower porosity and increasing for higher porosity (Heijs and Lowe, 1995; Richardson et al., 2002). Using the permeability data gathered from experimental flux values of S-PACs, a Kozeny constant was calculated for each data point and averaged to produce an integer value of 6. The Carman-Kozeny equation was not able to predict the permeability of PAC data from its particle size, likely due to the minimal resistance of the PAC layer as compared to the membrane resistance. The flux values computed by COMSOL are as expected given the error associated with the average Kozeny constant of 6; the computed fluxes are shown alongside the measured flux values for comparison (Table 5.7). The Kozeny constant was applied to calculate permeability used as an input to Darcy flow physics and only particle size was changed in each case. PAC permeability was not predicted by the Carman-Kozeny equation and instead permeability was directly calculated from the measured flux.

The largest deviation occurred for the 6-hrs S-PAC, for which the calculated Kozeny number was 13.4, thus implying that the cake formed by 6-hrs S-PAC may have had a higher porosity than predicted by random packing theory. Since the porosity used in the calculation is the theoretical maximum packing for randomly ordered spheres, it is unlikely that the smallest particles and longest milled particles would result in a higher void volume. Instead, it is more likely that the less milled particles contain more heterogeneity and angularity, thus the assumption of homogenous spheres is less valid and porosity under the random packing model is not accurate. With increased heterogeneity, the porosity decreases since smaller particles are able to fit in the gaps between larger particles.

Table 5.7. Use of experimental data and the Carman-Kozeny equation to determine carbon permeability within the COMSOL model using a Kozeny constant of 7.

Carbon	Size (μm)	Experimental Flux (m/s)	COMSOL Flux (m/s)
PAC	12.3	4.72×10^4	4.68×10^4
1 Pass	0.6281	4.49×10^4	4.48×10^4
15 min	0.4315	4.59×10^4	4.05×10^4
30 min	0.3982	4.37×10^4	3.93×10^4
1 hour	0.329	3.95×10^4	3.59×10^4
2 hours	0.3295	4.05×10^4	3.59×10^4
6 hours	0.2304	1.83×10^4	2.78×10^4

Boundary and Reaction Conditions

The inlet concentration was smoothed as a step function to ease model convergence. At time zero the concentration was 0 at the boundary, then it was increased via the smoothed step function until reaching its maximum value of 7×10^{-5} mol/m³, which corresponds to a concentration of 15 ppb of atrazine, after one minute. For the remainder of the simulation the concentration was held constant at the maximum value. The flow conditions were governed by a pressure of 10 psi at the inlet and 0 psi at the outlet.

First-order reaction kinetics were used to describe the adsorption reaction. Pseudo first-order reaction kinetics are descriptive of activated carbon adsorption when the bulk concentration is not a limiting factor. For adsorption reactions, the rate equation describes the reaction of a liquid-phase species with available adsorption sites to form the solid-phase species. In this form, it is necessary to track the changing concentration of the species as well as the changing availability of adsorption sites. By assuming a one-to-one conversion of adsorption sites to solid-phase species, the rate equation can instead be written in terms of the two species concentration in relation to the maximum concentration of adsorption sites, here denoted as θ , which is calculated from the Freundlich isotherm and the total surface area (Equations 5.1 and 5.2).

$$\theta = q_e SA = K_f C_e^{\frac{1}{n}} SA \quad \text{Eq. 5.1}$$

$$R = k_{ads} C_A (\theta - C_{AS}) \quad \text{Eq. 5.2}$$

CFD Results

All models were run over a duration of 50 minutes with a time step of 0.2 minutes, except 6-hrs S-PAC which was run for 100 minutes. The pellet radius dimension was resolved to a mesh of 10 linear elements. The only parameter changed between the model runs was the pellet size, which controlled the permeability and thus the flow rate and pressure drop over the packed bed. PAC data could not be modeled with the CFD geometry due to high heterogeneities in membrane coverage. The estimated cake height of 3 μm is the same for all carbons due to equal masses used and assumption of 37% porosity; however, PAC particle size is 12.3 μm , which is larger than the cake height. Thus, the PAC layer consists of areas with particle build up and areas without much carbon. The atrazine removal through PAC would be best modeled as an average of removals over various cake heights; that type of model is beyond the scope of this study.

The model reveals information about the pressure drop over both the cake and the membrane that are otherwise unobserved in experimental data, though can be calculated from known values. For the larger particles the cake did not provide much resistance so more of the pressure drop was over the membrane, while for the smaller particles the cake layer contributed a larger portion of resistance and less pressure drop occurred over the membrane; however, in all cases, the majority of the pressure drop was over the membrane (Figure 5.16).

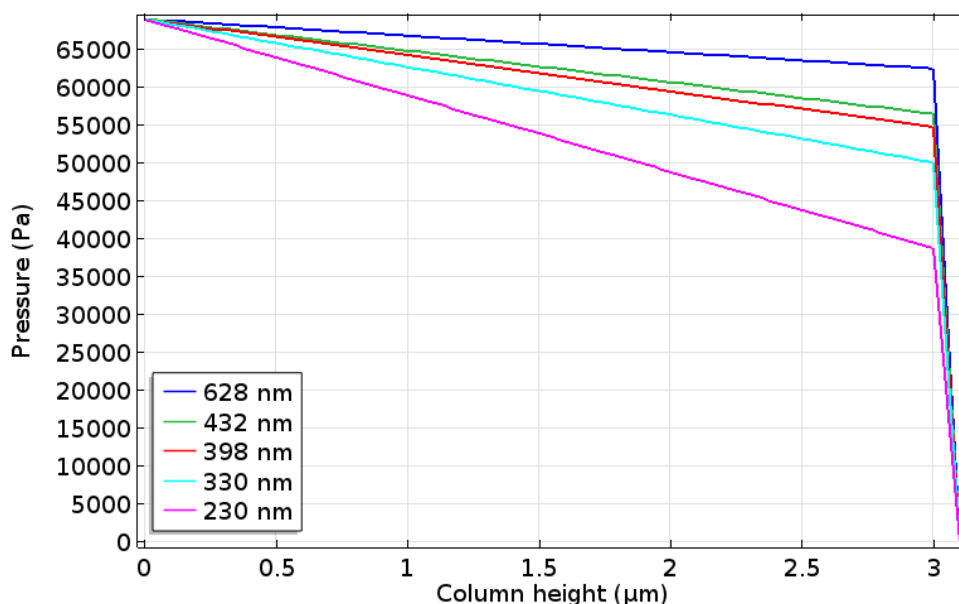


Figure 5.16. Pressure drop over 10 μm carbon columns on a membrane support. Columns with larger particle sizes see less pressure drop over the cake than those with smaller particle sizes.

1-pass S-PAC (628 nm) membrane coating data was fit with the following parameters: $D_s = 5 \times 10^{-10}$ cm²/min, $K_{fl} = 0.1$ cm/s, $K_F = 8$ mol/kg, $l/n = 0.1$, and $k_{ads} = 50$ (Figure 5.17). The Freundlich parameters correspond to a maximum adsorption site concentration of 1.29×10^{-6} mol/m². These parameters differ from the parameter results of HSDM modeling, which were not able to model the high removals in the membrane coating experiments.

When the best fit parameters for 628 nm were used with smaller particle sizes, the data of the smaller particles were not fit well. Since only 1-pass S-PAC saw significant breakthrough experimentally—other S-PACs resulted in near complete removal similar to the data for 15 min S-PAC (432 nm)—the parameters fit to 1-pass S-PAC can be used as a large particle control. The model reveals an intuitive result in the concentration over time

in the 632 nm carbon cake, which is shown in six panels in Figure 5.18. As the inlet concentration diffuses and reacts within the pellets, the full mass of incoming species is removed. Over time, the ability of carbon near the inlet has reduced ability to remove the species and concentrations are higher further and further down the column until the permeate concentration is considered to have broken through. Running the model for a longer time period would result in saturation of the column and a permeate concentration equal to the inlet concentration.

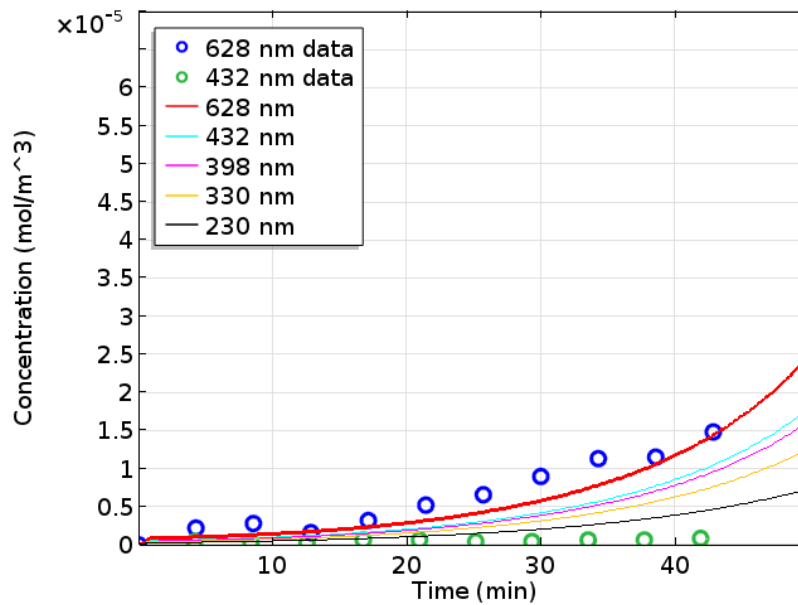


Figure 5.17. Permeate concentration of models with all S-PAC sizes using parameters for best fit of 1-pass S-PAC data. $D_s = 5 \times 10^{-10}$ cm²/min, $K_{fl} = 0.1$ cm/s, $K_F = 8$ mol/kg, $1/n = 0.1$, and $k_{ads} = 50$. Parameters that result in good fits to 1-pass data (628 nm) do not result in good fits for other S-PAC data.

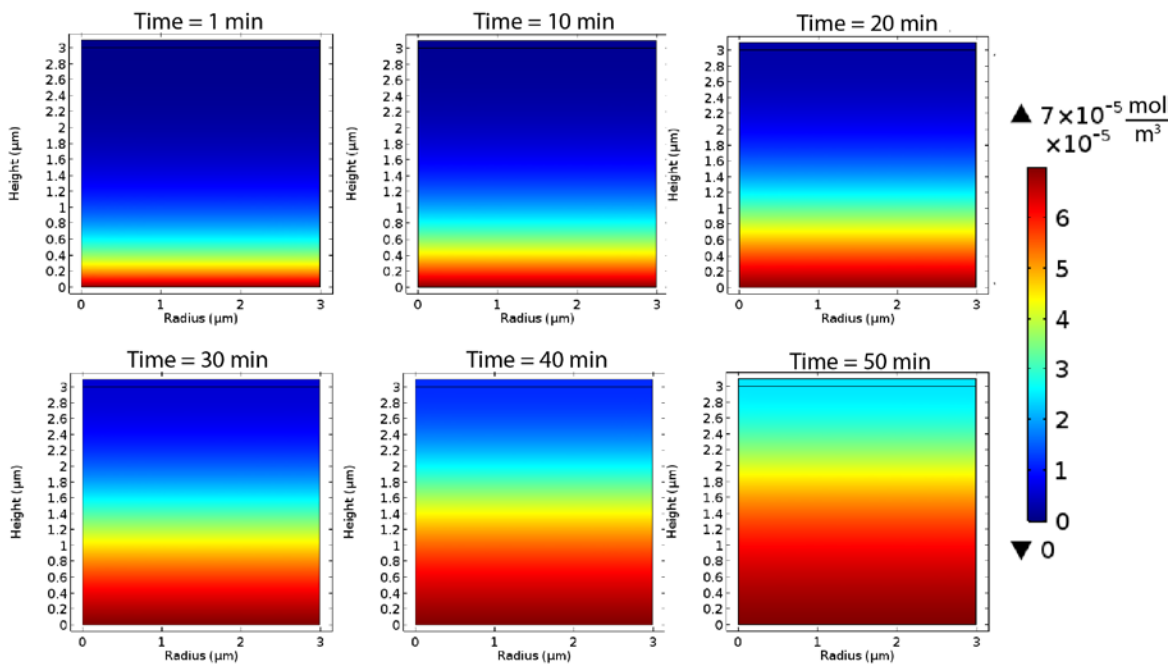


Figure 5.18. Concentration over the height of the simulated 628 nm carbon cake at various time points in the simulation.

Parameters were chosen by trial and error to best fit the remaining S-PAC data sets. All models used the isotherm parameters used to fit the 1-pass data set, $K_F = 8 \text{ mol/kg}$ and $1/n = 0.1$, as well as the values $K_{fl} = 0.1 \text{ cm/s}$ and $k_{ads} = 50$ (Figure 5.19). 15-min (432 nm) and 30-min (398 nm) were fit well with $D_s = 1.5 \times 10^{-6} \text{ cm}^2/\text{min}$, while 1-hr, 2-hrs (330 nm) and 6-hrs (230 nm) were best fit with $D_s = 5 \times 10^{-7} \text{ cm}^2/\text{min}$. Compared to the diffusivity that best fit the 1-pass data set, the remaining S-PACs required much larger values and the trend is non-linear since the smallest particles were fit with a smaller diffusivity than the intermediate sized particles.

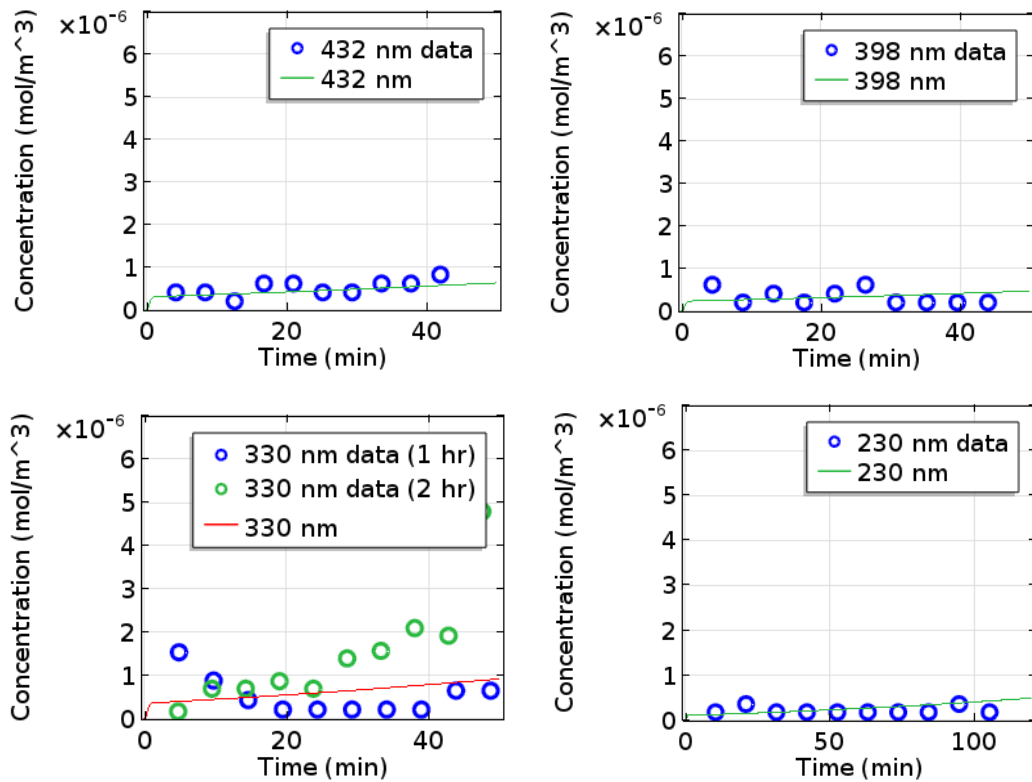


Figure 5.19. Permeate concentration of best fit models for S-PAC sizes except 1 pass. All models used the same isotherm parameters. 15 min (432 nm) data and 30 min (398 nm) data were modeled with $D_s = 1.5 \times 10^{-6} \text{ cm}^2/\text{min}$, while 1 hr, 2 hrs (330 nm) and 6 hrs (230 nm) data were modeled with $D_s = 5 \times 10^{-7} \text{ cm}^2/\text{min}$.

A benefit of the computational model is the ability to describe movement of species within the pellets as well as within the bed. In all models, the penetration of species into the particles was limited. The graphs in Figure 5.20 show the diffused liquid-phase species concentration and the adsorbed surface-phase concentration from the 230 nm model; the results are representative of the pellet concentrations resulting from all of the models. The lack of species presence within the pellet is an unexpected result. A postulation of the mechanism of S-PAC adsorption suggests that S-PAC utilizes a higher fraction of adsorbent volume than PAC due to a constant penetration depth into particles that limits

PAC volume utilization (Matsui et al., 2011). The COMSOL model instead predicts a limited diffusion distance despite the smaller particle size, though the models are not necessarily in conflict since larger particles may have the same limited penetration depth.

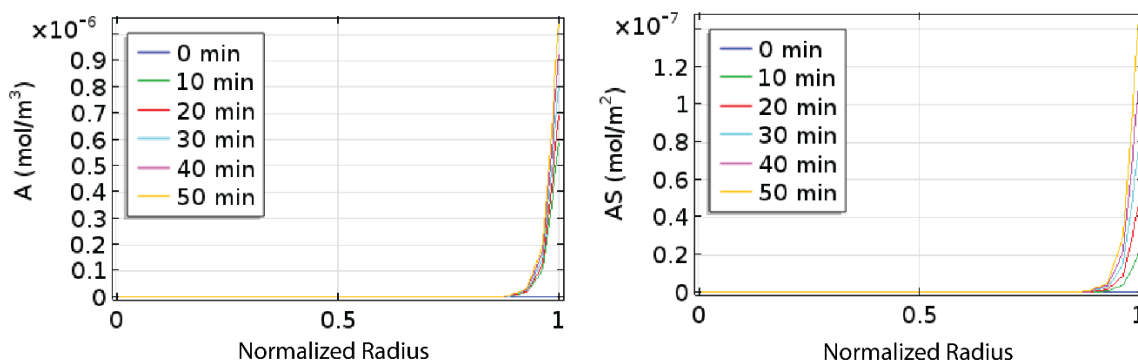


Figure 5.20. Concentrations within a pellet situated at $z = 2 \mu\text{m}$. Left: Concentration of liquid-phase species. Right: Concentration of solid-phase species.

Discussion

Using the HSDM model and best fit isotherm parameters, S-PAC data were fit with surface diffusion coefficients on the order of $10^{-11} \text{ cm}^2/\text{min}$, while the COMSOL model fit data with surface diffusion coefficients on the order of $10^{-6} \text{ cm}^2/\text{min}$. It is worthwhile to note that the models, which use the same fundamental principles of mass transfer, were fit to two different data sets: one as a batch contactor and one as a membrane coating.

The Freundlich isotherm parameters used in the COMSOL model, $K_F = 8 \text{ mol/kg}$ and $I/n = 0.1$, translate to $K_F = 34000 (\mu\text{g/mg})(\text{L}/\mu\text{g})^{1/n}$ and $I/n = 0.1$, which is a much larger coefficient than the best fit isotherm found for the HSDM model, $K_F = 11 (\mu\text{g/mg})(\text{L}/\mu\text{g})^{1/n}$ and $I/n = 0.4$. The Freundlich coefficient is generally a factor relating to the adsorption capacity while the Freundlich exponent is related to the adsorption affinity

or bonding strength, though the parameters are intertwined (Adams and Watson, 1996). A better comparison is between the equilibrium solid-phase concentration calculated using the Freundlich parameters. Given a concentration of 15 $\mu\text{g/L}$, the isotherm parameters used in the COMSOL model predict a solid-phase concentration of 222.1 $\mu\text{g/mg}$, while the parameters used in the HSDM model predict a solid-phase concentration of 32.5 $\mu\text{g/mg}$. While these values don't tell us absolute information about the properties of WC800 S-PAC, they indicate that superfine activated carbons, especially used as membrane coatings, act as super performing adsorbents.

A point of discrepancy in the treatment of Freundlich parameters is due to averaging. In finite element modeling, parameters are evaluated over small mesh volumes, while isotherm experiments produce parameters that are averaged over the entire particle volume. In the computational model, the level of adsorption achieved in the outer particle region is governed by the Freundlich parameters and therefore the equilibrium concentration must be higher than the average value in order to achieve the high removals observed in data.

Table 5.8. Summary of model parameter results for the best fit to each data set through HSDM modeling and CFD modeling. For comparison, the Freundlich equilibrium, q_e , is calculated for each set of Freundlich parameters for a concentration of 15 ppb atrazine.

Carbon	Size [μm]	HSDM model				CFD model			
		K_F [$\mu\text{g}/\text{mg}^*$ ($\text{L}/\mu\text{g}$) ^{1/n}]	1/n	q_e [$\mu\text{g}/\text{mg}$]	D_s (cm^2/min)	K_F [mol/kg]	1/n	q_e [$\mu\text{g}/\text{mg}$]	D_s (cm^2/min)
PAC	12.3	6	0.8	52.4	4.23E-11				
1 pass	0.6281	6	0.4	17.7	2.00E-12	20	0.15	199.2	5.00E-10
15 min	0.4315	11	0.4	32.5	4.64E-12	8	0.1	222.1	5.00E-10
30 min	0.3982	11	0.4	32.5	1.42E-11	8	0.1	222.1	1.50E-06
1 hr	0.329	11	0.4	32.5	1.48E-11	8	0.1	222.1	1.50E-06
2 hrs	0.3295	11	0.4	32.5	3.05E-12	8	0.1	222.1	5.00E-07
6 hrs	0.2304	11	0.4	32.5	3.19E-12	8	0.1	222.1	5.00E-07

One possibility for variable surface diffusivity coefficients is the possibility that the model varies according to a parameter such as particle size. Studies have had mixed results in the correlation of surface diffusion coefficients fit to experimental data to other parameters, including particle size and pore volume distribution (Najm et al., 1990; Li et al., 2003). The surface diffusion coefficients found with the HSDM model and CFD model do not correlate with any of the material parameters measured for the produced S-PACs. However, the best fit parameters, taken as the surface diffusion coefficient and the Freundlich equilibrium concentration, correlated to the overall atrazine removal through carbon coatings (Figure 5.21). The HSDM parameters correlated with atrazine removal according to the equation $-27.73 + (3.065 \times 10^{11})D_s + 2.90q_e$ ($R^2 = 0.848$). CFD parameters correlated with atrazine removal according to the equation $-329.6 + (5.07 \times 10^6)D_s + 1.77q_e$ ($R^2 = 0.847$). While the correlation does not reveal information about the mechanism since atrazine removal is not a predictive factor, since atrazine removal is also correlated to a

combination of specific external surface area and oxygen content, the correlation is indicative of a relationship between the model fit and the carbon surface properties.

Lastly, the data set here only comprises the adsorption of one adsorbate to one carbon. Material parameters are not explored here that may reveal more about the mechanism for S-PAC adsorption. For example, varying the pore size distributions of the carbon adsorbent could determine whether the ratio of macropores to micropores is needed for S-PAC modeling. Variation of the adsorbate pK_a could reveal whether the surface charge as a result of oxidation interacts significantly with the ionization state of the adsorbed species. Completing additional experimental studies to expand the combination of adsorbate-adsorbent interactions would provide additional material parameters for understanding S-PAC adsorption.

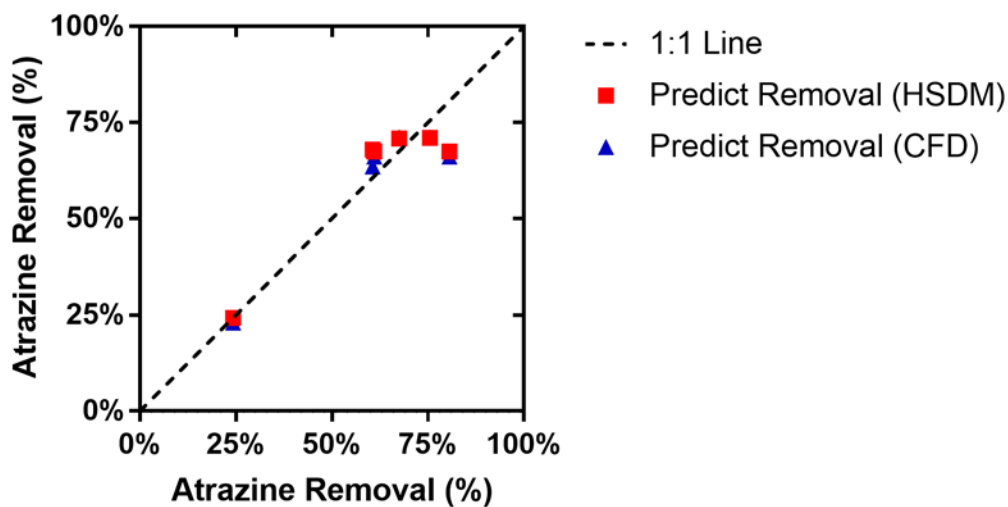


Figure 5.21. HSDM and CFD model parameters correlated to the overall atrazine removal through carbon coatings. The dashed line is provided for a 1:1 reference.

Conclusions

- Batch kinetics data were modeled well with HSDM after using the isotherm coefficient and exponent as fitting parameters in addition to the surface diffusion coefficient.
- CFD modeling was able to model atrazine adsorption despite the extremely limited cake thickness.
- Higher values of both isotherm parameters and surface diffusivity were needed to model atrazine removal through an S-PAC coating using CFD modeling as compared to HSDM.
- The results of both modeling approaches signify a high performing adsorbent exceeding expectations based on experimental isotherm measurements.
- A mechanism of S-PAC adsorption is not determined from the results, but specific external surface area appears to be a key factor in S-PAC coating success.
- Additional adsorbates and carbon combinations should be explored experimentally to increase data for parameter correlation.

CHAPTER SIX

CONCLUSIONS AND RECOMMENDATIONS

Summary and Conclusions

The work detailed here covered a novel method of activated carbon use in drinking water treatment, characterization of the new carbon material, and modeling of the application method. The method of applying S-PAC as a membrane coating, which was shown prior as an effective method to remove trace contaminants, is explored and analyzed from three different perspectives.

Chapter 3 explored aggregation to alleviate membrane fouling that revealed coagulant type and dosing as critical to the success of a direct filtration membrane process. In general, coagulant use led to increased membrane fouling instead of decreased fouling. If fouling reduction is required for an economically viable S-PAC process and chemical coagulants are used, precise dosing is required to avoid membrane fouling by metal precipitates. Other potential fouling control methods could be implemented to prevent marked flux decline and/or transmembrane pressure increase, such as low concentration S-PAC dosing, which would likely result in reduced contaminant removal, high concentration dosing to promote self-aggregation, or high frequency of backwashing.

Chapter 4 examined how S-PAC characteristics are affected by the material production process. Of the adsorption related parameters selected for measurement, surface chemistry and oxygen content changed significantly and unexpectedly as a result of milling. The results indicate the potential of the milling environment to drastically alter the surface functionality of activated carbon. The chemical changes do not negatively affect

carbon adsorption, and it is not yet clear whether the changes are key factors in the high performance of S-PAC. It is also possible that S-PAC production in an environment designed to reduce oxidation may result in carbon with significantly different performance. Such an environment could be devised by degassing the milling solvent to remove oxygen.

Chapter 5 continued the pursuit of understanding S-PAC adsorption mechanisms from a theoretical standpoint. The S-PACs produced in chapter 4 with varied characteristics removed atrazine quickly and completely in both a batch reactor system and a membrane coating system. While both analytical and computational models were able to fit the data, the parameters needed to achieve the fits were varied and differed from measured values. Additionally, the experimental performance of S-PAC greatly exceeded the performance that the models predicted from measured parameters. The results suggest that the physics of adsorption over characteristic lengths on the nano- to micro-scale could be different from conventional scales. The correlation of both the experimental data and the fitted model parameters, which resulted from modeling of two disparate data sets, to external surface parameters suggests that functionality on the surface is the key factor behind an adsorption mechanism that increases S-PAC performance far beyond theoretical expectations.

Recommendations for Future Work

Fouling Study with Backwash

In the membrane fouling study, only deposition of S-PAC was measured. However, in water treatment plants, microfiltration filters are backwashed to remove particulate buildup and regenerate flux capacity. Removal is especially important for adsorbents since

capacity becomes exhausted over time and replacement material is needed. It is not known how S-PAC, either aggregated or unaggregated, will respond to removal by hydraulic backwashing from polymeric membranes. For ceramic membranes, an example with backwashing exists. A direct filtration ceramic membrane system used S-PAC in conjunction with PACl and was successfully backwashed, even producing lower transmembrane pressure increase than trials with PAC (Matsui et al., 2009b).

It is possible that S-PAC will adhere to the membrane fibers and resist hydraulic backwashing, since the adsorption potentials that attract solutes can also result in surface attraction. In that case, exploration of a barrier between the S-PAC coating and the membrane surface such as a large molecule surfactant might be a solution to enhance the hydraulic removal of S-PAC coatings (Chen et al., 1992).

Submerged Membrane Study

The results of the aggregation study had high variation and one possible source of error is in transfer between the jar testing apparatus and the filtration apparatus. While in a drinking water plant with membrane filtration it would be necessary to transfer water from a flocculation basin to the membrane unit via pumping and piping, an alternative to those systems is a submerged membrane unit. With a submerged unit, the membrane is immersed at the end of the flocculation basin and negative pressure pulls water through the membrane for an outside-in operation. This setup avoids introducing turbulence between flocculation and membrane filtration. Bench-scale studies will reveal whether the breaking of floc via turbulent transfer was a major source of variability in the aggregation experiments. A study will also reveal whether submerged membranes are a solution to S-PAC application.

Further S-PAC Experimentation

Further experimental measurements of S-PAC in continuously stirred systems and membrane coating systems is recommended because there are still additional unknown parameters that may be relevant to the mechanism of S-PAC adsorption. Experiments should vary the types of carbon and the types of adsorbates. In regards to adsorbate variation, compounds can be varied over molecule size, polarity, planarity, and solubility; similar studies have been performed to understand PAC adsorption (Brooks et al., 2012; Apul et al., 2013). Non-environmentally relevant compounds may be useful for evaluating extremes.

In regards to carbon type, selecting an alternative carbon adsorbent with more homogenous properties may be useful in elucidating correlating material and adsorbate properties (Pelekani and Snoeyink, 2000). Activated carbon fiber (ACF) is an example of a bottom-up carbon adsorbent with controlled material properties. ACF also has a small diameter similar to S-PAC, but is not compatible with the models developed here. Taking the ACF production process as inspiration, bottom-up spherical carbon adsorbents can be produced, such as by hydrothermal reaction of soluble carbon precursors (Sun and Li, 2005; Pan et al., 2012). With a more controllable particle size and carbon structure, synthetic activated carbon nanospheres may reveal information about small-size adsorption mechanisms.

It is also recommended to incorporate additional material characterization. Since the external surface of S-PAC was discovered to be significant outcome of milling and a significant factor in adsorption performance, additional measurement of the surface is

warranted. The types of functional groups present on the surface can be estimated by Raman spectroscopy via bond structure information. Nuclear magnetic resonance (NMR) imaging can also be used to pinpoint chemical bonds as well as provide a more accurate estimate of surface element concentrations.

Any additional kinetics experimentation should be devised such that adsorbate removals are gradual over the course of the experiment. A significant difficulty in modeling the S-PAC results in chapter 5 is fitting of the model to extremely small atrazine values. Batch kinetics experiments should show concentration decline over multiple data points before reaching steady state. Membrane coating experiments should show breakthrough and concentration increase over multiple data points. Such results would be obtained by using a higher adsorbate to adsorbent ratio and/or longer experiment times.

Models with Additional Mechanisms

Two factors that were not considered in HSDM are the film transfer coefficient and penetration depth. These factors were present in the CFD model; however, constant values were used to limit the number of degrees of freedom. Analytical models with increased complexity should be explored, starting with film transfer incorporated into HSDM via mass balance and extending to such models as the branched pore kinetic model (BPKM) for multiple transport regions or the shell adsorption model (SAM) to describe equilibrium under the assumption of a limited penetration depth. While BPKM is an analytical model, the incorporation of multiple fitting parameters does not necessarily lead to increased understanding of the modeled system. Results of SAM modeling would be interesting in relation to the CFD results that predict very limited particle penetration.

There are many parameters that can be adjusted with modified coefficients to improve model fits. For example, like the Kozeny constant was determined empirically, values for porosity can be modified, removing the assumption of a fully compact random packed bed. An example is a model of PAC applied in a submerged membrane reactor, which does not observe heavy compaction, that was fit well with a membrane packing parameter (Vigneswaran et al., 2016). Conversely, an exceptionally compact bed may describe the S-PAC membrane coating better for the reason that heterogeneous particle size distributions could lead to higher packing efficiencies.

Other aspects that have not been touched on in this work are also worth exploring. Effects of pressure and fluid flow can be examined by modeling. Reynolds number regions may have effects on the transport of solutes outside primary streamlines. At high Reynolds number, the ratio of centric void flow to mean interstitial flow is much higher (Suekane et al., 2003). The experimental data set for such a study would involve velocities much faster than the ones presented here to produce Reynolds numbers on the order of 10–20. Lastly, theoretical mechanisms that incorporate surface functionality should be explored in response to correlations between adsorption and specific external surface area. This effort should be incorporated along with additional material characterization.

APPENDICES

Appendix A

HSDM Model

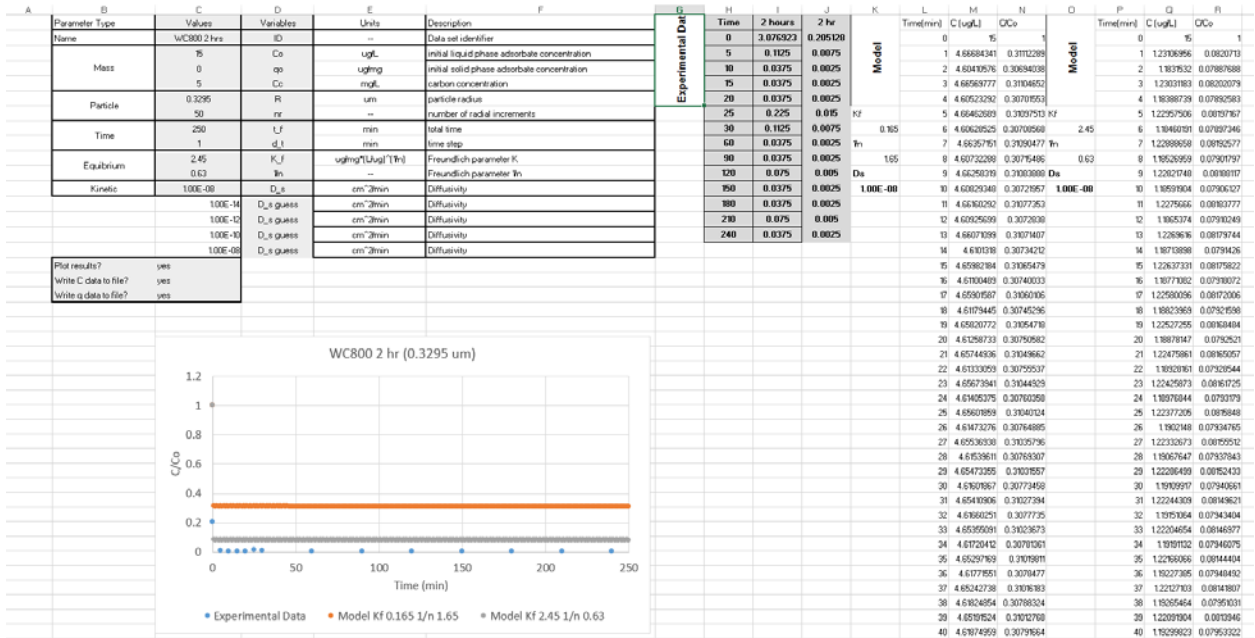


Figure A.1. Excel input file, HSDMin.xlsx, modified from To

Modified scripts, originally created by Priscilla To. Only modified HSDM and DsSearch to adapt for the data set used, base calculations are untouched.

```
function HSDM
% Author: Priscilla To, mod. Erin Partlan (2016)
% Description: HSDM for PAC batch adsorption system
% Uses finite difference method to solve for solid-phase concentration
of
% trace of trace compound (u=gr)
% Assumes
% -instantaneous equilibrium on surface between bulk liquid-PAC as
% described by Freundlich
% -spherical symmetry
% -well mixed system, neglect film diffusion at boundary
% -constant diffusivity and density
clear

% -----
----
% read input file (HSDM_in.xls)
% nf = 1/n
```

```

[inputfile,text] = xlsread('HSDMin.xlsx', 'C2:C19') ;
id = text (1) ;
plot = char(text(end-2)) ;
writeC = char(text(end-1)) ;
writeq = char(text(end));
dt = inputfile (7); % min
Ds = inputfile (10); % cmA2/min

% call function singleHSDM to solve for C and q numerically
[C_final, q, time, rad, m, n] = singleHSDM (Ds, inputfile);
Co = inputfile (1); % ug/L
C_over_Co = 0;
if Co ~= 0
    C_over_Co = C_final./Co;
end

if (isequal(plot,'yes') == 1)
    plotresults (id, C_final, C_over_Co, time, q, rad, n, dt) ;
end
if (isequal(writeC,'yes') == 1)
    writeCresults(id, time, C_final, C_over_Co);
end
if (isequal(writeq,'yes') == 1)
    writeqresults(id, time, rad, q, m, n) ;
end
if (isequal(plot,'yes')==1) || (isequal(writeC,'yes')==1) || ...
    (isequal(writeq,'yes')==1)
    writeinput(id, inputfile);
end

% -----
% ----- subfunctions -----
% -----

function plotresults (id, C_final, C_over_Co, time, q, rad, n, dt)
% Plot results of C/Co (or C if Co = 0)
    subplot(1,2,1);
    axis([0,1,0,inf])
    if C_over_Co == 0
        plot (time, C_final, '.b');
        ylabel ('C (ug/L)') ;
    else
        plot(time, C_over_Co, '.b');
        ylabel ('C/Co (ug/L) ' ) ;
    end
    xlabel('Time (min)');
    title([id, 'C profile']);
    hold on

    subplot(1,2,2);
    hold on

```

```

N = round([2; n/4; n/2; n*3/4; n]);
T = int2str((N-1)*dt);
t = ['t = ' ; 't = ' ; 't = ' ; 't = ' ; 't = ' ] ;
min = [' min'; ' min'; ' min'; ' min'; ' min'];
legendlabels = cat(2, t, T, min);
plot (rad, q(2:end,N(1)),'.m') ,
plot (rad, q(2:end,N(2)),'.r') ,
plot (rad, q(2:end,N(3)),'.c') ,
plot (rad, q(2:end,N(4)),'.b') ,
plot (rad, q(2:end,N(5)),'.k') ,
xlabel('Radius (um)');
ylabel( 'q' ) ;
title([id, 'q profile']);
legend (legendlabels);
hold off
return;
% -----
----
function writeCresults(id, time, C_final, C_over_Co);
% write C data to excel file with function write_xls
% writes results to excel file with name "id"
filename=char(id);
Clabel = {'Time(min)', 'C (ug/L)', 'C/Co'};
xlswrite(filename, Clabel, 'Sheet1', 'A1');
xlswrite(filename, time, 'Sheet1', 'A2');
xlswrite(filename, C_final, 'Sheet1', 'B2');
if C_over_Co ~= 0
    xlswrite(filename, C_over_Co, 'Sheet1', 'C2')
end
return
% -----
----
function writeqresults(id, time, rad, q, m, n );
% write q data to excel file with function write_xls
% writes results to excel file with name "id"
% Excel number of columns limited to 256
filename=char(id);
if n < 255
    qsmall = q;
    tsmall = time';
else
    qsmall = [ ] ;
    tsmall = [ ] ;
    for i = 1:ceil(n/255):n
        qsmall = [qsmall, q(:,i)];
        tsmall = [tsmall, time(i)];
    end
end
end
Qlabel = {'Time(min)'; 'Radius(um)='};
xlswrite(filename, Qlabel, 'Sheet3');
xlswrite(filename, rad, 'Sheet3', 'A3');
xlswrite(filename, tsmall, 'Sheet3', 'B1');
xlswrite(filename, qsmall(2:m,:), 'Sheet3', 'B3');

```

```

return;
%-----
-----
function writeinput(id, inputfile);
% write input parameters to file
    filename=char(id);
    Labels = {'File ID'; 'Co (ug/L)'; 'qo (ug/mg)'; 'Cc (mg/L)';...
             'R (um)'; 'nr (-)'; 'tf (min)'; 'dt (min)'; ...
             'K (ug/mg*L/mg^1/n)'; '1/n (-)'; 'Ds (cm^2/min)'} ;
    xlswrite(filename, Labels, 'Sheet2', 'A1');
    xlswrite(filename, id, 'Sheet2', 'B1');
    xlswrite(filename, inputfile(1:10), 'Sheet2', 'B2');
return;

function DsSearch
% Author: Priscilla To, mod. Erin Partlan (2016)
% Description: Fit Ds to experimental data using HSDM for batch
% adsorption system. Requires initial guess for Ds.
% If error is large, guess a new Ds.
% Uses finite difference method to solve for solid-phase concentration
of
% trace of trace compound (u=qr)
% Assumes
% -instantaneous equilibrium on surface between bulk liquid-PAC as
% described by Freundlich
% -spherical symmetry
% -well mixed system, neglect film diffusion at boundary
% -constant diffusivity and density

clear

% -----
-----
% read experimental data (input.xls)
% column 1 of data = Time (min)
% column 2 of data = Conc. (ug/L)

[data] = xlsread('HSDMin.xlsx', 'H:I');

% read input parameters
% nf = 1/n
[inputfile,text] = xlsread('HSDMin.xlsx', 'C2:C19');
id = text(1);
plot = char(text(end-2));
write = char(text(end));
Dsguess = inputfile(10:end); % initial guesses for Ds

% -----
-----
% fits input data to Ds, using least squares error
options = optimset ('Display', 'iter'); % set to display iterations

```



```

trackDs = [];
a = size (Dsguess);
for i = 1:1:a(1)
    [Ds,resnorm,residual,exitflag] = lsqnonlin
(@finddiff,Dsguess(i),0, ...
    1e-8,options,data,inputfile);
    trackDs = [trackDs; Dsguess(i), Ds, resnorm, exitflag];
end

format short e
disp(' ');
disp(' Guess Ds   Search Ds   Resnorm   Exitflag');
disp (trackDs);

if ((isequal(write, 'yes') == 1) || (isequal(plot, 'yes') == 1))
    [trackC_final, trackq, time] = runHSDM (a, trackDs, inputfile);
    if (isequal(plot, 'yes') == 1)
        plotresults (data, a, time, id, trackC_final, trackDs);
    end
    if (isequal(write, 'yes') == 1)
        writeresults (id, time, inputfile, trackDs, trackC_final,
data);
    end
end
end
% -----
% ----- subfunctions -----
% -----
function diffarray = finddiff (Ds,data,inputfile);
% 1) Calc C and q profile by HSDM given Dsguess
% 2) Compare differences from data points to calculated profiles.
%   If data does not match numerical steps, interpolate between points
% 3) Returns an array of differences (not yet squared)
[C_final, q , time, rad, m, n] = singleHSDM (Ds, inputfile);
diff = [];
C = [];
i = 1;
for i = 1:1:length(data)
    index = find(time > data(i,1));
    a = index (1);
    frac = (data(i,1) - time (a-1))/(time(a)-time(a-1));
    C = [C; frac * (C_final(a)-C_final(a-1)) + C_final(a-1)];
end
diffarray = data(:,2) - C;
return

% -----
% -----
function [trackC_final, trackq, time] = runHSDM (a, trackDs, inputfile)
% Runs HSDM model for fitted Ds
    trackC_final = [];

```

```

        trackq = [];
        for i = 1: 1:a(1)
            [C_final, q, time, rad, m, n] = singleHSDM
(trackDs(i,2),inputfile);
            trackC_final(:,i) = C_final';
            trackq = [trackq, q];
        end
    return

% -----
% -----
function plotresults (data, a, time, id, trackC_final, trackDs)
% Plots data and curve from search results
    hold on
    plot (data(:,1),data(:,2),'ok');
    for i = 1:1:a(1)
        if i==1            plot (time, trackC_final(:,1), '-k');
            elseif i==2    plot (time, trackC_final(:,2), '-b');
            elseif i==3    plot (time, trackC_final(:,3), '-c');
            elseif i==4    plot (time, trackC_final(:,4), '-r');
            else            plot (time, trackC_final(:,5), '-m');
        end
    end

    xlabel ('Time (min)');
    ylabel('C (ug/L)');
    title([id, 'Experimental and fitted C profiles']);
    D = [];
    E = [];
    for i=1:1:a(1)
        D = [D; 'Ds = ' ] ;
        E = [E; ' err = '];
    end
    DD = num2str(trackDs(:,2));
    EE = num2str(trackDs(:,3));
    legendlabels = cellstr(cat(2, D, DD, E, EE));
    legendlabels = cat(1, 'Expr data', legendlabels);
    legend(legendlabels);
hold off
return

% -----
% -----
function writesresults (id, time, inputfile, trackDs, C_final, data);
% Subfunction writes results to excel file with name "id"+fit
    filename=[char(id), ' fit'];
    T = {'Time (min)', 'C (ug/L)'};
    D = {'Guess Ds (cm^2/min)'; 'Search Ds (cm^2/min)';
'Error'; 'Exitflag'};
    xlswrite(filename, D, 'Sheet1', 'A1');
    xlswrite(filename, T, 'Sheet1', 'A5');
    xlswrite(filename, time, 'Sheet1', 'A6');
    xlswrite(filename, trackDs, 'Sheet1', 'B1');
    xlswrite(filename, C_final, 'Sheet1', 'B6');

```

```

    Labels = {'File ID', 'Co (ug/L)', 'qo (ug/mg)', 'Cc (mg/L)',
'R(um)', ...
    'nr (-)', 'tf(min)', 'dt(min)', 'K(ug/mg*L/mg^1/n)', '1/n
(-)'};
    xlswrite(filename, Labels, 'Sheet2', 'A1');
    xlswrite(filename, id, 'Sheet2', 'B1');
    xlswrite(filename, inputfile (1:9), 'Sheet2', 'B2');
    E = {'Experimental Data'};
    xlswrite(filename, E, 'Sheet2', 'D1');
    xlswrite(filename, T, 'Sheet2', 'D2');
    xlswrite(filename, data, 'Sheet2', 'D3');
return

function [C_final, q, time, rad, m, n] = singleHSDM (Ds, inputfile);

% Returns C_final and q profiles given input of Ds

Co = inputfile (1); % ug/L
qo = inputfile (2); % ug/mg
Cc = inputfile (3); % mg/L
R = inputfile (4) * 1e-4; % convert from um to cm
nr = inputfile (5); % number of radial increments
tf = inputfile (6); % min
dt = inputfile (7); % min
Kf = inputfile (8); % ug/mg * L/ug^1/n
nf = inputfile (9); % 1/n = unitless
    % Ds (cm^2/min) given as input

%
% %Values for debugging
% Co = 15; % ug/L
% qo = 0; % ug/mg
% Cc = 1; % mg/L
% R = 25 * 1e-4; % convert from um to cm
% nr = 50; % number of radial increments
% tf = 30000; % min
% dt = 1000; % min
% Kf = 2.83; % ug/mg * L/ug^1/n
% nf = 0.65; % 1/n = unitless
% Ds = 5e-8; % Ds (cm^2/min)
%

% -----
% -----
% define step size dr and dt
dr = R/nr;
m =(R/dr + 1); %nr + 1, so that r goes from 0:nr

```

```

n = tf/dt + 1; %nt + 1
% -----
----
% mass balances for total mass of trace compound in batch system
C_final(1) = Co;
Ctot = C_final(1) + qo * Cc;
% -----
----
% set up u(t=0) matrix for column vector (t=0 aka n=1)
% all u = qo*r
trackn = 1; % first time step, t=0
u = [];
for i = 1:1:m
    r = (i-1) * dr;
    u(i,trackn) = qo*r;
end
intm = int16(m);
qavg = calc_qavg(u(:,1),dr,R,m);
trackqavg(1) = qavg;
% -----
----
% Steps to solving at a single time step (repeat for each new time
step):
% 1) Make initial guess for C(t=trackn)
% 2) Use guess to calculate uguess(r=R)= R * Kf * C^1/n
% 3) Use Crank-Nicholson/finite differences method to solve for
u(r,trackn)
% 4) Use numerical integration to find q_avg = u/r
% 5) Use q_avg to calc C(t) = Ctot - q_avg*Cc
% 6) Compare C(t) to initial guess = error
% 7) Repeat 2 to 7, updating C(t) w/ new value until error w/in
tolerance

% Initial Guess
Cguess = 0;
uguess = R*Kf*Cguess^nf;

% set up tridiagonal constant matrix for simultaneous system of eqns to
% be solved by Thomas method
alpha = Ds * dt / (2* (dr)^2);
for i = 1:1:m-2
    a(i) = - alpha;
    b(i) = 1 + 2*alpha;
    c(i) = - alpha;
end
a(1) = 0;
c(intm-2)= 0;

% define d matrix
B = [];
for i = 1:1:m-3
    B(i,i) = 1 - 2 * alpha;
    B(i+1,i) = alpha;
    B(i,i+1) = alpha;

```

```

end
B(intm-2,intm-2) = 1 - 2 * alpha;
D = [];

for trackn = 2:1:n % solve for next time step
    Cguess = [];
    Ccalc = [];
    iter = 1;
    error = 1;
    while (abs(error(end)) > 1e-4)
        if iter == 1
            Cguess = 0;
            bound = Cguess;
        elseif iter == 2 % set next C(t) guess
            Cguess = [Cguess; Ccalc(end)];
        elseif (sign(error(end)) ~= sign(error(end-1)))
            bound = Cguess(end-1);
            Cguess = [Cguess; 0.5 * (Cguess(end) + bound)];
        else Cguess = [Cguess; 0.5 * (Cguess(end) + bound)];
        end

        uguess = R * Kf * double(Cguess(end))^nf; % ensure Cguess is
double-precision
D(intm-2) = alpha * (u(intm,trackn-1) + uguess);
d = B * u(2:intm-1,trackn-1) + D'; % update d matrix
utemp(1) = 0; % u(r=0) = 0
utemp(2:intm-1) = nextdt(a,b,c,d); % solv by Thomas method
utemp(intm) = uguess; % u(r=R) = u(m)
qavg = calc_qavg(utemp,dr,R,m);

        Ccalc = [Ccalc; (Ctot - qavg * Cc)];
        error = [error; Cguess(end)-Ccalc(end)];
        iter = iter + 1;
    end
    C_final(trackn) = Cguess(end);
    u(:,trackn) = utemp';
    trackqavg(trackn) = qavg;
end

% -----
% -----
% create time array
% calculate q (not defined at r=0)
time = [];
for i = 0:dt:tf
    time = [time; i];
end
rad = [];
q = [];
for i = 2:1:m
    rad = [rad; (i-1) *dr*10000];
    q(i,:) = u(i,:)/((i-1)*dr);
end

```

```

% executes thomas method given input of tridiagonal elements
function [utemp] = nextdt (a, b, c, d);
utemp = [];
h = [] ;
p = [] ;
h(1) = [c(1)/b(1)];
p(1) = [d(1)/b(1)];
l = length (a);

for k = 2:1:l
    h(k) = c(k)/(b(k) - a(k)*h(k-1));
    p(k) = (d(k)-a(k)*p(k-1)) / (b(k)-a(k)*h(k-1));
end

utemp(l) = p(l); % because h(l) = 0

for k = l-1:-1:1
    utemp(k) = p(k) - h(k) * utemp(k+1);
end

% calculate qavg = average q in spherical particle
% by numerical integration - trapezoidal rule
% requires input of a 1-dimensional array
function [qavg] = calc_qavg (u,dr,R,m);
sum=0;
for i = 1:1:m-1
    r1 = (i-1)*dr; % radius at i
    r2 = i * dr; % radius at i+1
    r1 = double(r1); % convert to double precision
    r2 = double(r2);
    u1 = u(i);
    u2 = u(i+1);
    sum = sum + (dr / 2 * (r1*u1+ r2*u2));
end;
qavg = 3 /R^3 * sum;
return;

function diffarray = finddiff (Ds,data,inputfile);
% function to
% 1) Calc C and q profile by HSDM given Dsguess
% 2) Compare differences from data points to calculated profiles.
% If data does not match numerical steps, interpolate.
% 3) Returns an array of differences (not yet squared)

[C_final, q , time, rad, m] = singleHSDM (Ds, inputfile);
% -----

```

```

% find difference between data and calculated cone
diff = [];
C = [];
i = 1;

for i = 1:1:length(data)
    index = find(time > data(i,1));
    a = index(1);
    frac = (data(i,1) - time(a-1))/(time(a)-time(a-1));
    C = [C; frac * (C_final(a)-C_final(a-1)) + C_final(a-1)];
end
diffarray = data(:,2) - C;
return;

```

REFERENCES

- Abram, J. C. (1973) The Characteristics of Activated Carbon, *Proceedings of the Conference on Activated Carbon in Water Treatment*.
- Adams, C. D. (2009) Pharmaceuticals, in *Contaminants of Emerging Environmental Concern*. Reston, VA: American Society of Civil Engineers, pp. 56–85.
- Adams, C. D. and Watson, T. L. (1996) Treatability of s-triazine herbicide metabolites using powdered activated carbon, *Journal of Environmental Engineering*, pp. 327–330.
- Adams, C., Loftin, K. A., Adams, C., Asce, M., Wang, Y., Loftin, K. and Meyer, M. (2002) Removal of antibiotics from surface and distilled water in conventional water treatment processes, *Journal of Environmental Engineering*, 128, pp. 253–260.
- Adham, S. S., Snoeyink, V. L., Clark, M. M. and Bersillon, J. (1991) Predicting and verifying organics removal by PAC in an ultrafiltration system, *Journal AWWA*, 83(12), pp. 81–91.
- Akmil Başar, C., Karagunduz, A., Keskinler, B. and Cakici, A. (2003) Effect of presence of ions on surface characteristics of surfactant modified powdered activated carbon (PAC), *Applied Surface Science*, 218(1–4), pp. 170–175.
- Allen, D. T. and Shonnard, D. R. (2001) *Green engineering: Environmentally conscious design of chemical processes*. Prentice Hall.
- Amaral, P., Partlan, E., Li, M., Lapolli, F., Mefford, O. T. T., Karanfil, T. and Ladner, D.

- A. (2016) Superfine powdered activated carbon (S-PAC) coatings on microfiltration membranes: Effects of milling time on contaminant removal and flux, *Water Research*, 100, pp. 429–438.
- Ando, N., Matsui, Y., Kurotobi, R., Nakano, Y., Matsushita, T. and Ohno, K. (2010) Comparison of natural organic matter adsorption capacities of super-powdered activated carbon and powdered activated carbon, *Water research*. Elsevier, 44(14), pp. 4127–4136.
- Ando, N., Matsui, Y., Matsushita, T. and Ohno, K. (2011) Direct observation of solid-phase adsorbate concentration profile in powdered activated carbon particle to elucidate mechanism of high adsorption capacity on super-powdered activated carbon, *Water Research*. Elsevier Ltd, 45(2), pp. 761–767.
- Apul, O. G., Hoogesteijn Von Reitzenstein, N., Schoepf, J., Ladner, D., Hristovski, K. D. and Westerhoff, P. (2017) Superfine powdered activated carbon incorporated into electrospun polystyrene fibers preserve adsorption capacity.
- Apul, O. G. and Karanfil, T. (2015) Adsorption of synthetic organic contaminants by carbon nanotubes: A critical review, *Water Research*, pp. 34–55.
- Apul, O. G., Wang, Q., Zhou, Y. and Karanfil, T. (2013) Adsorption of aromatic organic contaminants by graphene nanosheets: comparison with carbon nanotubes and activated carbon., *Water research*. Elsevier Ltd, 47(4), pp. 1648–54.
- ASTM Standard D3802-10 (2010) *Standard Test Method for Ball-Pan Hardness of Activated Carbon*. West Conshohocken, PA: ASTM International.
- Azizian, S. (2004) Kinetic models of sorption: A theoretical analysis, *Journal of Colloid*

and Interface Science, 276, pp. 47–52.

Badruzzaman, M., Westerhoff, P. and Knappe, D. R. U. (2004) Intraparticle diffusion and adsorption of arsenate onto granular ferric hydroxide (GFH), *Water Research*, 38(18), pp. 4002–4012.

Bakkaloglu, S. (2014) *Adsorption of synthetic organic chemicals: A comparison of superfine powdered activated carbon with powdered activated carbon*. Clemson University.

Barnes, K. K., Kolpin, D. W., Furlong, E. T., Zaugg, S. D., Meyer, M. T. and Barber, L. B. (2008) A national reconnaissance of pharmaceuticals and other organic wastewater contaminants in the United States — I) Groundwater, *Science of The Total Environment*, 402(2), pp. 192–200.

Berg, J. C. (2010) *An Introduction to Interfaces & Colloids: The Bridge to Nanoscience*. World Scientific.

Bhandari, A., Surampalli, R. Y., Adams, C. D., Champagne, P., Ong, S. K., Tyagi, R. D. and Zhang, T. (eds) (2009) *Contaminants of Emerging Environmental Concern*. Reston, VA: American Society of Civil Engineers.

Biniak, S., Pakula, M., Szymanski, G. and Swiatkowski, A. (1999) Effect of activated carbon surface oxygen-and/or nitrogen-containing groups on adsorption of copper (II) ions from aqueous solution, *Langmuir*, 15, pp. 6117–6122.

Biniak, S., Swiatkowski, A. and Pakula, M. (2007) Electrochemical studies of phenomena at active carbon-electrolyte solution interfaces, in Radovic, L. (ed.) *Chemistry & Physics of Carbon*. CRC Press, pp. 125–216.

- Bird, A. and Trimm, D. (1983) Carbon molecular sieves used in gas separation membranes, *Carbon*, 21(3), pp. 177–180.
- Boehm, H. P. (1994) Some aspects of the surface chemistry of carbon blacks and other carbons, *Carbon*, 32(5), pp. 759–769.
- Boehm, H. P. (2002) Surface oxides on carbon and their analysis: a critical assessment, *Carbon*, 40(2), pp. 145–149.
- Bowman, B. T. (1982) Conversion of Freundlich adsorption K values to the mole fraction format and the use of S_Y values to express relative adsorption of pesticides, *Soil Science Society of America Journal*, 46(4).
- Brar, S. K., Verma, M., Tyagi, R. D. and Surampalli, R. Y. (2009) Nanoparticles, in *Contaminants of Emerging Environmental Concern*. Reston, VA: American Society of Civil Engineers, pp. 416–445.
- Brooks, A. J., Lim, H. and Kilduff, J. E. (2012) Adsorption uptake of synthetic organic chemicals by carbon nanotubes and activated carbons, *Nanotechnology*. IOP Publishing, 23(29), p. 294008.
- Carman, P. (1956) Flow of gases through porous media.
- Carroll, T., King, S., Gray, S. R., Bolto, B. A. and Booker, N. A. (2000) The fouling of microfiltration membranes by NOM after coagulation treatment, *Water Research*, 34(11), pp. 2861–2868.
- Chakraborti, R. K., Atkinson, J. F. and van Benschoten, J. E. (2000) Characterization of alum floc by image analysis, *Environmental Science and Technology*, 34(18), pp. 3969–3976.

- Chellam, S. and Wiesner, M. R. (1993) Fluid mechanics and fractal aggregates, *Water Research*, 27(9), pp. 1493–1496.
- Chen, V., Fane, A. G. and Fell, C. J. D. (1992) The use of anionic surfactants for reducing fouling of ultrafiltration membranes: Their effects and optimization, *Journal of Membrane Science*, 67(2–3), pp. 249–261.
- Chern, J.-M. and Chien, Y.-W. (2001) Adsorption isotherms of benzoic acid onto activated carbon and breakthrough curves in fixed-bed columns, *Industrial & Engineering Chemistry Research*, 40(17), pp. 3775–3780.
- Clark, R. and Lykins, B. (1990) *Granular activated carbon: design, operation and cost*. Chelsea, MI: Lewis Publishers.
- Cook, D., Newcombe, G. and Sztajn bok, P. (2001) The application of powdered activated carbon for MIB and geosmin removal: predicting PAC doses in four raw waters., *Water research*, 35(5), pp. 1325–33.
- Crittenden, J. C., Berrigan, J. K., Hand, D. W. and Lykins, B. (1987) Design of rapid fixed-bed adsorption tests for nonconstant diffusivities, *Journal of Environmental Engineering*, 113(2), pp. 243–259.
- Crittenden, J. C., Reddy, P. S., Arora, H., Trynoski, J., Hand, D. W., Perram, D. L., Summers, R. S., Parimi Sanjay, R., Harish, A., Trynoski, J., Hand, D. W., Perram, D. L. and Summers, R. S. (1991) Predicting GAC performance with rapid small-scale column tests, *Journal - American Water Works Association*. American Water Works Association, 83(1), pp. 77–87.
- Crittenden, J. C., Trussell, R. R., Hand, D. W., Howe, K. J. and Tchobanoglous, G.

- (2005) Adsorption, in *Water Treatment: Principles and Design*. 2nd edn. Hoboken, NJ: John Wiley & Sons, Inc., pp. 1245–1358.
- Crittenden, J., Trussell, R. and Hand, D. (2012) *MWH's Water Treatment: Principles and Design*.
- Dabrowski, A., Podkoscielny, P., Hubicki, Z. and Barczak, M. (2005) Adsorption of phenolic compounds by activated carbon—a critical review, *Chemosphere*, 58, pp. 1049–1070.
- Dastgheib, S. A., Karanfil, T. and Cheng, W. (2004) Tailoring activated carbons for enhanced removal of natural organic matter from natural waters, *Carbon*, 42(3), pp. 547–557.
- Delle Site, A. (2001) Factors affecting sorption of organic compounds in natural sorbent/water systems and sorption coefficients for selected pollutants. A review, *Journal of Physical and Chemical Reference Data*, 30(1), pp. 187–439.
- Dixon, A. G. and Nijemeisland, M. (2001) CFD as a design tool for fixed-bed reactors, *Industrial & Engineering Chemistry Research*, 40(23), pp. 5246–5254.
- Dunn, S. E. and Knappe, D. R. U. (2013) *DBP precursor and micropollutant removal by powdered activated carbon (Web Report #4294)*. Denver, Colorado: Water Research Foundation.
- Ellerie, J. R. (2012) *Carbonaceous Adsorbants as Coatings for Ultrafiltration Membranes*. Clemson University.
- Ellerie, J. R., Apul, O. G., Karanfil, T. and Ladner, D. A. (2013) Comparing graphene, carbon nanotubes, and superfine powdered activated carbon as adsorptive coating

- materials for microfiltration membranes., *Journal of Hazardous Materials*. Elsevier B.V., 261C, pp. 91–98.
- EPA (2006) *WATER9*, EPA Office of Air Quality Planning and Standards.
- Ervin, V. (2015) *Introduction to Numerical Techniques*. Clemson University.
- Glucina, K., Do-Quang, Z. and Laîné, J. M. (1997) Assessment of a particle counting method for hollow fiber membrane integrity, *Desalination*, 113(2–3), pp. 183–187.
- Greenbank, M. and Spotts, S. (1993) Effects of starting material on activated carbon characteristics and performance, *Proceedings of WATERTECH Expo*.
- Gregory, J. (1975) Interaction of unequal double layers at constant charge, *Journal of Colloid And Interface Science*, 51(1), pp. 44–51.
- Gunjal, P. R., Ranade, V. V. and Chaudhari, R. V. (2005) Computational study of a single-phase flow in packed beds of spheres, *AIChE Journal*, 51(2), pp. 365–378.
- Guo, H., Wyart, Y., Perot, J., Nauleau, F. and Moulin, P. (2009) Low-pressure membrane integrity tests for drinking water treatment: A review, *Water Research*, 44, pp. 41–57.
- Gurr, C. J. and Reinhard, M. (2006) Harnessing natural attenuation, *Environmental science & technology*, May 1, pp. 2872–2876.
- Hamad, J. Z., Kennedy, M. D., Hofs, B., Heijman, S. G. J., Amy, G. and Schippers, J. (2008) *Super ground PAC in combination with ceramic micro-filtration II*.
- Heijman, S. G. J., Hamad, J. Z., Kennedy, M. D., Schippers, J. and Amy, G. (2009a) Submicron powdered activated carbon used as a pre-coat in ceramic micro-filtration, *Desalination and Water Treatment*. Desalination Publications, 9(1–3), pp. 86–91.

- Heijman, S. G. J., Rabinovitch, E., Bos, F., Olthof, N. and van Dijk, J. C. (2009b) Sustainable seawater desalination: Stand-alone small scale windmill and reverse osmosis system, *Desalination*, 248(1–3), pp. 114–117.
- Heijs, A. W. J. and Lowe, C. P. (1995) Numerical Evaluation of the Permeability and the Kozeny Constant for Two Types of Porous Media, *Phys. Rev. E*, 51(5), pp. 4346–4352.
- Hendricks, D. W. (2006) *Water treatment unit processes: physical and chemical*. CRC.
- Hernández, A. M., Labady, M. and Laine, J. (2014) Granular activated carbon from wood originated from tropical virgin forest, *Open Journal of Forestry*, 4, pp. 208–211.
- Ho, Y. S. (2004) Citation review of Lagergren kinetic rate equation on adsorption reactions, *Scientometrics*, 59(1), pp. 171–177.
- Ho, Y. S. and McKay, G. (1999) Pseudo-second order model for sorption processes, *Process Biochemistry*, 34(5), pp. 451–465.
- Howe, K. J. and Clark, M. M. (2006) Effect of coagulation pretreatment on membrane filtration performance, *Journal / American Water Works Association*, pp. 579–582.
- Huang, H., Spinette, R. and O’Melia, C. R. (2008) Direct-flow microfiltration of aquasols I. Impacts of particle stabilities and size, *Journal of Membrane Science*. Johns Hopkins Univ, Dept Geog & Environm Engn, Baltimore, MD 21218 USA. Johns Hopkins Univ, Bloomberg Sch Publ Hlth, Ctr Water & Hlth, Baltimore, MD 21205 USA. O’Melia, CR, Johns Hopkins Univ, Dept Geog & Environm Engn, 3400 N Charles St, Baltimore, MD 21, 314(1–2), pp. 90–100.
- Huber, M. M., Göbel, A., Joss, A., Hermann, N., Löffler, D., McArdell, C. S., Ried, A.,

- Siegrist, H., Ternes, T. A. and von Gunten, U. (2005a) Oxidation of pharmaceuticals during ozonation of municipal wastewater effluents: A pilot study, *Environment Science and Technology*. American Chemical Society, (39), pp. 4290–4299.
- Huber, M. M., Korhonen, S., Ternes, T. A. and von Gunten, U. (2005b) Oxidation of pharmaceuticals during water treatment with chlorine dioxide, *Water Research*, 39(15), pp. 3607–3617.
- Ismail, A. F. and David, L. I. B. (2001) A review on the latest development of carbon membranes for gas separation, *Journal of Membrane Science*, 193, pp. 1–18.
- Israelachvili, J. N. (2011) *Electrostatic Forces between Surfaces in Liquids, Intermolecular and Surface Forces*. Elsevier.
- Jain, P. and Pradeep, T. (2005) Potential of silver nanoparticle-coated polyurethane foam as an antibacterial water filter, *Biotechnology and Bioengineering*, 90(1), pp. 59–63.
- Jain, S., Yamgar, R. and Jayaram, R. V. (2009) Photolytic and photocatalytic degradation of atrazine in the presence of activated carbon, *Chemical Engineering Journal*, 148(2), pp. 342–347.
- Jia, Y. F. and Thomas, K. M. (2000) Adsorption of cadmium ions on oxygen surface sites in activated carbon, *Langmuir*. American Chemical Society, 16(3), pp. 1114–1122.
- Karanfil, T. and Kilduff, J. E. (1999) Role of granular activated carbon surface chemistry on the adsorption of organic compounds. 1. Priority pollutants, *Environmental Science and Technology*, 33(18), pp. 3217–3224.
- Karanfil, T., Kitis, M., Kilduff, J. E. and Wigton, A. (1999) Role of granular activated carbon surface chemistry on the adsorption of organic compounds. 2. Natural

- organic matter, *Environmental Science and Technology*, 33(18), pp. 3225–3233.
- Kim, H. S., Katayama, H., Takizawa, S. and Ohgaki, S. (2005) Development of a microfilter separation system coupled with a high dose of powdered activated carbon for advanced water treatment, *Desalination*, 186(1–3), pp. 215–226.
- Knappe, D. R. U., Matsui, Y., Snoeyink, V. L., Roche, P., Prados, M. J. and Bourbigot, M.-M. (1998) Predicting the capacity of powdered activated carbon for trace organic compounds in natural waters, *Environmental Science and Technology*, 32(11), pp. 1694–1698.
- Ko, D. C. K., Porter, J. F. and McKay, G. (2002) A branched pore model analysis for the adsorption of acid dyes on activated carbon, *Adsorption*, (1987), pp. 305–317.
- Ladner, D. A., Steele, M., Weir, A., Hristovski, K. and Westerhoff, P. (2012) Functionalized nanoparticle interactions with polymeric membranes, *Journal of Hazardous Materials*, 211–212, pp. 288–295.
- Lagergren, S. (1898) Zur theorie der sogenannten adsorption gelöster stoffe, *Kungliga Svenska Vetenskapsakademiens. Handlingar*, Band 24(4), pp. 1–39.
- Lee, C. W., Bae, S. D., Han, S. W. and Kang, L. S. (2007) Application of ultrafiltration hybrid membrane processes for reuse of secondary effluent, *Desalination*, 202(1–3), pp. 239–246.
- Leverenz, H. L., Tchobanoglous, G. and Asano, T. (2011) Direct potable reuse: a future imperative, *Journal of Water Reuse and Desalination*, 1(1), p. 2.
- Li, L., Quinlivan, P. A. and Knappe, D. R. U. (2002) Effects of activated carbon surface chemistry and pore structure on the adsorption of organic contaminants from

aqueous solution, *Carbon*, 40, pp. 2085–2100.

Li, M. (2014) *Effects of Natural Organic Matter on Contaminant Removal by Superfine Powdered Activated Carbon Coupled with Microfiltration Membranes*. Clemson University.

Li, Q., Snoeyink, V. L., Mariñas, B. J. and Campos, C. (2003) Elucidating competitive adsorption mechanisms of atrazine and NOM using model compounds, *Water Research*, 37(4), pp. 773–784.

Lipp, P., Müller, U., Hetzer, B. and Wagner, T. (2009) Characterization of nanoparticulate fouling and breakthrough during low-pressure membrane filtration, *Desalination and Water Treatment*, 9(2008), pp. 234–240.

Liu, G., Ma, J., Li, X. and Qin, Q. (2009) Adsorption of bisphenol A from aqueous solution onto activated carbons with different modification treatments., *Journal of hazardous materials*, 164(2–3), pp. 1275–80.

Lopez-Ramon, M., Stoeckli, F., Moreno-Castilla, C. and Carrasco-Marín, F. (1999) On the characterization of acidic and basic surface sites on carbons by various techniques, *Carbon*, 37(1999), pp. 1215–1221.

Lua, A. C. and Jia, Q. (2009) Adsorption of phenol by oil-palm-shell activated carbons in a fixed bed, *Chemical Engineering Journal*, 150, pp. 455–461.

Luo, Y., Guo, W., Ngo, H. H., Nghiem, L. D., Hai, F. I., Zhang, J., Liang, S. and Wang, X. C. (2014) A review on the occurrence of micropollutants in the aquatic environment and their fate and removal during wastewater treatment, *Science of the Total Environment*, 473–474, pp. 619–641.

- Malvern Instruments (no date) Zeta potential: An Introduction in 30 minutes, *Zetasizer Nano Series Technical Note. MRK654-01*.
- Martin, R. J. (1980) Activated carbon product selection for water and wastewater treatment, *Ind. Eng. Chem. Prod. Res. Dev.*, 19, pp. 435–441.
- Matsui, Y., Aizawa, T., Kanda, F., Nigorikawa, N., Mima, S. and Kawase, Y. (2007) Adsorptive removal of geosmin by ceramic membrane filtration with super-powdered activated carbon, *Journal of Water Supply: Research and Technology—AQUA*, 56(6–7), p. 411.
- Matsui, Y., Ando, N., Sasaki, H., Matsushita, T. and Ohno, K. (2009a) Branched pore kinetic model analysis of geosmin adsorption on super-powdered activated carbon., *Water research*. Elsevier Ltd, 43(12), pp. 3095–103.
- Matsui, Y., Ando, N., Yoshida, T., Kurotobi, R., Matsushita, T. and Ohno, K. (2011) Modeling high adsorption capacity and kinetics of organic macromolecules on super-powdered activated carbon., *Water research*. Elsevier Ltd, 45(4), pp. 1720–8.
- Matsui, Y., Fukuda, Y., Inoue, T. and Matsushita, T. (2003) Effect of natural organic matter on powdered activated carbon adsorption of trace contaminants: characteristics and mechanism of competitive adsorption., *Water research*, 37(18), pp. 4413–24.
- Matsui, Y., Hasegawa, H., Ohno, K., Matsushita, T., Mima, S., Kawase, Y. and Aizawa, T. (2009b) Effects of super-powdered activated carbon pretreatment on coagulation and trans-membrane pressure buildup during microfiltration., *Water research*. Elsevier Ltd, 43(20), pp. 5160–70.

- Matsui, Y., Murai, K., Sasaki, H., Ohno, K. and Matsushita, T. (2008) Submicron-sized activated carbon particles for the rapid removal of chlorinous and earthy-musty compounds, *Journal of Water Supply: Research and Technology—AQUA*, 57(8), p. 577.
- Matsui, Y., Murase, R., Sanogawa, T., Aoki, N., Mima, S., Inoue, T. and Matsushita, T. (2005) Rapid adsorption pretreatment with submicrometre powdered activated carbon particles before microfiltration., *Water Science and Technology*, 51(6–7), pp. 249–56.
- Matsui, Y., Murase, R., Sanogawa, T., Aoki, N., Mimi, S., Inoue, T. and Matsutshita, T. (2004) Micro-ground powdered activated carbon for effective removal of natural organic matter during water treatment, *Water Science and Technology: Water Supply*, 4(4), pp. 155–163.
- Matsui, Y., Nakao, S., Taniguchi, T. and Matsushita, T. (2013) Geosmin and 2-methylisoborneol removal using superfine powdered activated carbon: shell adsorption and branched-pore kinetic model analysis and optimal particle size., *Water research*. Elsevier Ltd, 47(8), pp. 2873–80.
- Matsui, Y., Sakamoto, A., Nakao, S., Taniguchi, T., Matsushita, T., Shirasaki, N., Sakamoto, N. and Yurimoto, H. (2014) Isotope microscopy visualization of the adsorption profile of 2-methylisoborneol and geosmin in powdered activated carbon, *Environmental Science and Technology*, 48, pp. 10897–10903.
- Matsui, Y., Sanogawa, T., Aoki, N., Mima, S. and Matsushita, T. (2006) Evaluating submicron-sized activated carbon adsorption for microfiltration pretreatment, *Water*

Science and Technology:Water Supply, 6(1), pp. 1–8.

Matsui, Y., Yoshida, T., Nakao, S., Knappe, D. R. U. and Matsushita, T. (2012)

Characteristics of competitive adsorption between 2-methylisoborneol and natural organic matter on superfine and conventionally sized powdered activated carbons., *Water research*. Elsevier Ltd, 46(15), pp. 4741–9.

McDougall, G. J. (1991) The physical nature and manufacture of activated carbon,

Journal of the South African Institute of Mining and Metallurgy, 91(4), pp. 109–120.

Menendez, I. and Fuerte, A. B. (2001) Aging of carbon membranes under different environments, *PERGAMON Carbon*, 39, pp. 733–740.

Menendez, J., Illán-Gómez, M. and Radovic, L. (1995) On the difference between the isoelectric point and the point of zero charge of carbons, *Carbon*, 33(11), pp. 1655–1657.

Metawater Co Ltd (2011) Ceramic Membrane Filtration System, p. 8.

Müller, E. A. and Gubbins, K. E. (1998) Molecular simulation study of hydrophilic and hydrophobic behavior of activated carbon surfaces, *Carbon*, 36(10), pp. 1433–1438.

Najm, I. N., Snoeyink, V. L., Suidan, M. T., Lee, C. H. and Richard, Y. (1990) Effect of particle size and background natural organics on the adsorption efficiency of PAC, *Journal - American Water Works Association*, 82(1), pp. 65–72.

Neely, J. and Isacoff, E. (1982) *Carbonaceous adsorbents for the treatment of ground and surface waters: Vol. 21. Pollution Engineering and Technology*. Marcel Dekker Inc., New York, United States.

Nyholm, N., Jacobsen, B. N., Pedersen, B. M., Poulsen, O., Damborg, A. and Schultz, B.

(1992) Removal of organic micropollutants at PPB levels in laboratory activated sludge reactors under various operating conditions: biodegradation, *Water Research*, 26(3), pp. 339–353.

Osantowski, R. and Wullschleger, R. (1986) *Evaluation of Activated Carbon for Enhanced COD Removal from Pharmaceutical Wastewater*. Cincinnati, OH: U.S. EPA.

Pan, K., Ming, H., Liu, Y. and Kang, Z. (2012) Large scale synthesis of carbon nanospheres and their application as electrode materials for heavy metal ions detection, *New Journal of Chemistry*, 36(1), p. 113.

Pan, L., Matsui, Y., Matsushita, T. and Shirasaki, N. (2016) Superiority of wet-milled over dry-milled superfine powdered activated carbon for adsorptive 2-methylisoborneol removal, *Water Research*. Elsevier Ltd, 102, pp. 516–523.

Pan, L., Takagi, Y., Matsui, Y., Matsushita, T. and Shirasaki, N. (2017) Micro-milling of spent granular activated carbon for its possible reuse as an adsorbent: Remaining capacity and characteristics, *Water Research*, 114, pp. 50–58.

Patni, A., Ludlow, D. and Adams, C. (2008) Characteristics of ground granular activated carbon for rapid small-scale column tests, *Journal of Environmental Engineering*, pp. 216–221.

Peel, R. G., Benedek, A. and Crowe, C. M. (1981) A branched pore kinetic model for activated carbon adsorption, *AIChE Journal*, 27(1), pp. 26–32.

Pelekani, C. and Snoeyink, V. L. (1999) Competitive adsorption in natural water: role of activated carbon pore size, *Water Research*, 33, pp. 1209–1219.

- Pelekani, C. and Snoeyink, V. L. (2000) Competitive adsorption between atrazine and methylene blue on activated carbon: the importance of pore size distribution, *Carbon*, 38(10), pp. 1423–1436.
- Pikkarainen, A. T., Judd, S. J., Jokela, J. and Gillberg, L. (2004) Pre-coagulation for microfiltration of an upland surface water, *Water Research*, 38(2), pp. 455–465.
- Quinlivan, P. A., Li, L. and Knappe, D. R. U. (2005) Effects of activated carbon characteristics on the simultaneous adsorption of aqueous organic micropollutants and natural organic matter., *Water research*, 39(8), pp. 1663–73.
- Raymond, J. W., Rogers, T. N., Shonnard, D. R., Kline, A. A. and Rogers, T. N. (2001) A review of structure-based biodegradation estimation methods, *Journal of Hazardous Materials*, 84, pp. 189–215.
- Rice, J., Wutich, A. and Westerhoff, P. (2013) Assessment of de facto wastewater reuse across the U.S.: Trends between 1980 and 2008, *Environmental Science and Technology*, 47(19), pp. 11099–11105.
- Richardson, J. F., Harker, J. H. and Backhurst, J. R. (2002) Flow of fluids through granular beds and packed columns, in *Chemical Engineering*. Butterworth-Heinemann, pp. 191–236.
- Roy, D., Wang, G. T. and Adrian, D. D. (1993) A simplified solution technique for carbon adsorption model, *Water Research*, 27(6), pp. 1033–1040.
- Rushton, A., Ward, A. S. and Holdich, R. G. (2008) *Solid-Liquid Filtration and Separation Technology*. John Wiley & Sons.
- Russel, W. B., Saville, D. A. and Schowalter, W. R. (1992) *Colloidal Dispersions*.

Cambridge University Press.

- Saufi, S. M. and Ismail, A. F. (2004) Fabrication of carbon membranes for gas separation—a review, *Carbon*, 42, pp. 241–259.
- Schäfer, A. I., Schwicker, U., Fischer, M. M., Fane, A. G. and Waite, T. D. (2000) Microfiltration of colloids and natural organic matter, *Journal of Membrane Science*, 171(2), pp. 151–172.
- Scott, G. D. and Kilgour, D. M. (1969) The density of random close packing of spheres, *Journal of Physics D: Applied Physics*. IOP Publishing, 2(6), pp. 863–866.
- Shimodaira, N. and Masui, A. (2002) Raman spectroscopic investigations of activated carbon materials, *Journal of Applied Physics Raman Spectrum of Graphite Journal of Applied Physics*, 92(10).
- Smíšek, M. and Černý, S. (1970) *Active carbon: manufacture, properties and applications*. Elsevier Publishing Company.
- Snoeyink, V. L. and Chen, A. S. C. (1985) Removal of organic micropollutants by coagulation and adsorption, *Science of the Total Environment*, 47, pp. 155–167.
- Stackelberg, P. E., Furlong, E. T., Meyer, M. T., Zaugg, S. D., Henderson, A. K. and Reissman, D. B. (2004) Persistence of pharmaceutical compounds and other organic wastewater contaminants in a conventional drinking-water-treatment plant, *Science of the Total Environment*, 329(1–3), pp. 99–113.
- Stoeckli, F., Huguenin, D. and Greppi, A. (1993) Primary and secondary filling of micropores in active carbons, *Journal of the Chemical Society, Faraday Transactions*. The Royal Society of Chemistry, 89(12), p. 2055.

- Stoquart, C., Servais, P., Bérubé, P. R. and Barbeau, B. (2012) Hybrid membrane processes using activated carbon treatment for drinking water: A review, *Journal of Membrane Science*. Elsevier B.V., 411–412, pp. 1–12.
- Studebaker, M. (1957) The chemistry of carbon black and reinforcement, *Rubber Chemistry and Technology*, 30(5), pp. 1401–1483.
- Stumm, W. and Morgan, J. J. (1942) Chemical Aspects of Coagulation, *American Water Works Association*, 54(8), pp. 971–994.
- Suekane, T., Yokouchi, Y. and Hirai, S. (2003) Inertial flow structures in a simple-packed bed of spheres, *AIChE Journal*, 49(1), pp. 10–17.
- Sun, X. and Li, Y. (2005) Hollow carbonaceous capsules from glucose solution., *Journal of colloid and interface science*, 291(1), pp. 7–12.
- Tessmer, C. H., Vidic, R. D. and Uranowski, L. J. (1997) Impact of oxygen-containing surface functional groups on activated carbon adsorption of phenols, *Environmental Science and Technology*. American Chemical Society, 31(7), pp. 1872–1878.
- Thill, A., Veerapaneni, S., Simon, B., Wiesner, M., Bottero, J. Y. and Snidaro, D. (1998) Determination of structure of aggregates by confocal scanning laser microscopy, *J. Colloid and Interface Sci.*, 204, pp. 357–362.
- Thiruvengkatachari, R., Shim, W. G., Lee, J. W. and Moon, H. (2004) Effect of powdered activated carbon type on the performance of an adsorption-microfiltration submerged hollow fiber membrane hybrid system, *Korean Journal of Chemical Engineering*, 21(5), pp. 1044–1052.
- Thomas, J. W. (1995) *Numerical Partial Differential Equations*. Springer New York.

- Thomas, P. M. and Foster, G. D. (2005) Tracking acidic pharmaceuticals, caffeine, and triclosan through the wastewater treatment process, *Environmental Toxicology and Chemistry*. Wiley Periodicals, Inc., 24(1), p. 25.
- To, P. C.-W. (2008) *Desorption of trace contaminants from activated carbon: effect of strongly-competing and pore-blocking background organic matter on desorption kinetics*. University of Illinois at Urbana-Champaign.
- Toles, C. A., Marshall, W. E., Johns, M. M., Wartelle, L. H. and McAloon, A. (2000) Acid-activated carbons from almond shells: physical, chemical and adsorptive properties and estimated cost of production, *Bioresource Technology*, 71(1), pp. 87–92.
- Vigneswaran, S., Chaudhary, D. S., Ngo, H. H., Shim, W. G., Moon, H., Chaudhary, D. S., Ngo, H. H., Shim, W. G. and Moon, H. (2016) Application of a PAC-membrane hybrid system for removal of organics from secondary sewage effluent: Experiments and modelling, *Separation Science and Technology*, 38(10), pp. 2183–2199.
- Waite, T. D., Schäfer, A. I., Fane, A. G. and Heuer, A. (1999) Colloidal fouling of ultrafiltration membranes: Impact of aggregate structure and size, *Journal of Colloid and Interface Science*, 212(2), pp. 264–274.
- Wang, J., Guan, J., Santiwong, S. R. and Waite, T. D. (2008) Characterization of floc size and structure under different monomer and polymer coagulants on microfiltration membrane fouling, *Journal of Membrane Science*, 321, pp. 132–138.
- Weber JR, W. J., Meginley, P. M. and Katz, L. E. (1991) Sorption phenomena in subsurface systems: Concepts, models, and effects on contaminant fate and

transport, *Wat. Res*, 25(5), pp. 499–528.

Westerhoff, P., Yoon, Y., Snyder, S. and Wert, E. (2005) Fate of endocrine-disruptor, pharmaceutical, and personal care product chemicals during simulated drinking water treatment processes., *Environmental Science and Technology*, 39(17), pp. 6649–63.

Wu, S. H. and Pendleton, P. (2001) Adsorption of anionic surfactant by activated carbon: Effect of surface chemistry, ionic strength, and hydrophobicity, *Journal of Colloid and Interface Science*, 243, pp. 306–315.

Xu, P. and Yu, B. (2008) Developing a new form of permeability and Kozeny–Carman constant for homogeneous porous media by means of fractal geometry, *Advances in Water Resources*.

Yalcin, M. and Arol, A. I. (2002) Gold cyanide adsorption characteristics of activated carbon of non-coconut shell origin, *Hydrometallurgy*, 63(2), pp. 201–206.

Yan, X. M., Shi, B. Y., Lu, J. J., Feng, C. H., Wang, D. S. and Tang, H. X. (2008) Adsorption and desorption of atrazine on carbon nanotubes, *Journal of Colloid and Interface Science*, 321(1), pp. 30–38.

Žalac, S. and Kallay, N. (1992) Application of mass titration to the point of zero charge determination, *Journal of colloid and interface science*, 149(1), pp. 233–240.

Zeng, Z. and Grigg, R. (2006) A criterion for non-Darcy flow in porous media, *Transport in Porous Media*, 63, pp. 57–69.

Zhang, S., Shao, T., Bekaroglu, S. S. K. and Karanfil, T. (2009) The impacts of aggregation and surface chemistry of carbon nanotubes on the adsorption of

synthetic organic compounds, *Environmental Science and Technology*, 43(15), pp. 5719–5725.

Zhang, S., Shao, T. and Karanfil, T. (2011) The effects of dissolved natural organic matter on the adsorption of synthetic organic chemicals by activated carbons and carbon nanotubes., *Water research*. Elsevier Ltd, 45(3), pp. 1378–86.

Zhang, S., Shao, T., Kose, H. S. and Karanfil, T. (2010) Adsorption of aromatic compounds by carbonaceous adsorbents: a comparative study on granular activated carbon, activated carbon fiber, and carbon nanotubes, *Environmental Science and Technology*, 12(864), pp. 6377–6383.

Zhang, W., Crittenden, J., Li, K. and Chen, Y. (2012) Attachment efficiency of nanoparticle aggregation in aqueous dispersions: modeling and experimental validation., *Environmental Science and Technology*, 46, pp. 7054–62.